A Photoelastic Study of Roof Truss-Roof Interactions in a Multilayered Mine Model

by

George M. Neall III

Thesis submitted to the Graduate Faculty of the
Virginia Polytechnic Institute and State University
in partial fulfillment of the requirements for the degree of

Master of Science

in

Mining Engineering

APPROVED:

Christopher Haycocks

Christopher Haycocks

J. Richard Lucas

J. Richard Lucas

Lawrence Adler

Lawrence Adler

May, 1975

Blacksburg, Virginia

LD
5655
V855
1975
N43
c.2

Acknowledgements

I would like to thank Dr. Christopher Haycocks, Committee Chairman,for his guidance, help, and suggestions, not only in the preparation of this thesis, but also in the actual model experimentation. Sincere thanks are also extended to Dr. J. Richard Lucas and Dr. Lawrence Adler for their guidance and help. Thanks are also extended to Dr. H. F. Brinson and Professor C. W. Smith of the Engineering Mechanics Department for their many comments and suggestions on the technical aspects of the model analysis and correlation with a prototype, and to James M. Townsend for his comments and criticism of the experimental and theoretical work. Finally, I would like to thank Virginia Polytechnic Institute and State University and the Fossil Fuel Division of the Energy Research and Development Administration, former Office of Coal Research, whose financial assistance made this project possible.

TABLE OF CONTENTS

LIST OF FIGURES

LIST OF TABLES

INTRODUCTION

Only recently has the energy crisis, predicted by many experts for years, had real impact upon our nation. It has been clearly demonstrated by them that conservation of our natural resources is urgently required because there is but a limited supply available. We must improve on existing technology so that energy which is available can be more efficiently used. This process will not occur overnight, and present resources must be utilized to the fullest extent possible.

Realization of this dilemma has been painful because of the sudden restriction in the supplies of petroleum and natural gas. Though reserves of petroleum and natural gas are low, there is an abundance of coal, and it appears that it will play an increasingly more important role in providing energy. This means that large tonnages must be mined cheaply and efficiently, so that production can keep abreast of demand. Of utmost important in coal mining is proper roof support. Without it, not only is production impaired, but lives are endangerd. Good roof support is not only a problem of the coal mining company and its personnel, but concerns everyone touched by the energy crisis.

Roof support in underground coal mines has been, and continues to be, a major problem to the design engineer and to production personnel. Modern high-capacity mines require large capital expenditures and assurances that output will be sufficient and continuous through the life of the mine to justify these investments. Good roof support, therefore, is required not only for the safety of personnel involved,

but also for the assurance that equipment damage and production stoppages due to roof failure will be minimal. The mechanical and resin anchored roof bolt today fulfills much of the above needs when properly used, however there have been and will continue to be numerous roof-control problems which will require even more effective support techniques. As early as 1959 it was recognized that obliquely installed roof bolts had advantages over the conventional perpendicularly installed bolts. Widespread use of this method has not occurred, however, due to the lack of design criteria and the difficulty of drilling inclined holes with existing equipment.

A modification of the obliquely installed roof bolt, the roof truss, utilizes the support concept of post-stressing and has been very effective in preventing roof falls which could not be controlled by other means. It has not been used extensively, however, again due to the above mentioned difficulties, among others. Development of design criteria, and an understanding of how the roof truss works would not only enable this support method to be utilized to its optimum potential, but would also help promote more general acceptance of this support technique.

Roof-truss optimization may be approached basically from three directions: field work, laboratory studies, and theoretical considerations. The length of time required to obtain useful data from field studies seemed prohibitive, so it was decided to approach the problem via the theoretical approach and through the use of laboratory model experiments. Because of the many assumptions and guesses which

must be made to apply theory to such a complicated problem as this, the laboratory approach seemed to be most promising.

Primary emphasis was therefore placed on obtaining laboratory data, with secondary emphasis placed on corroborating laboratory work with the theoretical solutions.

LITERATURE REVIEW

Roof-Truss Research

Although the use of roof trusses as a means of support in coal mines is fairly new, many mines have been quick to accept this support method simply because other methods of roof support have failed. Surprisingly enough however, there is very little literature describing roof-truss implementation and installation.

Kegel (1969) describes extensive field application and testing of roof trusses which proved effective in supporting roof strata which could not be supported effectively by roof bolts or standard timbering. He also describes multiple-truss installations, smaller span trusses used within larger span trusses, which have been successfully employed in spans up to 40 feet.

Sheorey, Verma, and Singh (1973) statically analyzed the roof truss and recommended the following:

1. Roof truss inclination from horizontal, θ, should preferably be 60^{o}, but in no case less than 45^{o}.
2. The optimum distance between the hole and blocking point depends on block size and hole to hole span, as seen in Figure 1.

Gambrell and Haynes (1970) constructed a one-piece photoelastic model of a mine opening from PLM-4B, a high modulus epoxy, and compared the shear stresses of a truss supported roof with an inclined bolted roof. The truss supported roof proved to be superior because compressive stresses parallel to the opening were produced, whereas in the inclined bolted model tensile stresses parallel to the opening

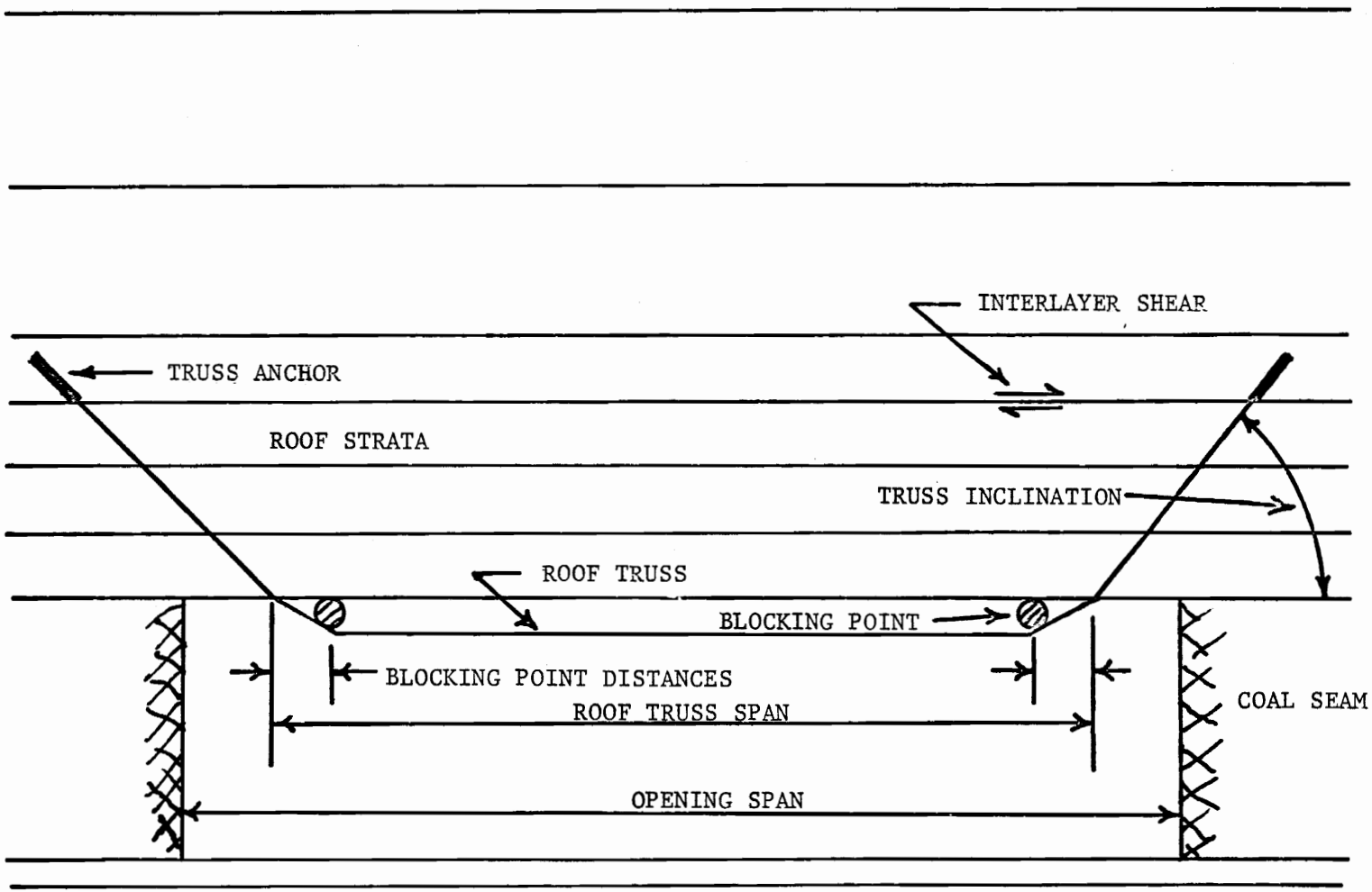

Figure 1. Schematic of Roof-Truss Installation in Photoelastic Mine Model.

were developed in the roof strata.

White (1970) discusses the field installations of over 30,000 roof trusses, of which less than 1% have failed due to truss breakage. In addition, he describes several multiple truss installations and discusses their yield load capacity.

Before the invention of the roof truss numerous experiments with conventional roof bolts were performed. Publications by Hugon (1959), Schvermann (1960), Singh and Chugh (1968), and Tincelin and Sinoc (1964) acknowledged that inclined roof bolts are more effective than perpendicularly installed roof bolts.

Van Ham and Tsur-Lavie (1969) constructed a composite (multi-layered) high modulus plastic photoelastic model and externally loaded it to simulate a distributed load. They then experimented with perpendicular and oblique roof bolts to determine which was the more effective support method. Among their conclusions were:

1. The reinforcement factor (RF = safety factor of bolted roof/safety factor of unbolted roof) of the obliquely bolted roof was greater than the perpendicularly bolted roof for a given set of conditions.
2. The RF of obliquely bolted roofs does not relate directly to mid-span deflections.
3. Soft interlayer inclusions decrease the RF, but with oblique roof bolts, it still remains relatively high.

Model Studies of Mine Structure

There are two basic approaches which may be taken in modelling mine structures, physical modelling and mathematical modelling. Mathematical modelling may be further broken down into closed form solutions and interative or numerical solutions.

The use of physical and mathematical models to explain and predict prototype behavior is by no means new. Frocht (1948) helped pioneer the use of photoelastic models to solve a multitude of problems ranging from stress concentration factors to three-dimensional stress analyses of complex models. The method is still widely used today in numerous fields of study ranging from fracture mechanics to stress determination in field situations, to composite model analyses, and has proven itself to be a valuable experimental technique. Similarly, scale model studies involving materials similar to the prototype have been conducted with much success.

Since the advent of the modern digital computer, numerous different types of mathematical models have been devised to solve problems for which closed form solutions do not exist. One of these methods is the finite-difference method. With this method, the boundary conditions are chosen, the model is discretised, and employing numerical differentials, which can be obtained by a Taylor's series expansion, a series of simultaneous equations can be derived and solved.

More recently, the finite-element method has been successfully applied to complex problems as will be discussed later.

In the particular area of mining, numerous investigators have

employed either photoelastic mine models or mine models of rock-like material with varying degrees of success.

Hobbs (1966, 1968, 1969, 1970) conducted a number of two dimensional scale model studies of strata movement around mine roadways. He employed a rock-like material made of various sand and cement mixtures so that the material properties of the model could be changed considerably. The multilayered models were inserted in a loading frame and various combinations of vertical and horizontal loads were applied. Failures similar to those encountered in mines could then be simulated. Similar tests were also conducted by Everling (1964) and Jacobi and Everling (1960).

Other mine model studies utilizing the photoelastic technique were employed. Agarwal (1968) described tests performed on a composite model with a circular opening. Bieniawski and Van Tonder (1969) studied the stress distribution and rock fracturing around an opening in a photoelastic mine model. Lang (1964) described research whereby photoelastic model studies combined with in-situ testing provided an acceptable forecast of the deformational behavior inside a tunnel. All of these tests, however,were concerned with externally loaded models and not gravity loaded as occurs in nature. The results of a gravity loaded and an externally loaded model may not differ greatly for such problems as pillar loads and floor heave. Larger discrepancies can be expected though when the immediate roof is being analyzed. This is because interlayer separation can occur in a gravity loaded model, whereas in an externally loaded model, since layer or beam deflection is a

function of overburden loading, no bed separation occurs. Because of this, differences not only in stress magnitudes but also in stress directions can be expected, significantly changing the effects resulting from a particular type of support.

Numerous investigators such as Panek (1952) and Hoek (1956) realized this and gravity loaded models utilizing a centrifuge to furnish the required body loading were built. Since the models were made of rock or a rock-like material laws of similitude were fulfilled. Several problems, however, are inherent with this method. The main problem encountered was in obtaining and recording strain and deflection measurements. Also, since the centrifugal force varies as a function of the distance from the center of rotation, complexities in scaling were encountered.

Mandel (1964) and Thakur (1968) discussed some of the problems associated with scale-model testing, with particular attention directed to similitude of model and prototype. Basically, the more variables which are present such as modulus of elasticity, geometrical properties, material density and others, the more complicated is the task of determining a scale factor to relate model stresses to prototype stresses. A scale factor might be relatively easily derived for a gravity loaded model of a rock-like material whose geometrical properties are similar to the prototype, whereas the problem of determining a scale factor for a gravity-loaded model with significantly different elastic moduli and geometrical properties from the prototype would be almost insurmountable.

Rankilor and McNicholas (1968) and Rankilor (1971) described the preparation and testing of a multi-layered mine model constructed from a low-modulus photoelastic material (solithane 113, or polyurethane). From their research, they constructed a subsidence development curve which related favorably with field examples even though no scale factor could be applied initially. The main advantage of this material is that normal gravity loading is sufficient to produce measureable deflections and because of this no centrifuges or loading devices are required.

THEORETICAL INVESTIGATION OF ROOF-TRUSS MECHANICS

In spite of the difficulties which are encountered in an investigation of this type, it was decided that a theoretical approach might provide valuable information which could be applied to the proposed model studies. After some initial investigation, several theoretical methods of predicting roof-truss performance were selected.

Elastic-Beams Approach

To determine whether or not the experimental values could be correlated with closed form theoretical solutions, a series of computations using beam flexure formulas was performed. Since the model represents only partially clamped beams, the solution should lie somewhere between the solutions for a simple beam and a fixed end beam.

The unsupported model opening's midspan deflection using simple beam equations, as seen in Figure 47 in the appendix, assuming only the immediate five rooflayers, each .3 in. high, contribute to the distributed load across the bottom rooflayer, should be approximately 1.31 in. The midspan deflection of a fixed-end beam would be 1/5 th. of this or .26 in. The second answer is more reasonable, but both seem to be too high for unsupported deflections. If the bottom layer were loaded by a distributed load equal to its weight, the deflection which might be expected would be 1/5 th. of the deflections which are mentioned above, or between .26 in. and .052 in.

If blocking point reactions 1.25 in. from the ribs were 1.0 lb. (.001 kips) each, the upward deflection which might be expected would be approximately 4.30 in. This seems to be completely unreasonable

though, even if one were to assume that the actual upward deflection were 1/4 th. of this or 1.08 in. This is probably due to the fact that the strata above the lowermost layer restrict its movement, effectively increasing its moment of inertia. As the moment of inertia increases, the deflection would decrease.

If the vertical anchor force reactions are assumed to contribute to the deflection, and it is assumed that the vertical load spreads out in a pyramid fashion, traveling outwards one unit for every two units downwards, its effect can be calculated. For a 45^{o} inclined hole, the anchor force would be approximately 0.7 lb. if the blocking point reaction were 1.0 lb., and would be located almost directly over the edge of the opening. The downward deflection which would be expected from it is approximately 1.95 in.

In any event, if the above figures are added, either for the simple-beam case or for a clamped-beam case, the answer indicates that the model should be deflecting upwards and not down. Again, this is probably due to the effects mentioned above concerning the moment of inertia of the roof layers. It has been known for some time that rocks exhibit different mechanical properties depending on the orientation of the specimen being tested. Since the moment of inertia seems to vary for the model material, which is isotropic and homogeneous, it is not unreasonable to assume that a similar property is exhibited by rock strata surrounding a mining opening.

Figure 2 shows an idealization of the type of loading situation being dealt with. In the theoretical solution only several of the loading

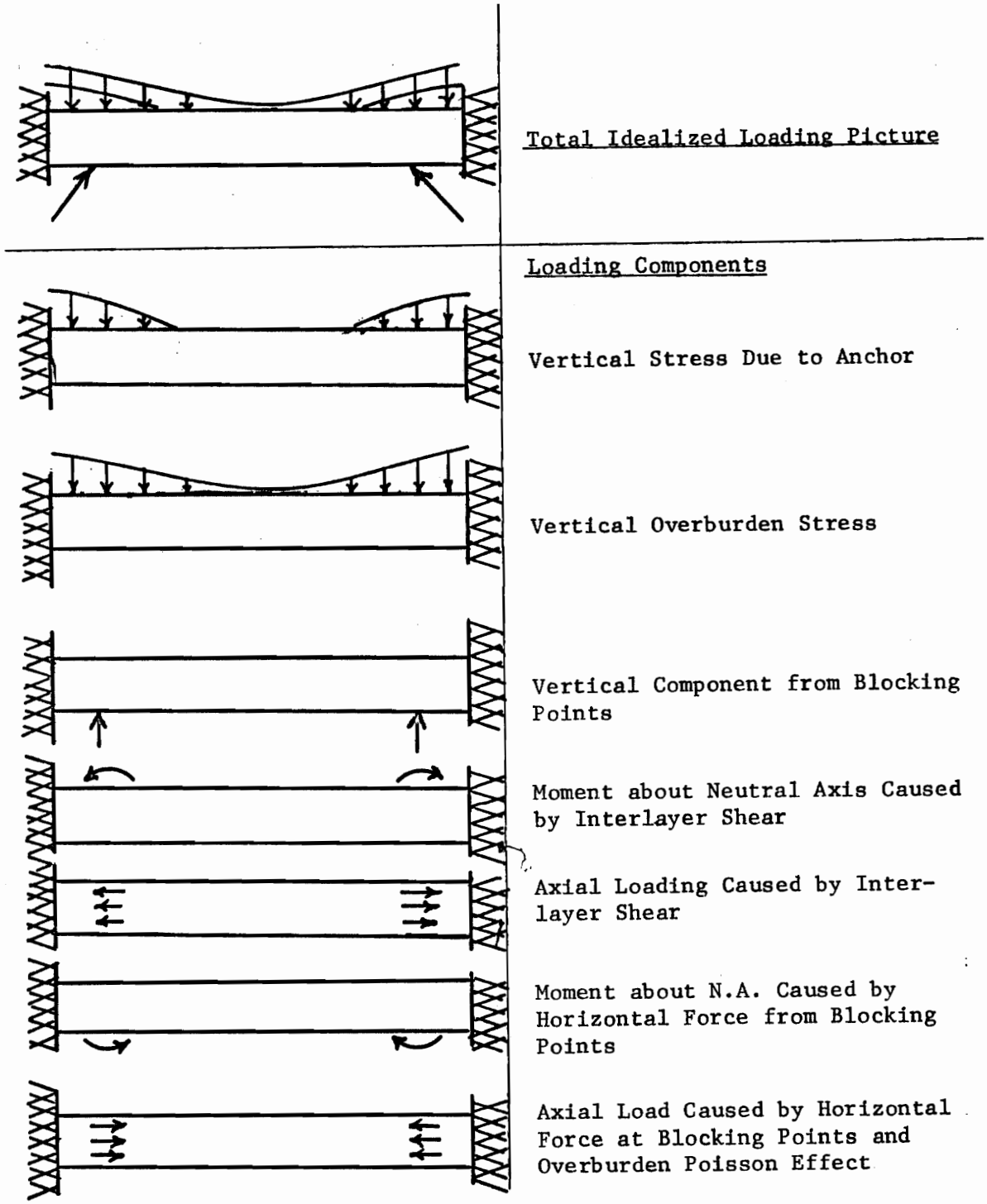

Figure 2. Separation of Loads in Idealized Truss Supported Roof. (Loads produce tension or compression in idealized beam.)

components are accurately known. The vertical stress due to the overburden and anchorage are not accurately known because an arching effect is taking place. In an attempt to overcome this, an unsupported mine model was constructed,and deflection measurements were taken every quarter inch across the opening. With this, it was thought a loading function might be constructed by employing numerical differentials to determine the fourth differential of the elastic curve. This approach was not acceptable, though, because the numerical operators demanded an accuracy of at least four places, whereas the accuracy of the cathetometer was only to three decimal places. Because of this, large fluctualtions between tension and compression were realized, and the resulting answer made no sense.

Because the above mentioned arching effect takes place, the vertical stress due to the anchor cannot be accurately determined. Similarly, interlayer shear is a function of the vertical loading from above, so the moment about the neutral axis and the axial loading attributable to it are unknown.

The only information which is accurately known are the reactions at the blocking points. The end result of the above analysis is that the closed from theoretical solutions rely a great deal on guesses and assumptions when such a complicated problem as this is being considered, and there is most certainly a fairly large error associated with this.

Rock-Load Solution

Terzaghi proposed an inelastic method of calculating the roof support which would be required based on the type of 'ground' encountered. Through extensive field investigation he categorized the types of rock commonly encountered depending on the bed dip and the number and characteristics of discontinuities, such as joints, which are present. From this he constructed a table, with each category, such as moderately blocky and seamy, and the heights to which failure might occur expressed as a constant multiplied by the width and height of the opening. A reproduction of this table as it appeared in Rock Tunneling with Steel Supports may be seen in Table 1. As may be seen from this table, some coal mine roofs may behave as very blocky and seamy, and, thus, the height of rock above the opening which will have to be supported to avoid roof failure can exceed the opening width. With this is mind a series of graphs was constructed as seen in Figures 3-8, which represent the weight of various shaped roof failures as a function of the height of the potential failure. Failure shapes may vary considerably depending on rock types, discontinuities present, and the stress field encountered. For an average roof truss spacing of 4 ft. and a 10 ft. high square-shaped failure, which would present the worst failure shape, the vertical load required to support the failed material is greater than 130,000 lb. Assuming the blocking point resultant acts at a 45^{o} angle, the required tension at both truss anchors is approxiamtely 85,000 lb. This, however, exceeds the allowable load of 10,000 lb. (average for 50 ksi steel)

Table 1

Rock load H_p in feet of rock on roof of support in tunnel with width B (ft) and height H_t (ft) at depth of more than 1.5 $(B + H_t)$.[1] (after Terzaghi, in Rock Tunneling with Steel Supports)

Rock Condition	Rock Load H_p, ft.	Remarks
1. Hard and intact	zero	Light lining, required only if spalling or popping occurs.
2. Hard stratified or schistose[2]	0 to 0.5B	Light support
3. Massive, moderately jointed	0 to 0.25B	Load may change erratically from point to point
4. Moderately blocky and seamy	0.25B to $0.25(B+H_t)$	No side pressure
5. Very blocky and seamy	$(0.35 \text{ to } 1.10)(B+H_t)$	Little or no side pressure

[1]The roof of the tunnel is assumed to be located below the water table. If it is located permanently above the water table, the values given for types 4 to 6 can be reduced by fifty per cent.

[2]Some of the most common rock formations contain layers of shale. In an unweathered state, real shales are no worse than other stratified rocks. However, the term shale is often applied to firmly compacted clay sediments which have not yet acquired the properties of rock. Such so-called shale may behave in the tunnel like squeezing or even swelling rock.

If a rock formation consists of a sequence of horizontal layers of sandstone or limestone and of immature shale, the excavation of the tunnel is commonly associated with a gradual compression of the rock on both sides of the tunnel, involving a downward movement of the roof. Furthermore, the relatively low resistance against slippage at the boundaries between the so-called shale and rock is likely to reduce very considerably the capacity of the rock located above the roof to bridge. Hence, in such rock formations, the roof pressure may be as heavy as in a very blocky and seamy rock.

Table 1 (continued)

Rock Condition	Rock Load H_p, ft.	Remarks
6. Completely crushed but chemically intact	$1.10(B+H_t)$	Considerable side pressure. Softening effect of seepage towards bottom of tunnel requires either continuous support for lower ends of ribs or circular ribs.
7. Squeezing rock, moderate depth	$(1.10 \text{ to } 2.10)(B+H_t)$	Heavy side pressure, invert struts required. Circular ribs recommended
8. Squeezing rock, great depth	$(2.10 \text{ to } 4.50)(B+H_t)$	(same as above)
9. Swelling rock	Up to 250 ft. irrespective of value of $(B+H_t)$	Circular ribs required. In extreme cases use yielding support.

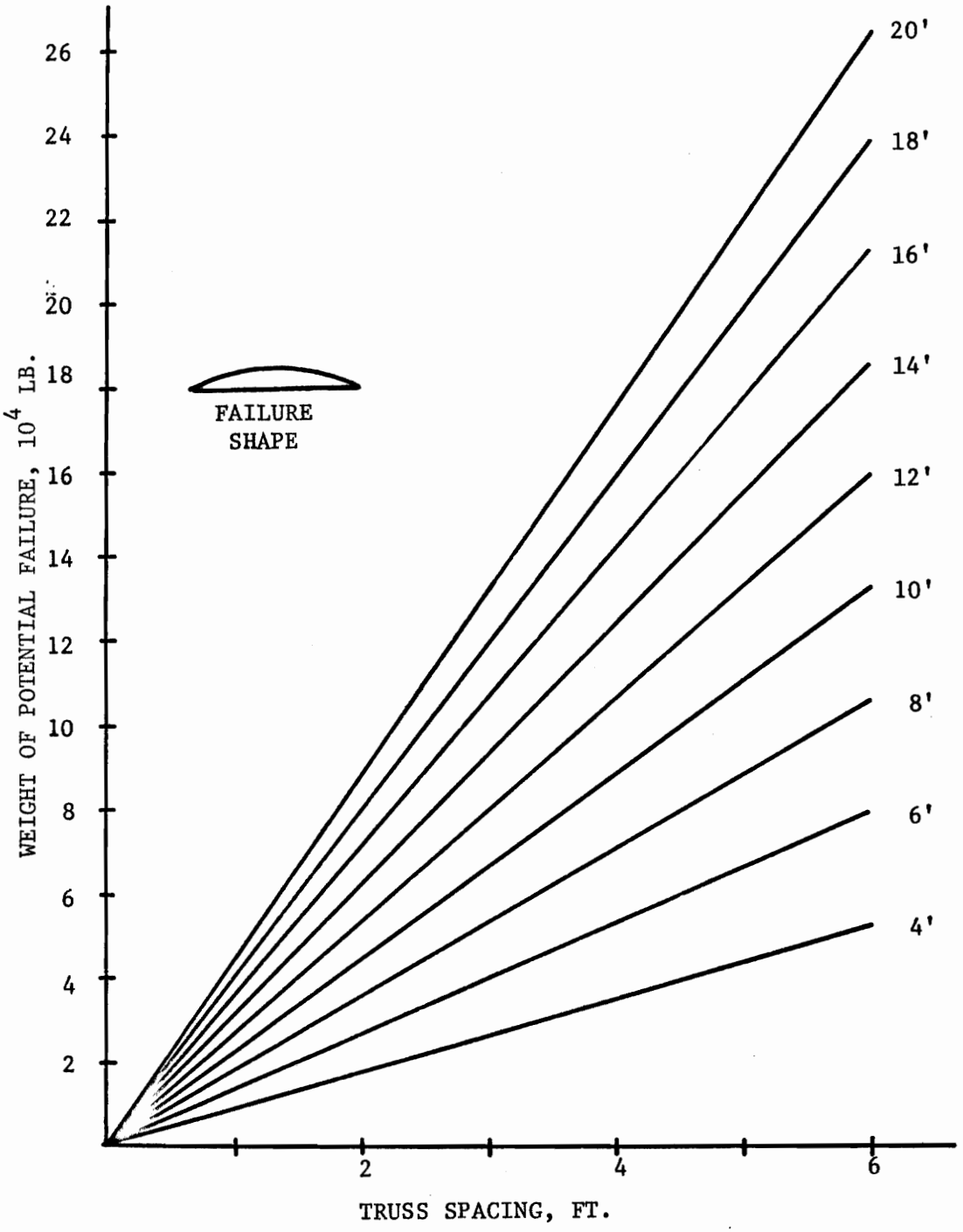

Figure 3. Weight of Parabolic-Shaped Failure Zone, for 20' Opening, as a Function of Failure Height. (See appendix 1 for derivation.)

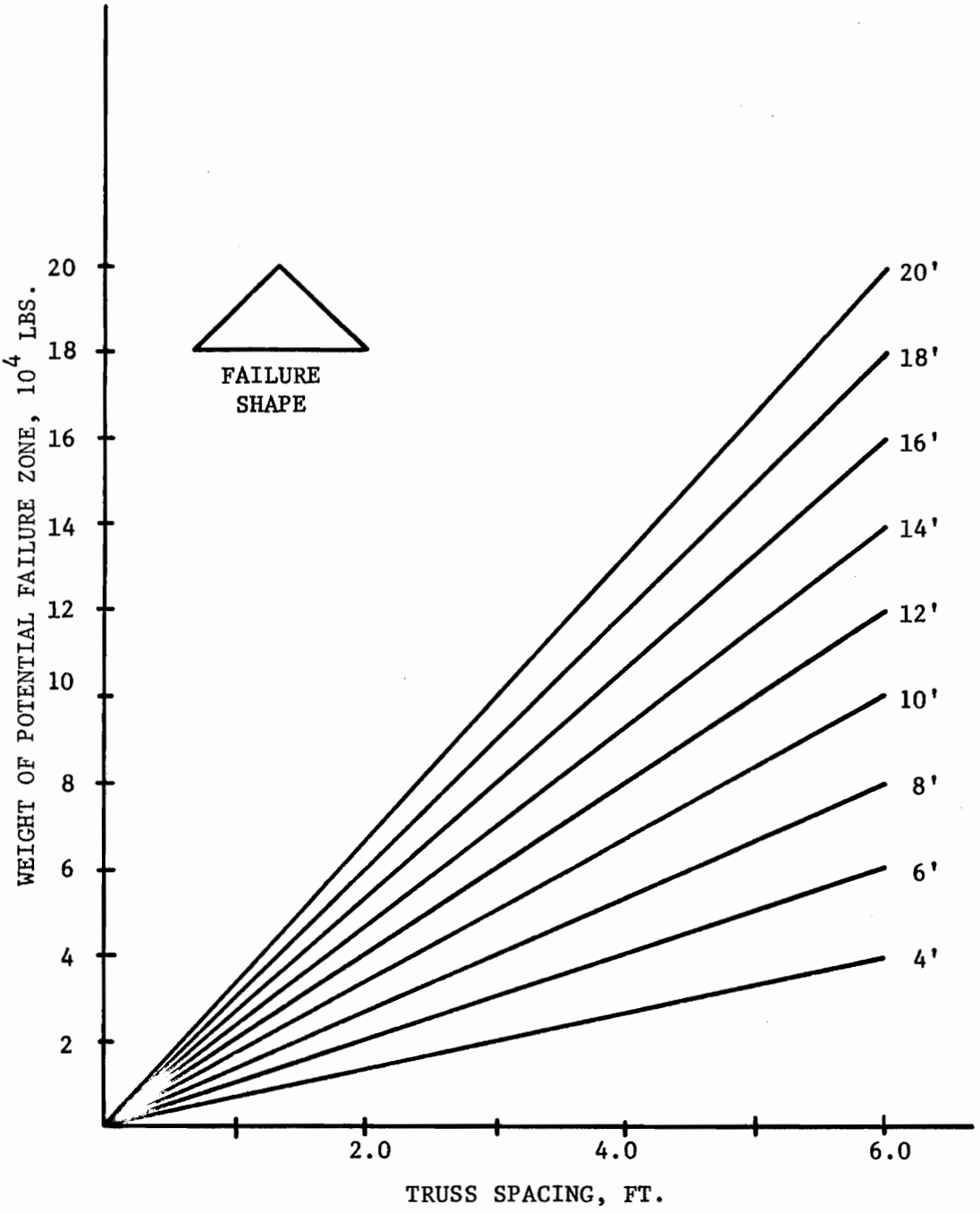

Figure 4. Weight of Triangular-Shaped Failure Zone, for a 20' Opening, as a Function of Failure Height. (See Appendix 1 for derivation.)

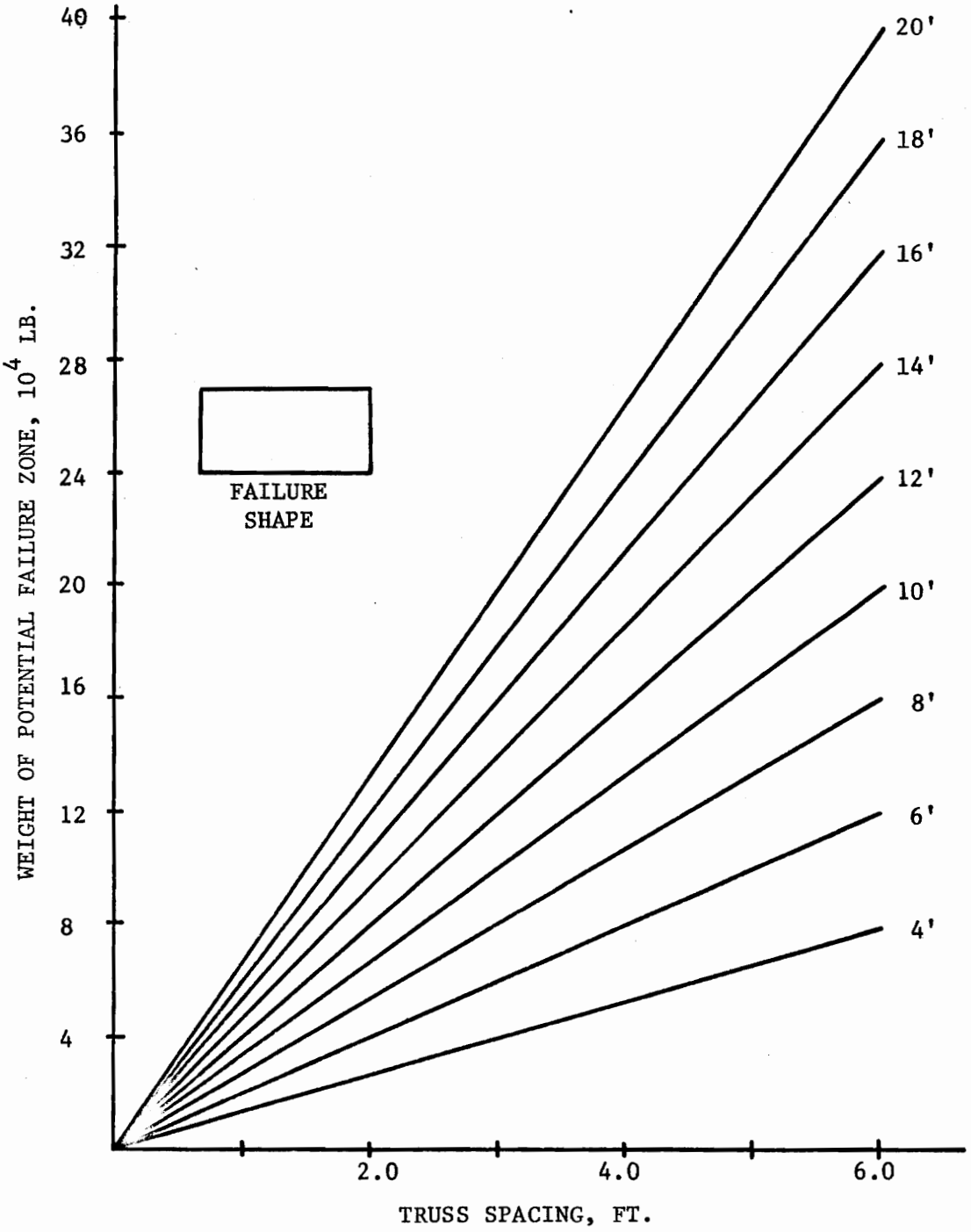

Figure 5. Weight of a Rectangular-Shaped Failure Zone, for a 20' Opening, as a Function of Failure Height. (See Appendix 1 for derivation.)

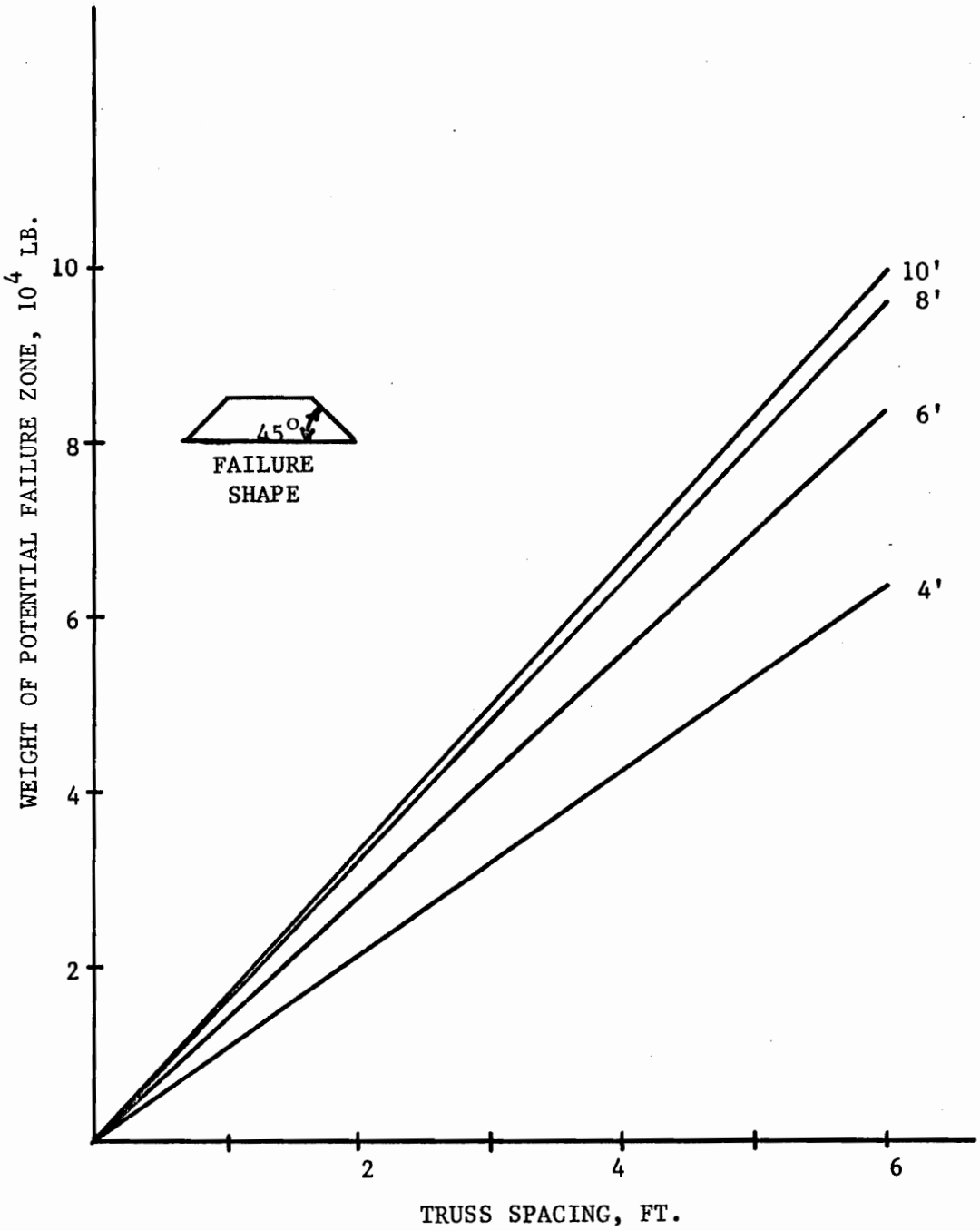

Figure 6. Weight of a Parallelogram-Shaped Failure Zone, for a 20' Opening, as a Function of Failure Height. (See Appendix 1 for derivation.)

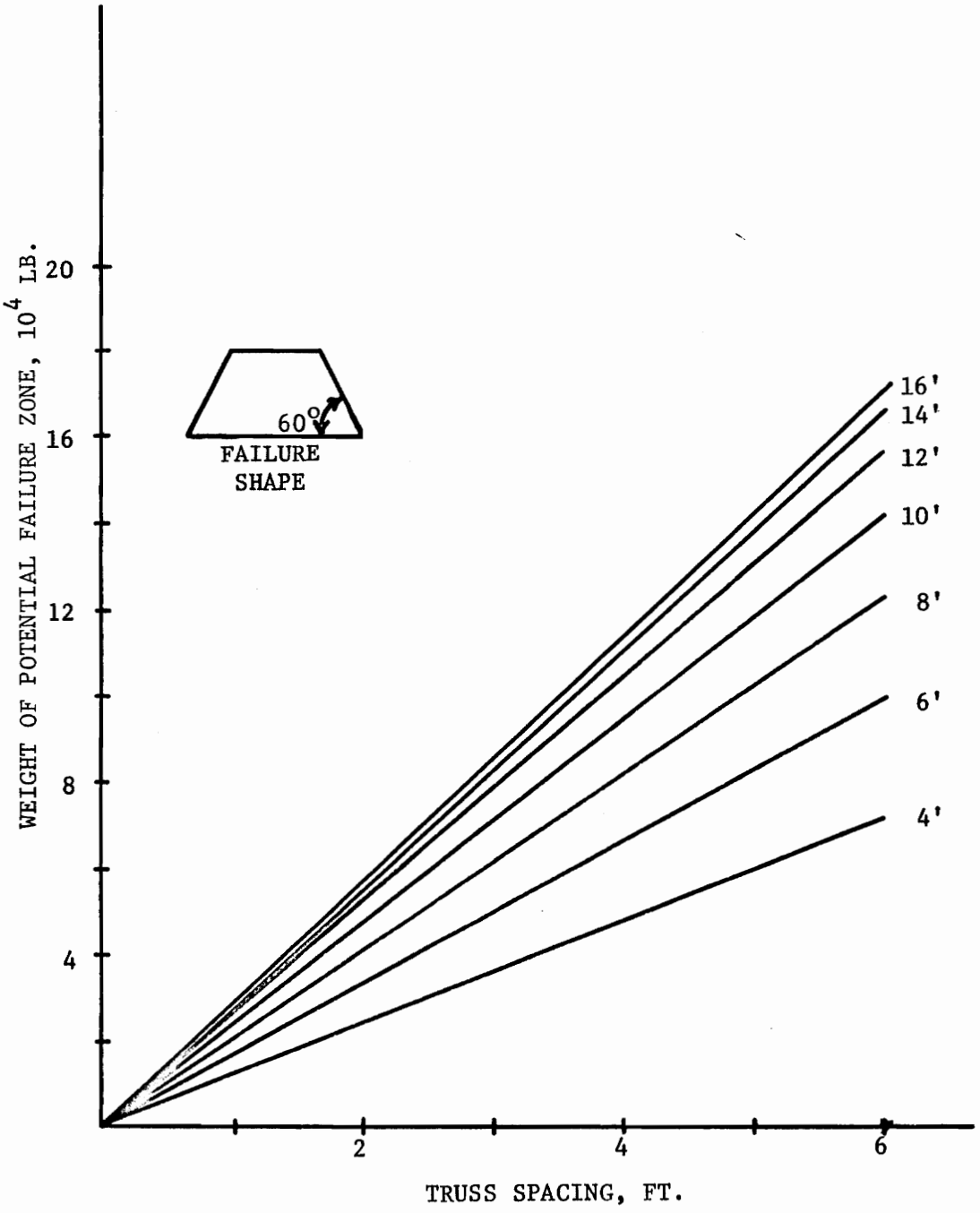

Figure 7. Weight of a Parallelogram-Shaped Failure Zone, for a 20' Opening, as a Function of Failure Height. (See Appendix 1 for derivation.)

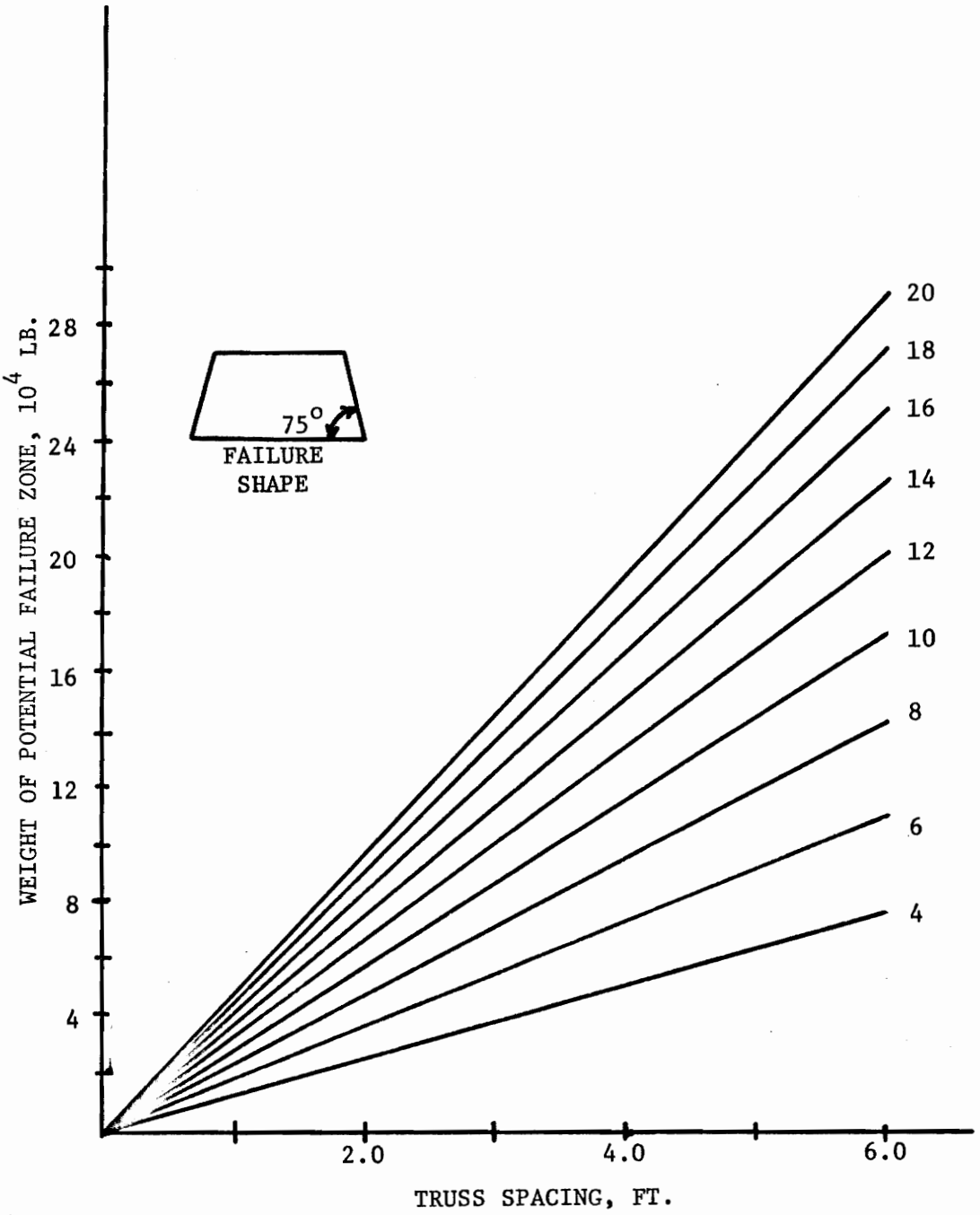

Figure 8. Weight of a Parallelogram-Shaped Failure Zone, for a 20' Opening, as a Function of Failure Height. (See Appendix 1 for derivation.)

for a 3/4 in. diameter bolt, especially when it is considered that the midspan tension is greater than anchor tension because of the friction loss at the blocking points (approximately 1.4 times greater depending on angle on contact, and frictional coefficients),as seen in Figure 9. From the above considerations the weight of the potential failure zone which would be supported can be calculated assuming a 30 percent loss of tension across the blocking point:

$$(T_b)\ (r)\ (n)\ (\sin 45^o) = SC$$

$$(10{,}000)\ (.70)\ (2)\ (.707) = 10{,}000\ \text{lb.}$$

Where:

T_b = allowable truss tension

r = efficiency (1 - coefficient of friction)

n = 2 (double anchor)

SC = Support Capacity

This would indicate that roof trusses spaced on 4 ft. centers could only prevent a square roof fall of less than 2 ft. Actual field installations, however, have proven otherwise, and have prevented falls of greater than 8 ft.

Roof-Reinforcement Analysis (Transformation of Sections)

Approaching the problem of truss support from another direction, one could assume that the truss transforms the potential failure zone into a large beam with only the truss capable of sustaining tension. Since it would be undesirable for the roof deflection to mobilize the tension in the truss, the truss would be tensioned when it was installed, and would be analagous to a prestressed concrete beam. The main reason

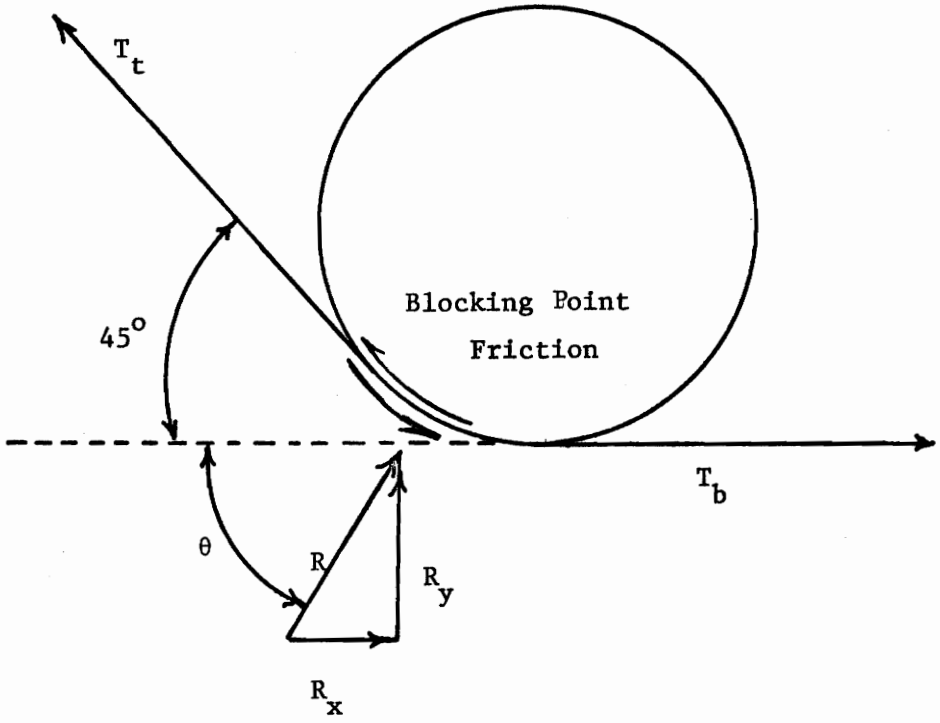

$$T_b - T_b\mu = T_t \qquad R_x = T_b - .707\ T_t \qquad R_y = .707\ T_t$$

Figure 9. Free-Body Diagram Illustrating Friction Loss Across Blocking Point

for prestressing the support is to limit deflection. If deflection were not limited, a shear failure might develop before the tensile failure, in which case the reinforcing material would not have served its intended purpose. For a 4 ft. thick partially-clamped externally loaded beam spanning 20 ft., the moment at midspan is greater than that for a clamped beam and less than that for a simple beam, therefore a conservative solution should result by using simple beam formulas. Assuming again that 10 ft. of the overlying rock strata will fail, the distributed load across the beam is approximately 1670 psf for a unit weight of 166 pcf.

Two distinct cases of truss useage might be considered. The first is the installment of a truss adjacent to the working face, where only a small portion of the ultimate load and deflection have developed. The second is the truss installment in an area where failure appears imminent if immediate support action is not taken. Since the second case presents the worse problem, it will be considered here. Assuming that prior to failure the modulus of elasticity is 6×10^6 psi, a method familiar to designers of reinforced concrete, transformation of sections, may be used to determine not only the truss tension required to prevent a tensile failure of the rock (assuming the rock cannot support tension) but also the resulting compressive stress in the roof. If the center of the truss is 3 in. from the roof, the neutral axis of a 4 ft. square rock beam may be found using transformation of sections, and is located 0.18 ft. from the top of the beam, as seen in Figure 10 and as calculated below:

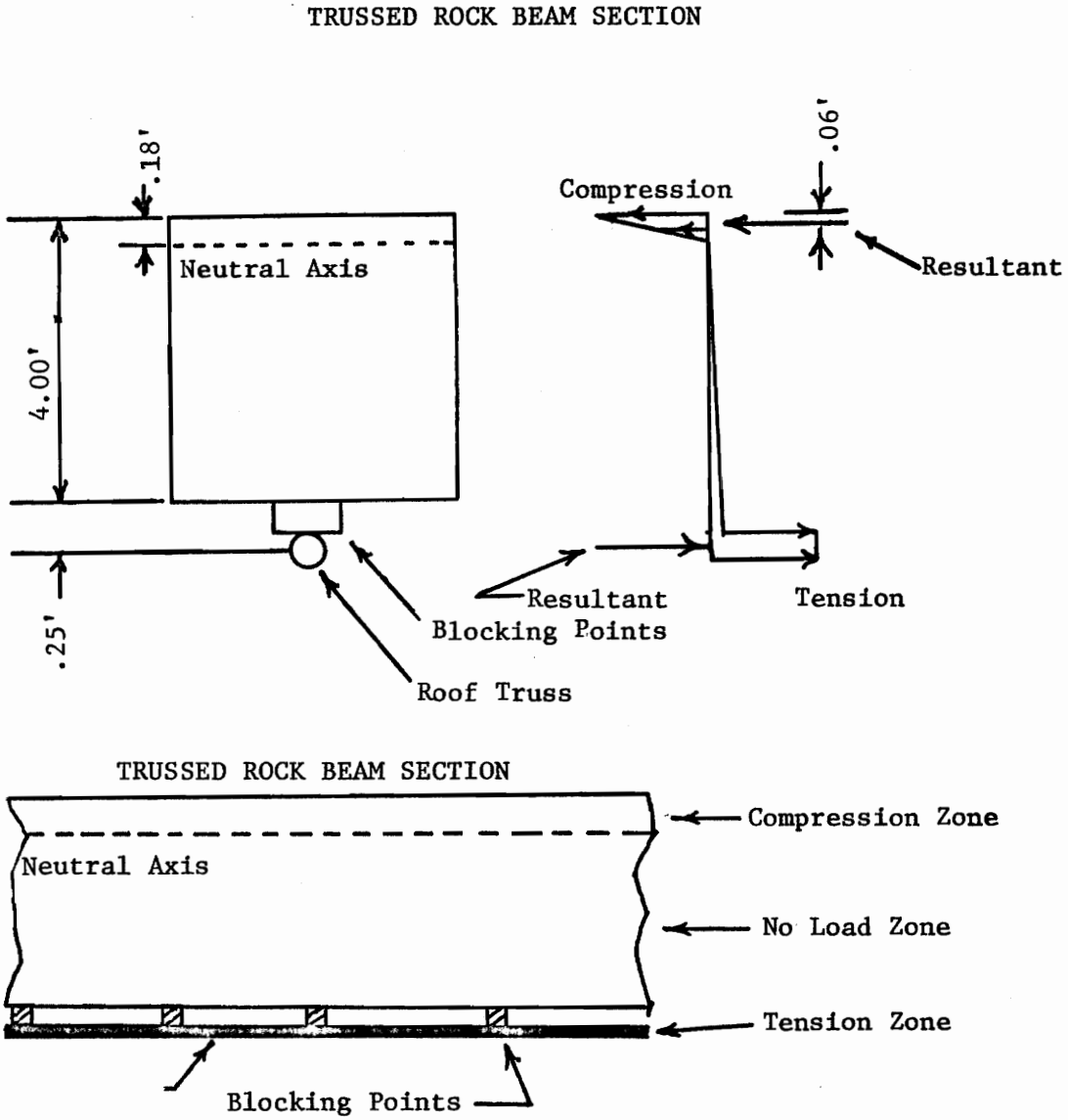

Figure 10. Diagram Illustrating Rock Beam as a Non-tension Material, with Roof Truss Supplying Necessary Tensile Strength.

Ratio of initial elastic moduli = 30/6 = 5

Truss area (3/4" diam.) = .4416 sq.in.

Transformed truss area = (5)(.4416) = 2.208 sq.in. = .015 sq.ft.

Summing the first moment of areas about the neutral axis,

$$(4)(c_t)(c_t/2) = (0.0153)(4.25-c_t)$$

Solving using the quadratic equation,

$$(-b \pm (b^2 - 4ac)^{1/2})/2a \quad , \quad c_t = .1767 \text{ ft., or } .18 \text{ ft.}$$

For a simply supported beam 4 ft. square spanning 20 ft. with an external load of 10 ft. of rock (6680 lb./ft.) the moment which could be expected at midspan is approximately 334,000 ft.lb. Since the tension-carrying capacity of the steel and the compression-carrying capacity of the rock acting as a couple some distance apart must resist this moment, and since the sum of the tension must equal the sum of the compression, the tension required in the steel roof truss may be calculated. The resultant of the compressive forces acts approximately 0.06 ft. from the top of the beam while the resultant of the tensile forces acts at a point 4.25 from the top of the beam. The moment arm may then be calculated and is 4.19 ft. Thus, the required tension in the truss may be calculated as follows:

$$T_s = M/4.19 = 334,000/4.19 = 79,700 \text{ lb.}$$

Again, this is more than the allowable load for a 3/4 in. truss. Assuming that the truss has been tensioned to its allowable load of 10,000 lb., however, and that the resultant at the blocking points is approximately 7000 lb. at a 45° angle (5000 lb. vertical and horizontal force), the upward moment imparted by the blocking points can be

subtracted from the downward moment of 334,000 ft.-lb. (simple beam formulas). The required truss tension to support the remaining moment is still too large, however. This suggests that the support effected by the roof truss involves a much more complicated interaction than has been assumed or that one or more incorrect assumptions have been made.

Finite-Element Analysis

Since the previous theoretical approaches to the roof-truss support problem appear to have failed, a simplified finite-element model was constructed as seen in Figure 11, and a stress analysis of the model was attempted using the two-dimensional finite-element program developed by Wilson (1963). To use this particular finite element program, the structure or model is first divided into a number of triangular-shaped elements. Each nodal point and each element of the model is then given a number. The coordinates of the nodal points are then determined, and the preceding information is coded for computer consumption.

The stresses and strains which are calculated are for a massive type of rock,or a single-piece model,so no bed separation or sliding can occur.

The basic assumption is the use of this program is that initially straight lines remain straight in their displaced position. Based on this assumption and the implied assumptions with it, the stiffness of an element, which is an expression for the corner forces resulting from unit corner displacements, may be determined by the following matrix equation:

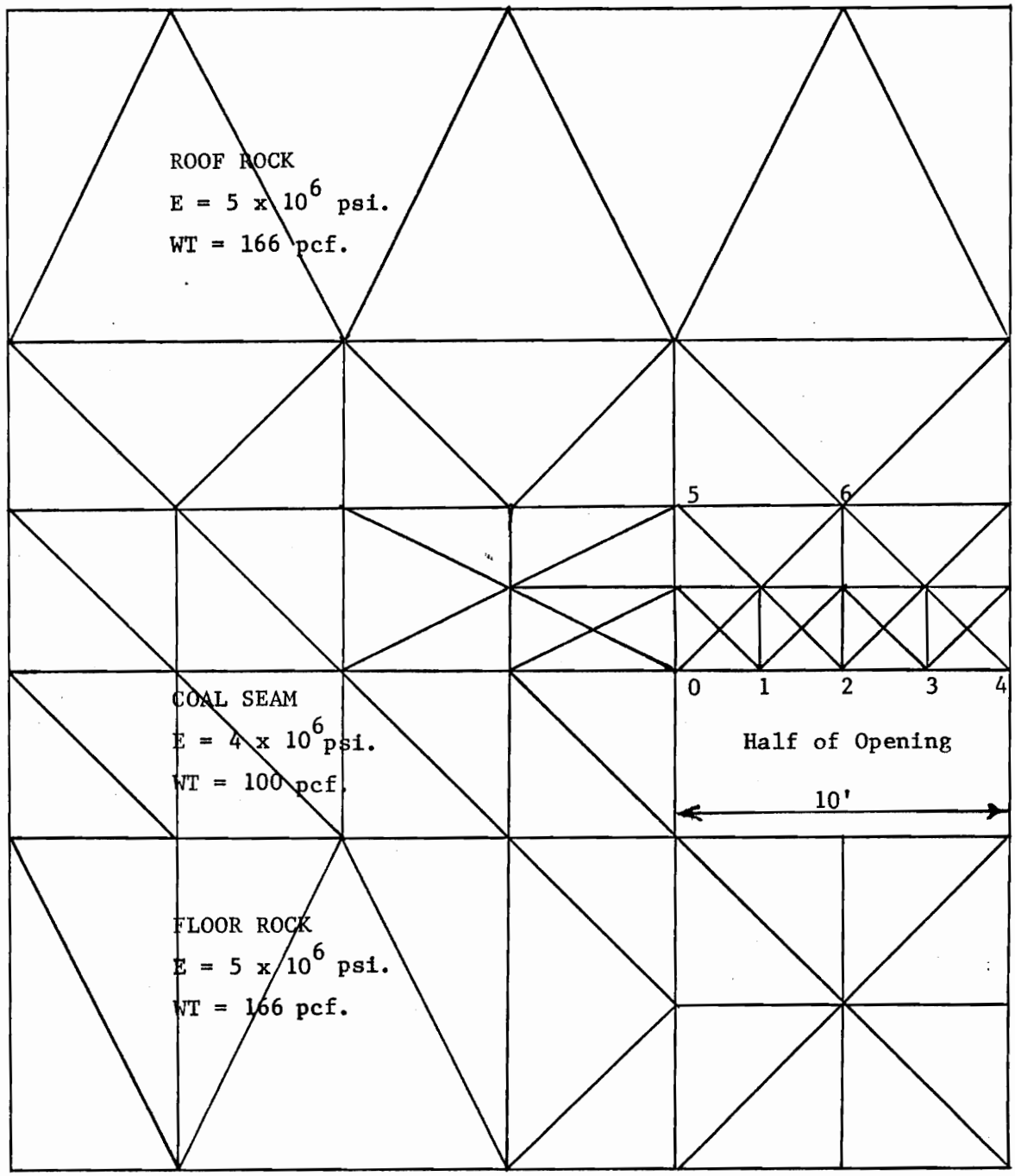

Figure 11. Finite-Element Grid Used in Analysis of Mine Model (Model is Symmetrical, so Only Half Need be Analyzed).

$$\begin{bmatrix} \varepsilon_x \\ \varepsilon_y \\ \gamma \end{bmatrix} = \frac{1}{a_j b_k - a_k b_j} \begin{bmatrix} b_j - b_k & 0 & b_k & 0 & -b_j & 0 \\ 0 & a_k - a_j & 0 & -a_k & 0 & a_j \\ a_k - a_j & b_j - b_k & -a_k & b_k & a_j & -b_j \end{bmatrix} \begin{bmatrix} u_i \\ v_i \\ u_j \\ v_j \\ u_k \\ v_k \end{bmatrix}$$

Where: a_j, a_k, b_j, b_k are element dimensions

$u_i, u_j, u_k, v_i, v_j, v_k$ are displacements in the u and v directions of the respective nodal point.

More concisely,

$$[\varepsilon] = [A][r]$$

In this program the stress-strain relationship is of the form:

$$[\sigma] = [C][\varepsilon]$$

Where: C is the 3 x 3 matrix of constants which are solutions to the linear displacement field.

The stiffness matrix can then be derived by a direct approach involving energy considerations, and is defined as:

$$[K] = \int [A]^T [C][A] \, da,$$

the integral being evaluated over the area of the triangular element.

The equilibrium of the complete system of elements can be expressed as:

$$[R] = [K][r]$$

The use of the above equation and the Gauss-Seidel iteration procedure involves the repeated calculation of new displacements from the equation:

$$r_n^{(s+1)} = k_{nn}^{-1} \left[R_n - \sum_{i=1,n-1} k_{ni} r_i^{(s+1)} - \sum_{i=n+1,N} k_{ni} r_i^{(s)} \right]$$

Where, n is the number of the unknown.

s is the cycle of iteration.

Although this procedure is not as efficient in the solution of the stiffness matrix as is more modern finite-element programs, since it was designed for use of smaller capacity computers, it was nevertheless selected because it was readily available. Data was entered into this program as seen in Figure 11. The iteration cycles was set at 500 and the resulting deflections and stresses at the points in question were recorded and compared with experimental photoelastic evaluations. Several computer runs were made to permit observation of how support varies with blocking-point reactions and anchor loads. The first run simulated deflections which would occur as a result of overburden stress with no mining operation. In the second run an opening was inserted but with no roof support. In the subsequent three runs blocking point reactions were increased to 2500 lb. to 5000 lb. to 10000 lb. in both the X and Y directions at nodal point number 1. Anchor reactions for the above were 1500 lb., 3000 lb., and 6000 lb., respectively at nodal point number 5. Subtracting the deflections and stresses of the points in question of the first run (no opening) from the subsequent runs permitted comparison of absolute values of deflections and stresses due solely to the presence of the mining opening. Raw computer data and data corrected for the initial no-opening deflection and stress may be seen in Tables 2 and 3. Several notes should be made concerning the input data at this point. Since the program is a two-dimensional one, it views reactions at nodal points, such as the blocking-point reactions

Table 2

Midspan Roof Reactions, from Finite-Element Analysis, as a Function of Blocking-Point Reactions

Model Description	X-Load	Y-Load	Comparable Tension	Deflection x 10^{-3} ft.	X-Stress psf
No Openign				-0.2274	283.
Unsupported				-0.3846	2116.
Supported	2500	2500	3500	-0.3759	1633.
Supported	5000	5000	7000	-0.3673	1150.
Supported	10000	10000	14000	-0.3501	184.

Table 3

Corrected Midspan Roof Reactions, from Finite-Element Analysis (see Table 4)

Model Description	Comparable Tension	Deflection x 10^{-3} ft.	% Reduction Deflection	Stress psf	% Reduction Stress
Unsupported		-011572	0	1833	0
Supported	3500	-011460	7	1350	26
Supported	7000	-0.1399	11	867	53
Supported	14000	-011227	22	-99	105

inserted, as being continuous and not as point or rectangular-shaped loads as is actually the case. This must be scaled as has been done to simulate real loading conditions. As such, blocking-point reactions of 2500 lb. simulate an opening with trusses, tensioned to achieve the above value, placed every foot. This, ideally, would also model an opening with trusses, tensioned to achieve blocking point reactions of 10000 lb., placed every 4 ft.

A plot of the computer output (corrected for no-opening deflections and stresses) may be seen in Figure 12. It is interesting to note that both plots are linear, with the plot of reduction of stress, which is comparable to reduction of fringe order, being almost 5 times as steep as the plot of reduction of deflection.

From the preceding discussion it is apparent that the problem of roof truss-roof interations is too complex to approach theoretically, at least by the simple methods used. The finite-element solution seemed to be reasonable in some respects, although it is unlikely that the reduction in stress and midspan deflection would have been linear.

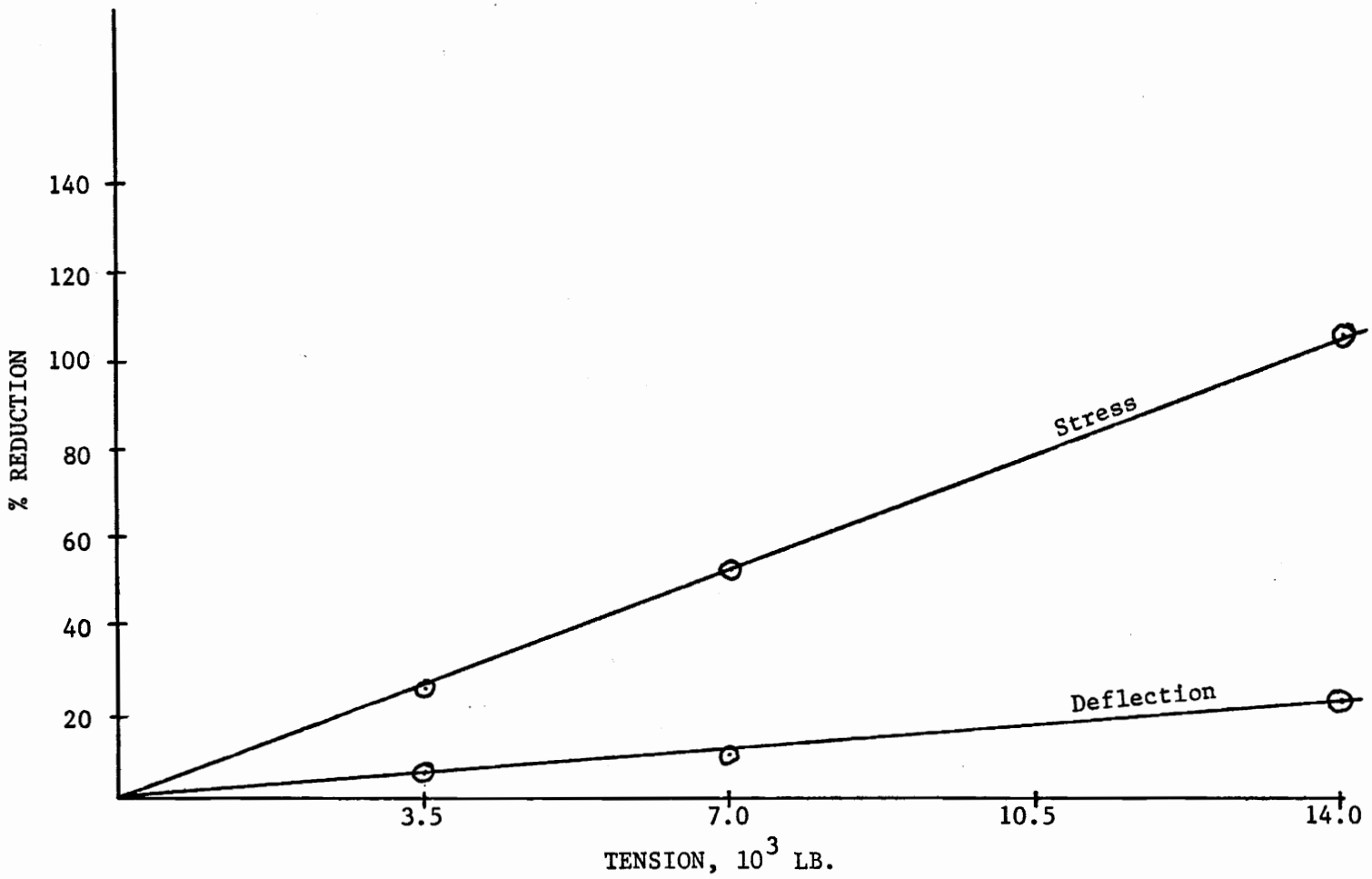

Figure 12. % Reduction of Midspan Stress and Deflection, from Finite-Element Analysis.

EXPERIMENTAL INVESTIGATION OF ROOF-TRUSS BEHAVIOR

Experimental Techniques

There are numerous methods available for the stress analysis of models. Each method has advantages and disadvantages depending on the type of model being studied, the information which is desired from the nodel analysis, the accuracy which is required, the effort required to perform the necessary measurements, and the cost of the materials and equipment required.

Based on previous research on roof support and mine model studies, is appeared that a multi-layered, body-loaded model would give the most pertinent and reliable results mainly because layer deflections and stresses can be independent of each other and bed separation can occur. In addition, very different stress pictures result from using multi-layered models. A simple relationship between the tension of the truss and the support which results seemed to be the most desirable way to present data.

Considering the above, the methods which were thought to be of potential value in the mine model analysis were investigated as follows:

1. Strain gage methods
2. Mechanical interferometer methods
3. Holographic methods
4. Grid methods
5. Photoelastic methods

Methods involving strain gages were rejected mainly because the

application of a strain gage to a low modulus material as must be employed would significantly change the mechanical properties of the model material. Results obtained using this method would be extremely difficult to evaluate.

Mechanical interferometer and holographic methods employ light travelling through a transparent material to measure the variations in thickness over the model. Because of this, two pictures of the resulting fringes, one in the unloaded state and one in the loaded state, are required for fringe order determination. The resulting fringes relate the sum of the principal stresses to the strain normal to the plane of the model. Normally, these methods are employed in conjunction with photoelastic measurements, which relate the relative retardation of the light rays passing through the model to the difference of the principal stresses, so that both the major and minor principal stresses may be determined without resorting to the use of numerical stress separation techniques. Because of the complexities involved with the use of these methods, and because basically the same information can be obtained through the use of photoelasticity, they were also rejected as a means of analyzing the mine model.

Grid methods may be broken down into basically two groups. The first would be the simple employment of a grid in the model, and the measurement of the unstressed and stressed distances between two grid points. A simple calculation involving these lengths will yield the average strain between the two points in question. The second group can be characterized by the Moirė method. In this method, finely gridded

lines are deposited or scribed on the model and on a plate or lens adjacent to the model, both having the same line spacing or pitch, and both being accurately aligned. When the model is stressed and undergoes strain, the pitch of the grid lines on the model changes and light passing through the model grid lines and the reference grid lines produces fringes. These fringes are directly related to the strain in the model. Knowing the material properties of the model, one may determine the stress. In both cases, however, relatively large strains are required, such as might be involved in plasticity and viscoelasticity problems, before the strain sensitivity of the methods is sufficient to produce accurate results. The modulus of a material suitable for a body loaded mine model study is approximately 1000 psi. The tension which might be expected at the extreme fiber of the lowermost rooflayer at midspan of the mine opening is between 1 and 2 psi. This would mean that a strain of .001 in./in. had taken place. According to Durelli and Riley (1956), optical measurements of grid displacements can be accurate to $\pm$0.0002 in. Thus, the error involved under ideal circumstances would be $\pm$20 percent with a grid method, and in actuality would probably be up to $\pm$50 percent. Similar accuracies may be expected using the Moiré method. In addition, both methods yield stresses at the surface of the model, or at some plane within the model, which may not be an accurate representation of the total stress picture in the model.

The photoelastic method of stress analysis relies on the relative retardation of the vector components of light propogating through a model to produce interference fringes which are directly related to the diff-

erence of the principal stresses. As such, fringes indicate the stress as averaged through the model, which is desirable in this particular case. Preparation work involved in making a photoelastic model is probably the same, or less, than that required by the above mentioned methods. The time required for performing an experiment should be considerably less than other methods which require numerous optical measurements. Accuracy of the method is good. Since the fringe order which might be expected is greater than 1, and since fractional order fringes can readily be determined to $\pm$ 1/50 fringe order, no accuracy problems should be encountered. In addition, the method is a full-field method, providing information at every point in the model. Even if only one or two points are utilized for readings, information is available at other points which may indicate that the model is not properly constructed, etcetera. In addition, with this procedure, tests could be repeated employing the full field capability of the method. The model which would be analyzed represents a two-dimensional analog of a three-dimensional problem. As such, some error might be involved, but this should be small (less than 10 percent). This method would not be applicable as outlined above for the study of the stress in the immediate vicinity of the roof truss. To do this, the photoelastic model would need to be changed considerably, possibly employing stress-freezing techniques, or one of the above rejected methods could be employed.

Frocht (1941) established that when the lateral dimensions of a model are 4 times (or greater) the thickness, plane stress theoretical approaches give excellent results. Because of the complex nature of

the model, it would be difficult to relate either a plane strain or a plane stress mathematical model to the entire photoelastic model. A combination of these would be required to approach the problem theoretically, or a three-dimensional approach would have to be taken. Near the opening, a plane-strain approach would have to be used because the thickness of the layers is not less than 1/4 of the beam width and height. This is because interlayer separation can occur and interlayer sliding is taking place. At some distance from the opening, the interlayer sliding is at a minimum, or zero, and interlayer separation does not occur. At this point, the model is effectively acting like a single-piece model, and the thickness is much less than 1/4 of the height and width, allowing a plane stress analogy to be employed.

The plastic selected for use is a low modulus polyurethane (PSM-4). Its modulus of elasticity is about 1000 psi., and its fringe constant is less than 1 psi./fringe/in. thickness.

Model Construction

Model construction consists of the machining of strips, or beams, of polyurethane suitable for the construction of the multilayered mine model and the design and construction of support components. Initial investigation and model construction using 1/4 in. thick polyurethane revealed several problems:

1. Machining had to be of higher quality than for normal two-dimensional photoelastic-model materials because very slight irregularities between layers produced unwanted stress concentrations making fringe interpretation difficult.
2. Fringes were of low order, necessitating the use of fractional fringe values.
3. Model stability was a problem when the height was greater than approximately 3 in.
4. The polyurethane layers had to be completely free of dust, dirt, and adhesive from the pressure sensitive tape.
5. Erroneous fringes could be introduced by careless stacking and sliding of the layers during model construction.

Because of the problems encountered, the following three steps were taken to improve the efficiency of material preparation:

1. A standard setup was devised so that the layers could be machined using a high speed router mounted on the spindle of a 36 in. milling machine, thus minimizing

irregularities and decreasing the time required for machining.

2. One inch thick polyurethane was selected and is currently being used, quadrupling fringe order, while allowing stable models as high as 18 in. to be constructed.
3. The polyurethane is thoroughly cleaned prior to the careful construction of the mine model.

The standard procedure used in machining the polyurethane was devised after considerable experimentation and testing, and was chosen because of the following reasons:

1. A modest machine shop generally has the necessary equipment such as a milling machine and a high speed router.
2. Precise pieces of plastic may be repeatedly machined.
3. The procedure is fairly simple, so that personnel with little or no related experience can acquire the basic technique in several hours.

The polyurethane presently being used in acquired in sheets 22 in. x 22 in. x 1 in. The only requirement of the milling machine is that its travel must accomodate the full length of the strips being machined.

The polyurethane sheet is trimmed on two parallel surfaces to remove any residual stresses left during casting. The sheet is then cut in half, so that the milling machine bed depth will accomodate each piece. One side of each piece is then machined smooth and a metal flatbar whose width is equal to or slightly less than the thickness of

the plastic is attached to this surface with pressure sensitive tape, thus ensuring that as the half is machined into smaller strips it will not bend and subsequently be machined straight.

A metal or wooden bed, surfaced with acrylic-plastic sheet or similar material is bolted to the bed of the milling machine. The protective paper is peeled off one side of the polyurethane sheet and this side is placed in contact with the acrylic sheet as seen in Figures 13 and 14. Slight pressure is generally required to make the cohesion between the two plastics sufficient to securely hold the polyurethane during machining. As strips are machined from the original sheets it may be necessary to use pressure-sensitive tape between the polyurethane and the acrylic sheet to prevent movement.

When the polyurethane has been properly aligned and secured on the acrylic sheet the rough edge is machined smooth. The sheet is then removed and a strip of the desired height is cut off on a band saw allowing sufficient material for the subsequent machining of the rough edge. This will have produced one strip, machined on one edge and rough on the other, approximately .05 in. to .1 in. larger than the required finished size. This procedure is repeated until the original sheets of plastic have been cut up into layers or strips each with one machined edge.

The wooden or metal bed is then removed and a machinist's vise is accurately aligned. A metal straight edge, 3/4 in. thick aluminum flatbar for example, is then clamped in the vise with approximately 1 1/4 in. above the vise, or about the thickness of the plastic plus

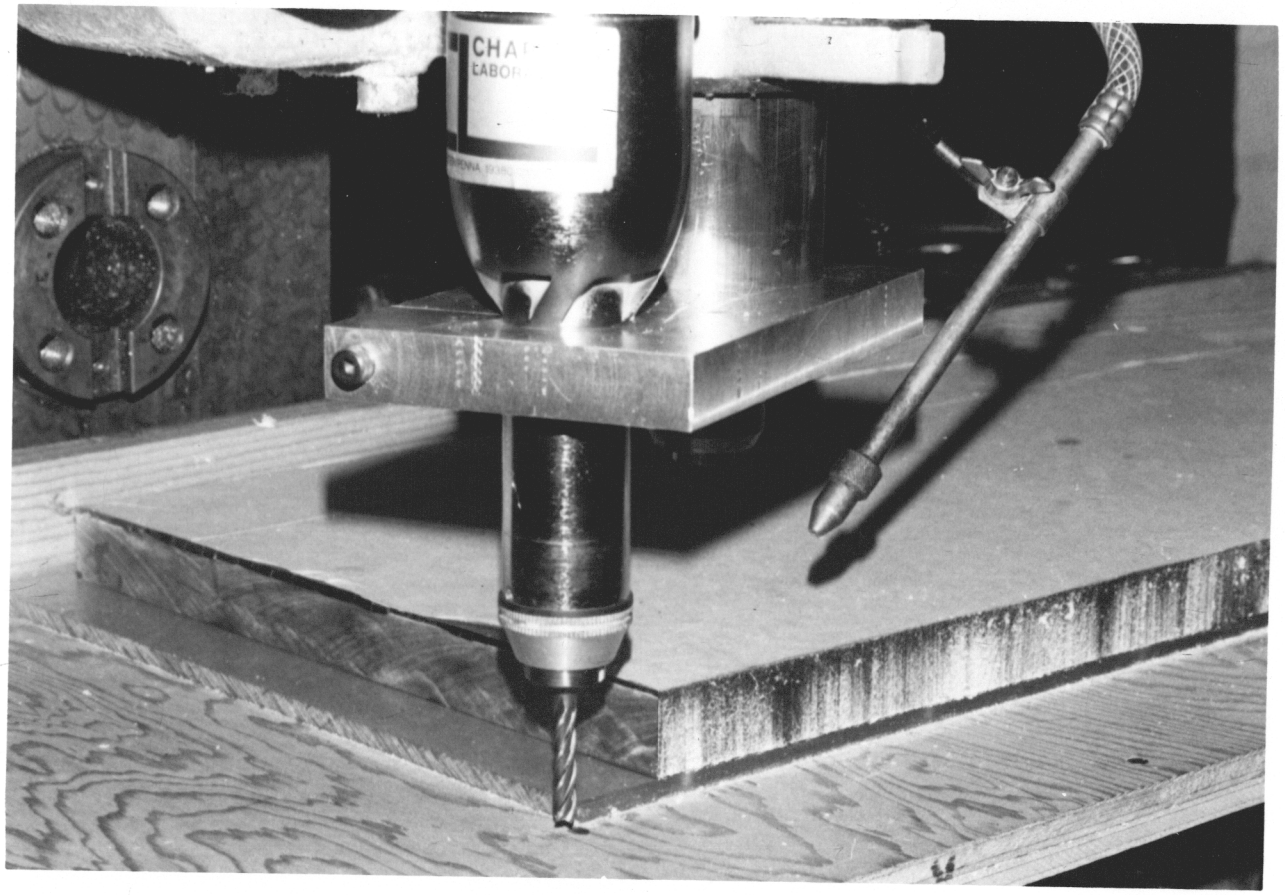

Figure 13. Initial Machining Procedure with Sheet of PSM-4 on Acrylic Bed.

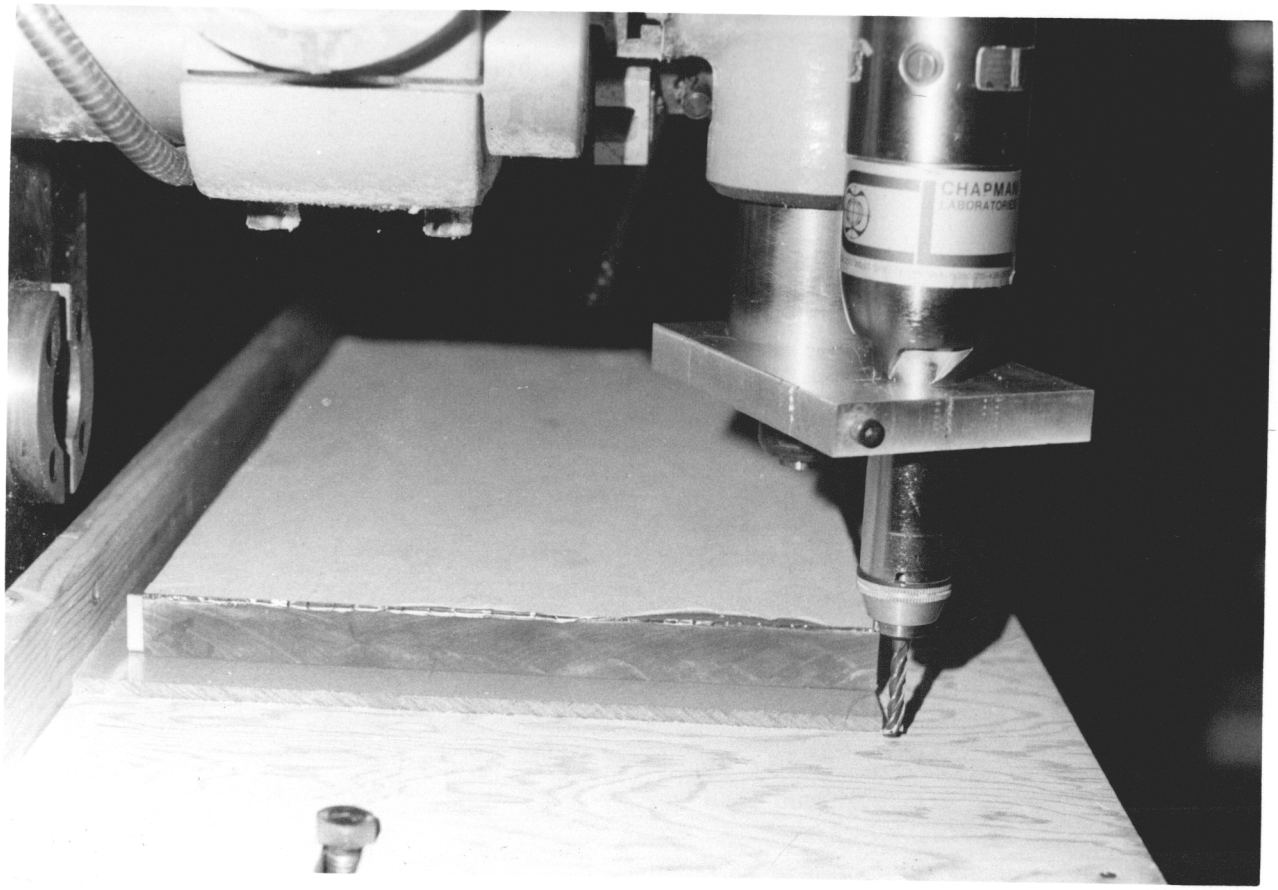

Figure 14. End View of Initial Machining Procedure, Edge Milled.

clearance. Using pressure-sensitive tape the machined edge of each plastic strip is attached to the straight edge and the rough edge is machined to specified dimensions as seen in Figure 15.

Several observations should be mentioned at this time. A high speed router, 25,000 rpm or greater, gives the best finishing results and can generally be easily mounted on the milling machine head. The maximum depth of cut generally should be limited to .025 in. or less with the final cut being about .01 in. This, combined with the use of a compressed air jet to clean and cool the cutter will eliminate the possibility of inducing thermal stresses due to heat build up. A portable routing table was tried for machining; however its results were generally not acceptable. The machined strips should be individually inspected to insure that no residual fringes are present. Stacking the strips on top of each other, machined edge to machined edge, ultimately reveals how well the machining has been performed. Even when great care is exercised during machining, very slight interlayer stress concentrations may occur, but should be minimal.

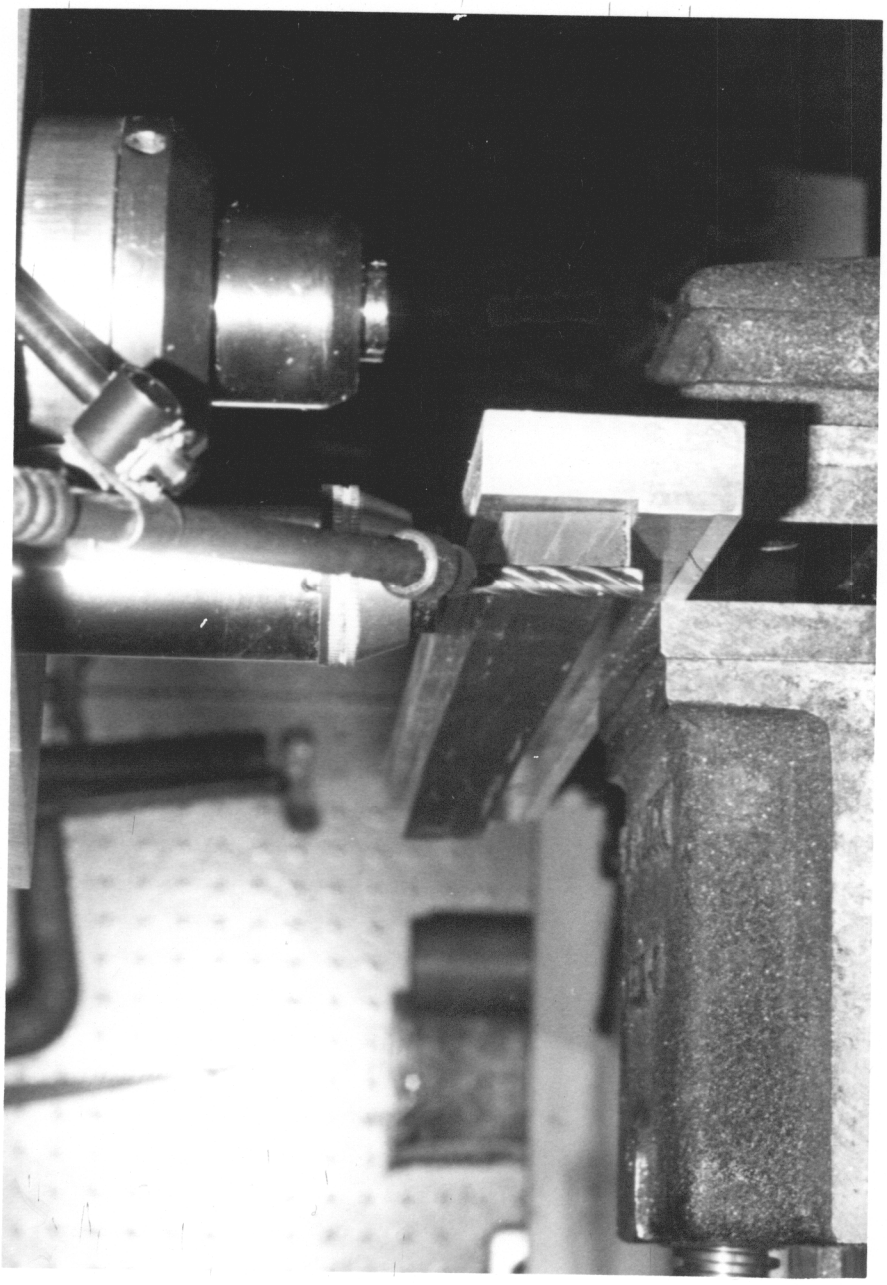

Figure 15. End View of Finished Strip after Final Milling Cut.

Experimental Procedure

The equipment employed in these experiments included an 18 in. diameter diffused light polariscope, a travelling X-Y coordinate cathetometer, a camera for recording isoclinic and isochromatic fringes, a screw unloading device, and a miniature roof truss. The roof truss consisted of a tension spring, two miniature turnbuckles, two friction anchors, and some light gage iron wire.

The photoelastic model is carefully constructed one layer at a time to reduce the possibility of inducing undesirable interlayer shear stresses. Experimental work by Rankilor (1971) on a similarly constructed gravity loaded mine model showed that model stability is not a problem unless the height to model thickness ratio exceeds 10:1. Similar tests were conducted, and models with a height of 18 in. (height:thickness ratio of 18:1) were constructed. Because of the difficulty in building models this high, model height was standardized at 10 in., although construction of 12 in. high models may be easily achieved.

A screw unloading device is placed where the opening will be, as seen in Figure 16, allowing all layers to be laid perfectly flat. After the model is constructed, the device is lowered by means of four screws, allowing the roof strata to deflect downward. When there is no contact between the device and the roof strata it is removed, leaving the simulated mine opening completely unsupported as seen in Figure 17.

A fixed reference mark is located behind the opening. The distance

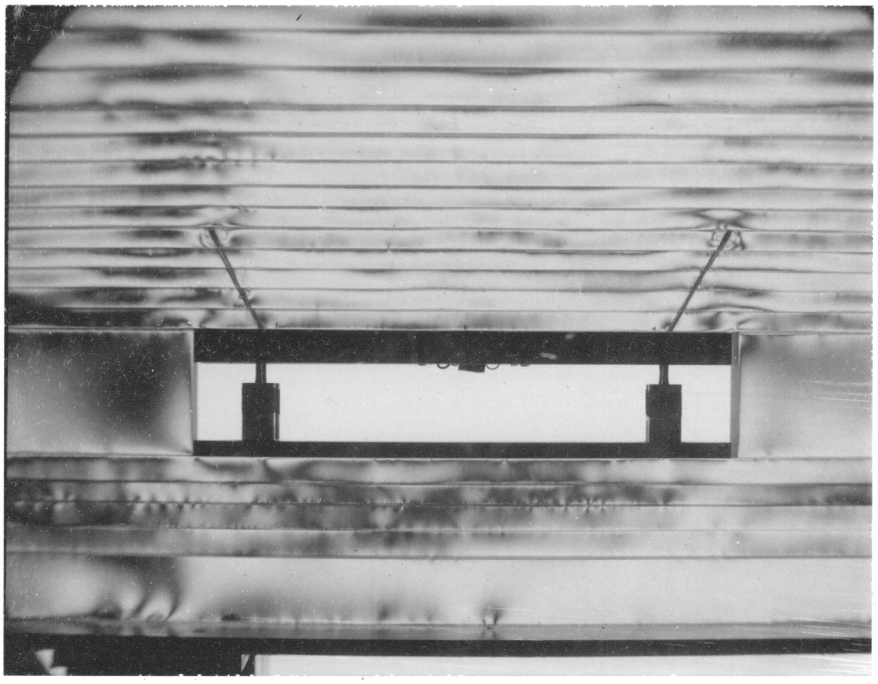

Figure 16. Unloading Device Supporting Photoelastic Mine Model.

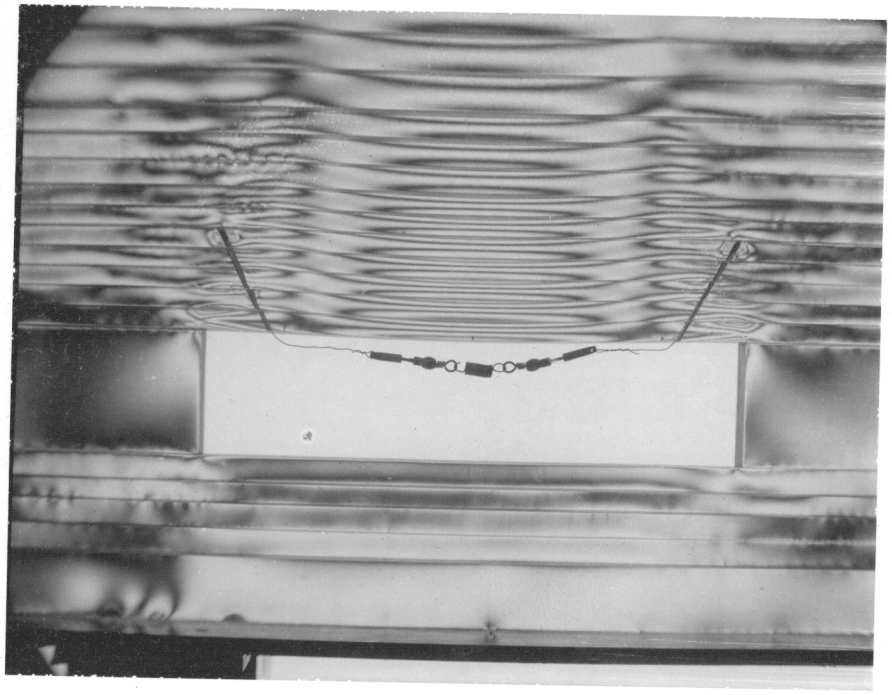

Figure 17. Completely Unsupported Mine Model.

between this mark and the lowermost point of the roof at midspan is measured with the X-Y coordinate cathetometer. This reading is repeated after the support is removed allowing the maximum deflection to be calculated. Midspan fringe order is recorded for each of the five immediate roof layers, however, since the fringe order for the lowermost layer is the greatest, it is used in calculating the percentage reduction of fringe order. The fringe orders of the overlying strata, though not used numerically, are a good indication of how well the model was initially built. Normally, the fringe order of the bottommost layer will be greater than the fringe order of the layer above, etcetera, for the unsupported opening. For the trussed opening, the fringe order will usually increase from the lowermost layer towards the middle layer, and then decrease from the middle layer to the top layer with the fringe order of the top layer approximately the same as the bottom. The full potential of the photoelastic method is not employed numerically, however, because of the complexities involved in obtaining the additional data and analyzing it.

When a blocking point is employed at midspan, fringe order readings at midspan do not give a good picture of what stress condition really exists in the roof strata. In this case, fringe orders have been taken approximately 1/3 of the distance from the midspan blocking point to the collar blocking points on both sides, and the results averaged. Deflection readings at midspan give good correlation if averaged over the roof and not shot solely on the depression caused by the blocking point. Inspecting Figure 19 will clarify the above description.

Fringe order readings would normally be taken approximately above the swivels which are located on the outside of the eyes which attach the tension spring to the turnbuckles.

The above readings are taken each time the truss tension is increased. In addition, the length of the truss tension spring is measured, allowing the truss tension to be calculated. Typical examples may be seen in Figures 18 and 19.

Deflection and fringe-order readings are compared with preceding readings to reduce the possibility of recording any incorrect figures. Any numbers which do not seem to follow the general trend established are double checked to insure their correctness.

Several parameters associated with roof-truss support were selected and studied. These parameters, as seen in Figure 1, were as follows:

1. Opening span
2. Truss span
3. Blocking-point configuration
4. Truss inclination
5. Number of trussed rooflayers (anchor depth)
6. Interlayer shear resistance.

Changing of the coal seam height was not studied as a parameter because of the small magnitude of the overburden stress being dealt with, and the resulting very small vertical strain in the coal seam. Had the overburden been on the order of several feet instead of 6 in., this would have been considered a parameter of interest.

Similitude will not be considered in the model because of the many

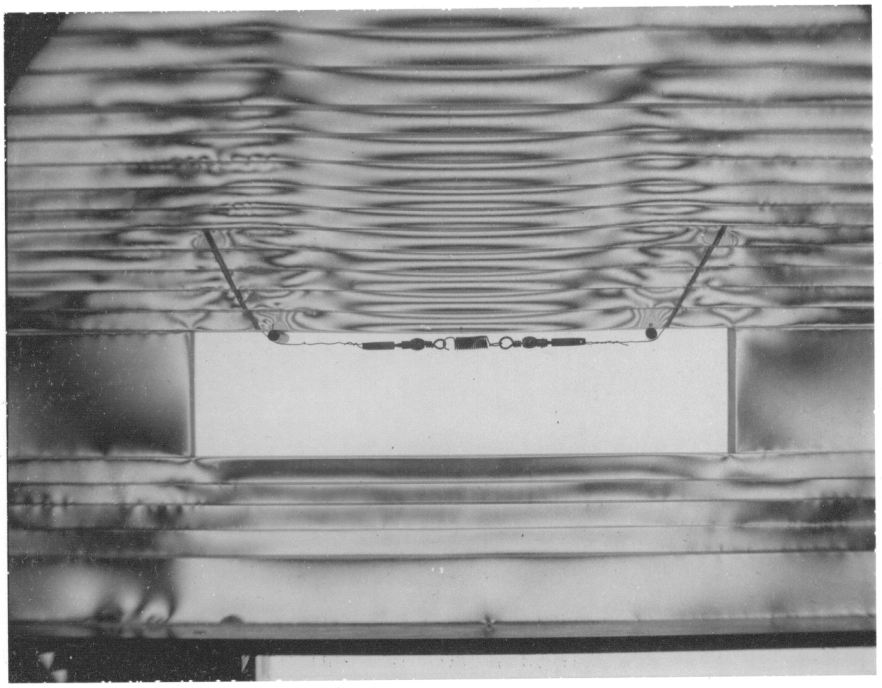

Figure 18. Mine Model with Roof Truss Installed (8" Opening, 6" Truss Span, 60° Inclination, .25" Blocking Point Distances.)

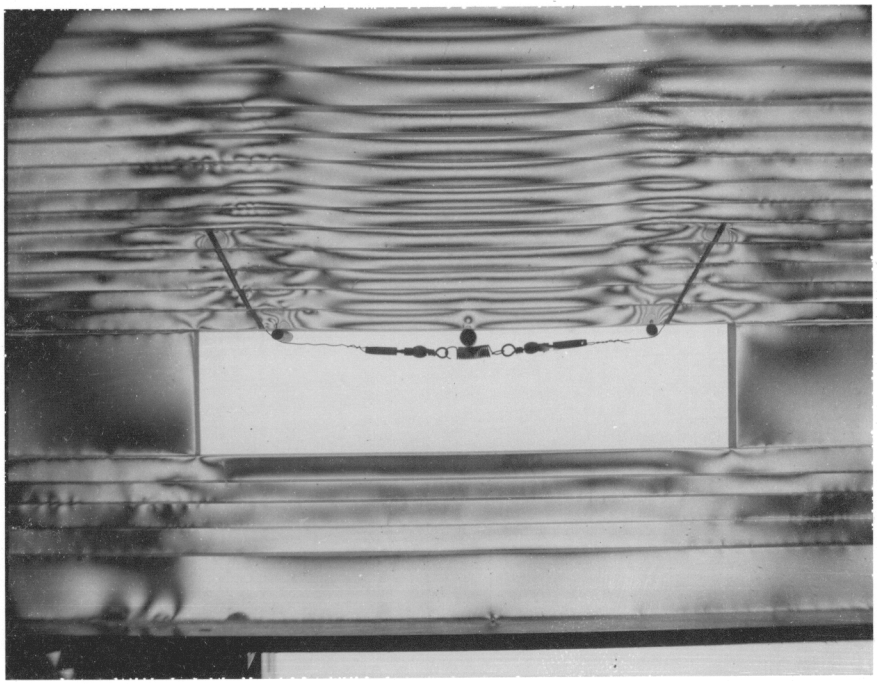

Figure 19. Mine Opening with Roof Truss (Note Midspan Blocking Point and Resulting Improvement in Fringe Order.)

varying properties between the model and prototype and the scaling complexities involved because of this, as pointed out in a previous section. In addition, because the values of the ratio of the shear strength of the model discontinuities to the model material shear strength (or tensile or compressive) is probably not the same as that of the prototype material (rock), further complexities in relating the stress in the model to the stress in the prototype are involved. It is hoped, therefore, that any trends which appear in the model studies may be checked in the field at a later date, and if corroborated, used in roof-truss support design.

Experimental Data Processing Procedures

A standard tension test was performed on the photoelastic material to determine its fringe constant of 0.46 psi/fringe/in. This value agreed well with that obtained by another test, the constant-moment beam-bending test. In both cases, the standard test was modified slightly to accomodate the unusual property of self-loading which the polyurethane exhibits. An accurate combination tension-compression scale reading to .05 lb. was used to record the load on the tension specimen and the beam specimen. In each test, a specimen of sufficient size was used so that any edge-loading effects had dissipated at the point of fringe order determination, the middle of the specimen. In each case, the specimen was slightly loaded until an integral order fringe appeared, and the fringe order and the corresponding load recorded. This fringe order consists of the fringe order due to the body loading and the fringe order due to the load of the scale. The load on the specimen was then increased until a higher integral order fringe appeared. Using this method, fractional fringe order determinations were not needed. Again, this new fringe order consists of the fringe order due to the body loading and the fringe order due to the higher load. Since the body loading is the same in both cases, their effects cancel each other. The difference in the loads applied by the scale, therefore, accounts for the fringe order change. Test data may be seen in Tables 4 and 5. The maximum shear stress, which is defined as follows:

$$\tau_{max} = (\sigma_1 - \sigma_2)/2$$

TABLE 4

Fringe-Value Determination
Tension Test

Test No.	n (fringes)	P (lbs.)	n/P (fringes/lb)
1	7.0	2.65	2.64
2	6.0	2.25	2.67
3	4.0	1.50	2.67
4	12.0	4.35	2.76
5	16.0	5.95	2.69
6	10.0	3.80	2.63
7	13.0	4.85	2.68
8	6.0	2.25	2.67
9	10.0	3.80	2.63
10	12.0	4.65	2.58
			Average = 2.662

$$\tau_{max} = \frac{nf}{t} = \frac{\alpha_1 - \alpha_2}{2}, \text{ but } \alpha_2 = 0$$

$$nf/t = \alpha_1/2 = P/2\,\omega t$$

$$f = P/2\omega n$$

If P = 10 lb., then n = 26.62

For $\omega = 0.408"$

$$f = (10.0)/(2)\ (.408)\ (26.62) = 0.4603 \text{ lb/in-fringe}$$

Fringe value = 0.46 psi/fringe/inch

TABLE 5

Fringe-Value Determination
Constant-Moment-Beam-Bending Test

Test No.	n (fringes)	M (in-lbs)	n/M (fringes/in-lb)
1	3.0	1.9	1.58
2	3.25	2.0	1.62
3	4.55	2.8	1.62
4	1.00	0.56	1.78
5	5.00	2.84	1.76
6	3.00	1.82	1.65
7	1.00	0.54	1.85
8	5.00	2.84	1.76

Average = 1.703

$$\tau_{max} = \frac{nf}{t} = \frac{\alpha_1 - \alpha_2}{2} = \frac{My}{2I} = \frac{My}{(2)(1/12)th^3}$$

If M = 10 in-lb, n = 17.03 fringes

For y = h/2 = 0.9475 in.

$I = (1/12)th^3$ t = 1.025 in.

$$f = \frac{6My}{nh^3} = \frac{(6)(10.0)(.9475)}{(.7.03)\ (6.805)} = 0.4905 \text{ psi/fringe/in.}$$

Fringe value = 0.49 psi/fringe/inch

where:

σ_1 = major principle stress

σ_2 = minor principle stress

may be determined by multiplying the fringe order by the fringe constant. On an interior point in the model the principle stresses may be determined if the isoclinics, which are the loci of points having constant principle stress direction, and the fringes, lines of maximum shear stress, are known. The most widely used method for obtaining this is the shear difference method of stress separation. Typical examples may be seen in any elementary text on photoelasticity or elasticity. The disadvantage of this method is that it is often very tedious not only to obtain the data, but to perform the necessary computations. The second disadvantage, however, may be overcome by the use of modern digital computers.

The problem of separating stresses can be greatly simplified, however, if one is dealing with stresses at a free boundary. For example, if a beam in bending were being analyzed and it were desired to determine the tension at the outermost fiber, knowing the following:

$$\sigma_{min} = \sigma_2 = 0$$

$$\tau_{max} = (\sigma_1 - \sigma_2)/2 = \sigma_1/2 = nf/t$$

where:

n = fringe order

f = fringe constant

t = thickness of model,

would reduce the problem to a quite simple one. The only problem left, then, is the determination of a starting point for counting fringe order. If a free corner is present the fringe order has to be zero at that point due to boundary conditions. In the mine model, since a fringe order count from a free corner was impractical, another approach had to be taken. This approach involved the neutral axis of a beam in bending. A basic rule from elementary mechanics is that at the neutral axis the maximum shear stress is zero, therefore, the fringe order is also zero. In white circularly polarized light the zero fringe is the only black fringe present and in many cases may be easily defined. Therefore, the integral order fringes may be determined simply by counting the number of fringes which appear between the zero fringe and the boundary. In most cases the integral fringe will not fall exactly on the boundary so the fractional order fringe, that which is added to the integral order, must be determined. The method which is most practical, and usually of sufficient accuracy, is the Tardy method of compensation. Using this method the analyzer is rotated until the integral order fringe appears at the boundary. The fractional fringe order is then defined as the ratio of the number of degrees of rotation required to achieve the above divided by 180. For example, if the analyzer were rotated 90^{o} to bring the integral order fringe to the boundary, then, assuming the integral order fringe were 2, the fringe order would be 2 plus 90/180 or 2.5.

From the deflection and fringe order readings the percentage reduction of fringe orders and deflections are calculated as follows:

$$\% \text{ Reduction} = \left(1 - \frac{\text{present reading}}{\text{unsupported reading}}\right) \times 100$$

For example, if the initial unsupported deflection were 4 mm., and some later deflection when the truss was tensioned were 3 mm., the percentage reduction of deflection would be 25. Percentage reduction of fringe order readings greater than 100 indicate that the principle stress has changed its mathematical sign from that of tension to compression.

Experiments in which only one variable has been changed are grouped together for later analysis. The appropriate experimental data is then coded and inserted into a computer plot program which produces a graph with the raw experimental data points plotted on it. Smooth curves are then drawn by hand through the data points and a series or family of curves results. From this the optimum truss configuration for the particular experimental conditions may be easily determined.

Initially, the experimental data was computer analyzed with a best-fitting polynomial curve resulting. Problems were encountered with this approach, however, because the polynomial curves often did not follow the general data trend which appeared to be present, even though the curves fit the data points fairly well. Because of this, the above described method was employed.

Some concern was expressed over the fact that the intial unsupported deflections were not the same, but varied considerably. Several tests were then repeated, and the plots of the percentage reduction of fringe

order and deflection vs. truss tension were compared. The plots of fringe order vs. tension were almost identical and posed no problem. The major differences that were noted were in the comparison of the reduction of deflection vs. truss tension. In the worst comparison, the difference varied 40 percent over a short section. Normally, however, differences were less than 15 percent. It should be noted, though, that the correlation of identical tests is dependent on the manner and care with which the models have been constructed. More reliable tests will therefore be obtained from an operator with some experience in building this type of model. Normally, this experience may be gained through several hours of careful model construction and evaluation.

Data Analysis

Experimental data has been related not only to midspan stress but also to midspan deflection. In a mine the roof has usually deflected only a fraction of what it would if it were completely unsupported, due to the support which is imparted by the adjacent face and roof bolts and trusses. It is still assumed, however, that when the truss is tensioned, the general support trend will exist, but that it will have shifted vertically on the Y-axis. Therefore, one would not expect to reduce deflections or stress as much in such an instance, as might be expected in a previously unsupported entry.

In many of the experiments, since the magnitude of the roof truss tension is greater than the overburden weight, it is felt that the lower portion of the curves will more accurately describe the reactions of a prototype mine roof. Extrapolation of experimental data from existing curves to higher truss tensions should not be attempted since large errors may result using this method. A better understanding of roof truss-roof interactions may be gained by studying Figure 2 in which the complex loading situation which exists has been separated into a number of idealized loads.

In the following discussion, families of curves, that is, series of curves with only one variable changed, have been visually analysed to determine not only if any trends are present, but also which truss configuration is the most efficient of those tested.

Effects of Angle of Truss Inclination Figures 20 and 21 and

Figures 22 and 23 show the effects that the angle of inclination of the roof truss has on the support effect on the mine model roof. Figure 20 seems to confirm previously mentioned work by Sheorey, Verma, and Singh, and indicates that the angle of truss inclination should be greater than 45^{o}, with the 60^{o} inclined truss being the best that was tested. The same results would be expected in Figure 21, however this is not true. The same trends which are exhibited in Figure 20 are not exhibited in Figure 21. Examining Figure 22, the 60^{o} inclined truss is the most efficient of those tested. Again, however, Figure 23 does not follow the same general trends. At present, no explanation can be proposed to explain why the percentage reduction of fringe order plots does not correspond to the percentage reduction of deflection plots. The same basic trend was exhibited in each of the plots of reduction of fringe order, though, and this was encouraging.

Effects of the Depth of Truss Anchorage Figures 24 and 25, 26 and 27, and 28 and 29 compare the support which results from varying the depth at which the truss is anchored. No general trends is apparent from the first four figures, however, in Figures 28 and 29, the same trend is present. It appears that the further away the anchorage is from the mine opening, the better is the support which results. This is what one would expect, and is not an unreasonable assumption. Again, no explanation can be proposed for the discrepancies between the first four figures.

Effects of Blocking Point Configuration Figures 30 and 31, 32 and

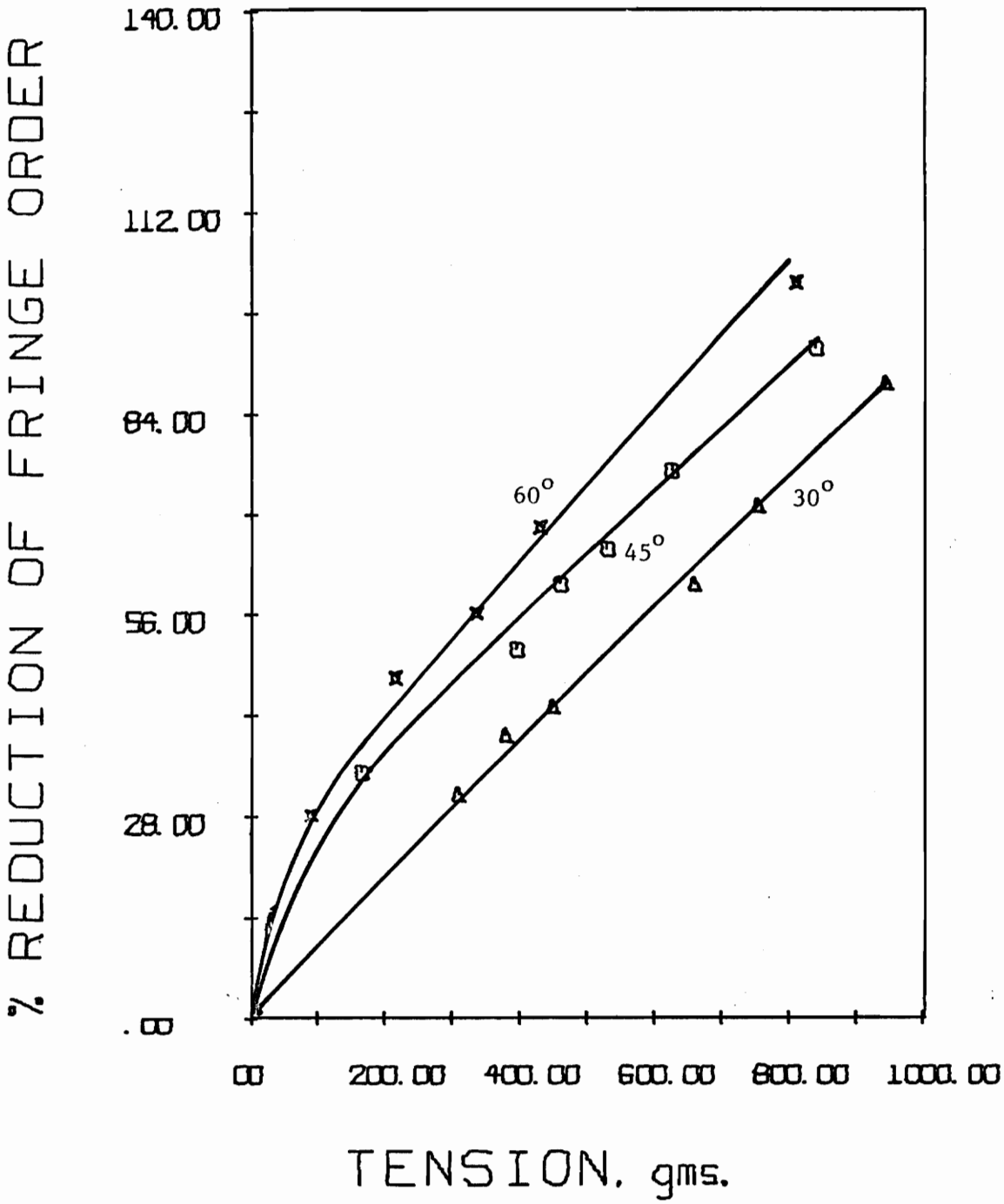

Figure 20. % Reduction of Fringe Order vs. Truss Tension as a Function of Truss Inclination (8" Span, 6" Truss Span, .25" Blocking-Point Distances, 5 Trussed Rooflayers).

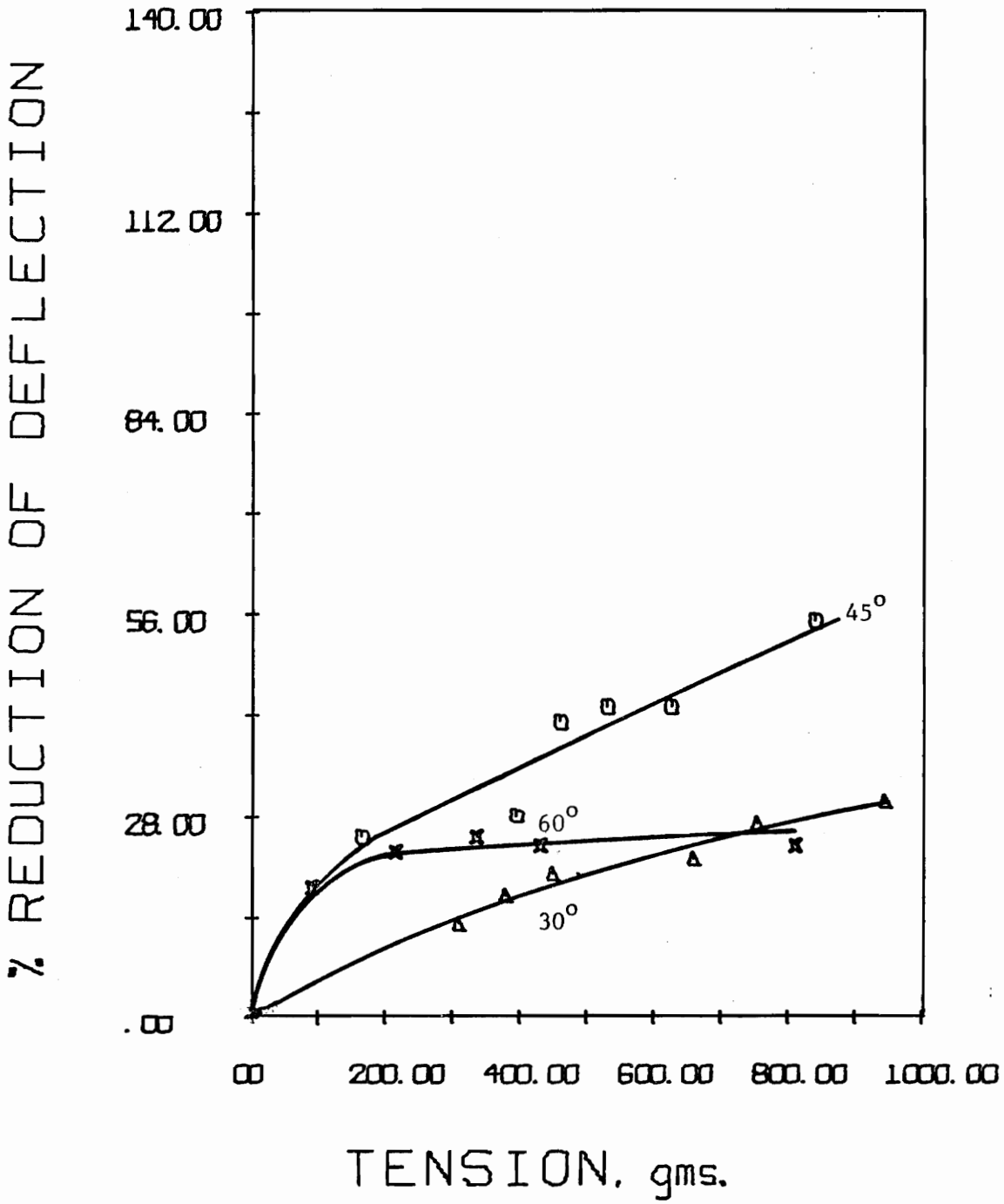

Figure 21. % Reduction of Deflection vs. Truss Tension as a Function of Truss Inclination (dimensions as in Figure 20).

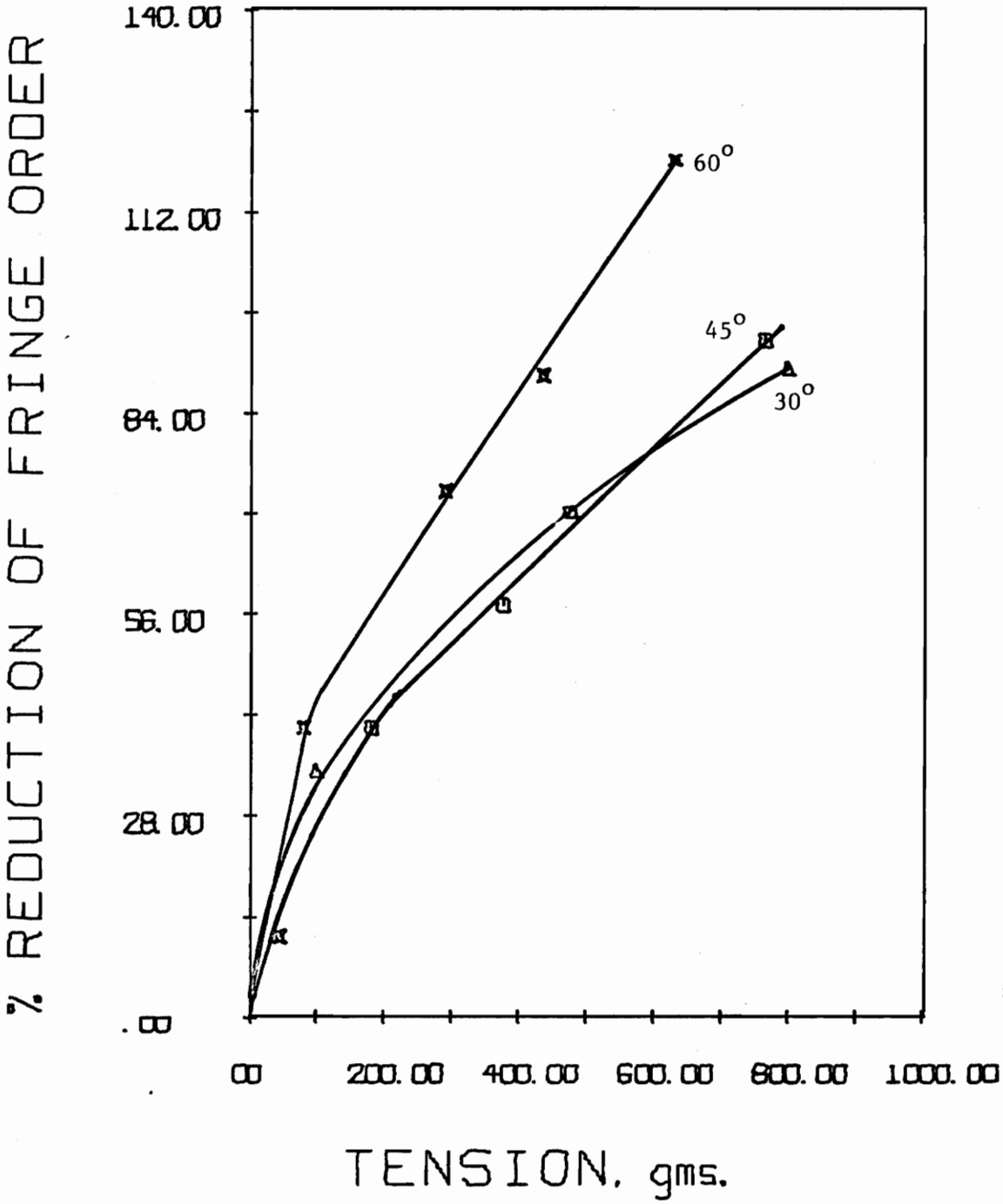

Figure 22. % Reduction of Fringe Order vs. Truss Tension as a Function of Truss Inclination (8" Span, 6" Truss Span, .25" and Midspan-Blocking Point Distances, 5 Rooflayers Deep).

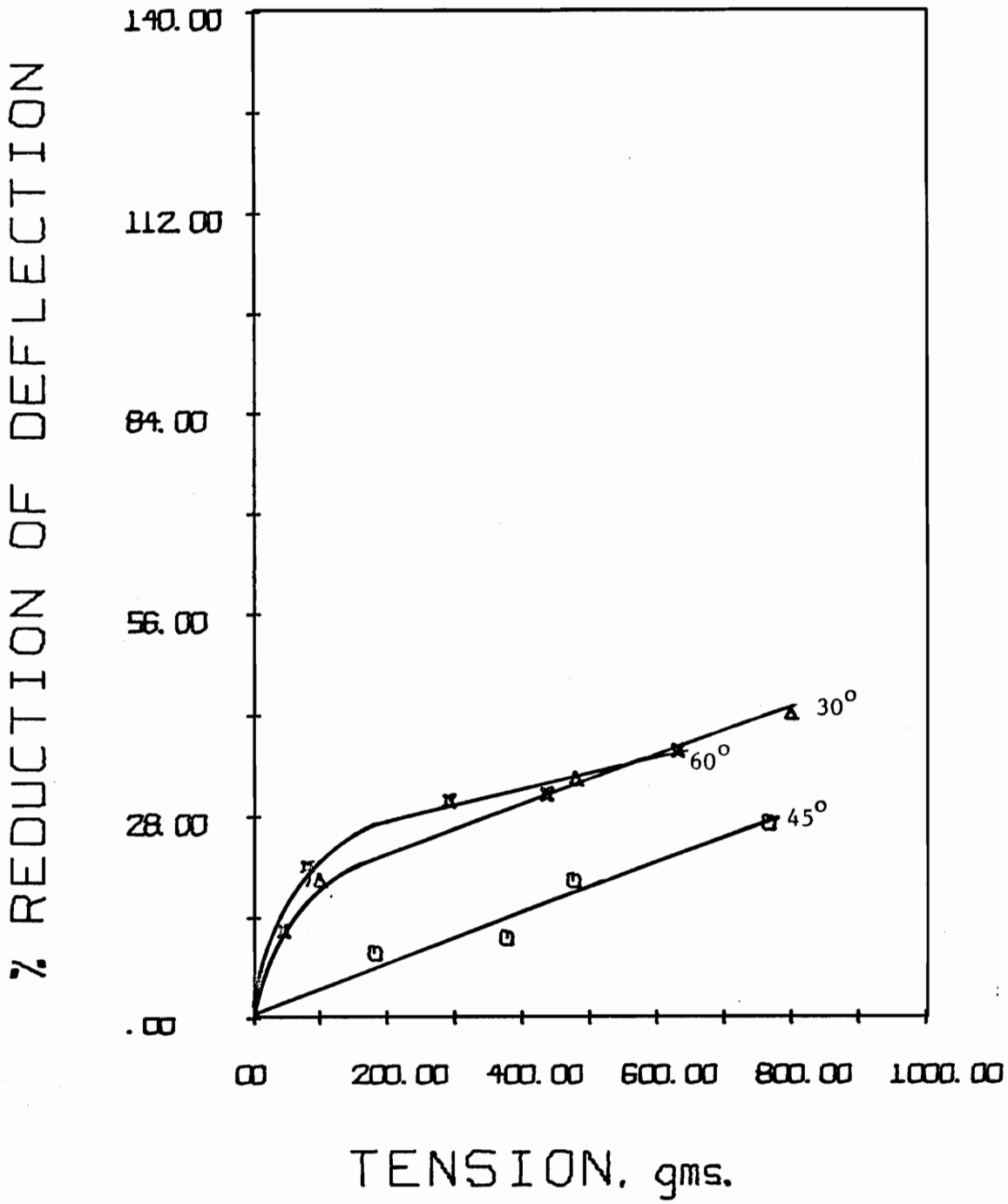

Figure 23. % Reduction of Deflection vs. Truss Tension as a Function of Truss Inclination (dimensions as in Figure 22).

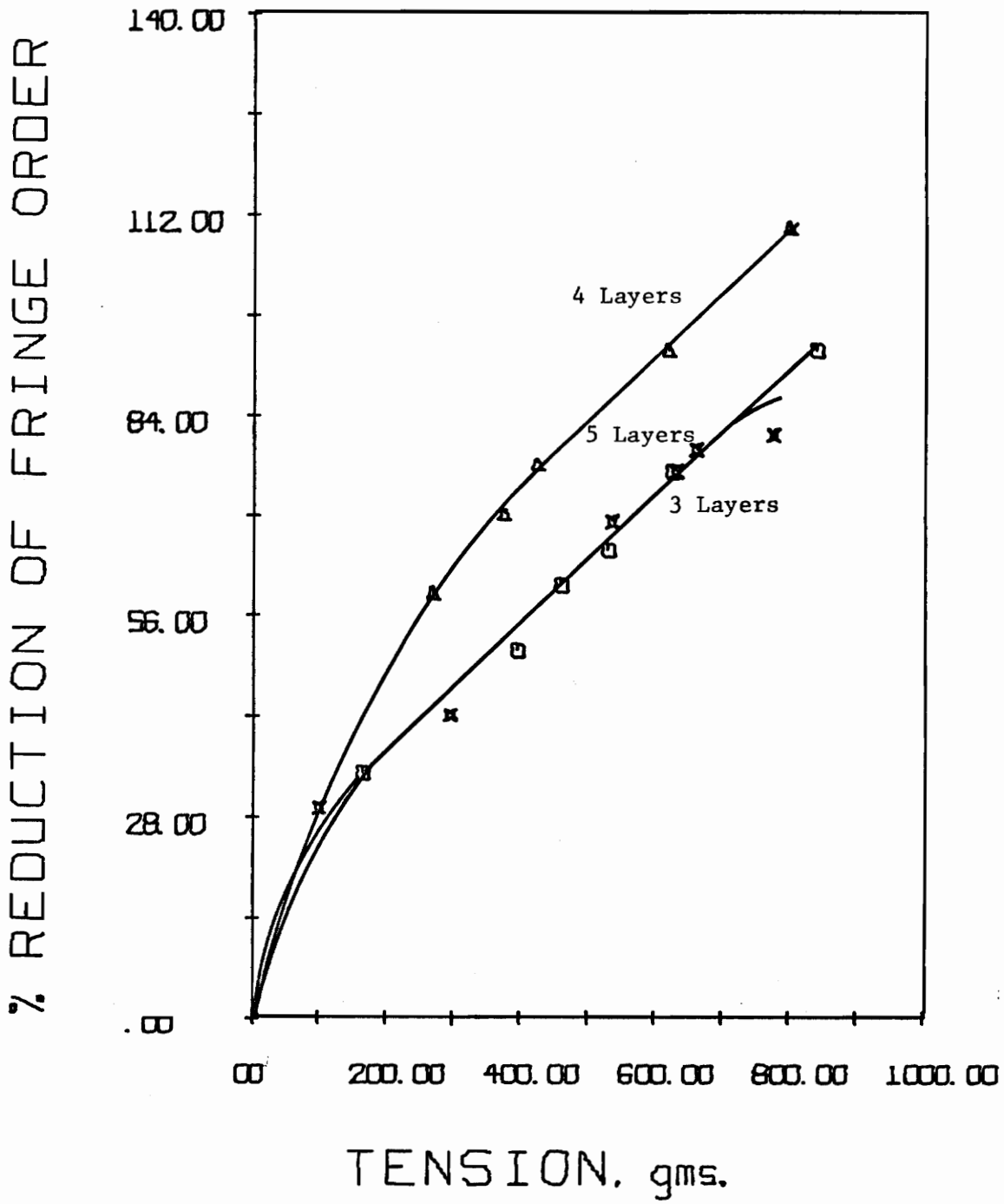

Figure 24. % Reduction of Fringe Order vs. Truss Tension as a Function of Number of Trussed Roof-layers (8" Span, 6" Truss Span, 45° Inclined Holes, .25" Blocking-Point Distances).

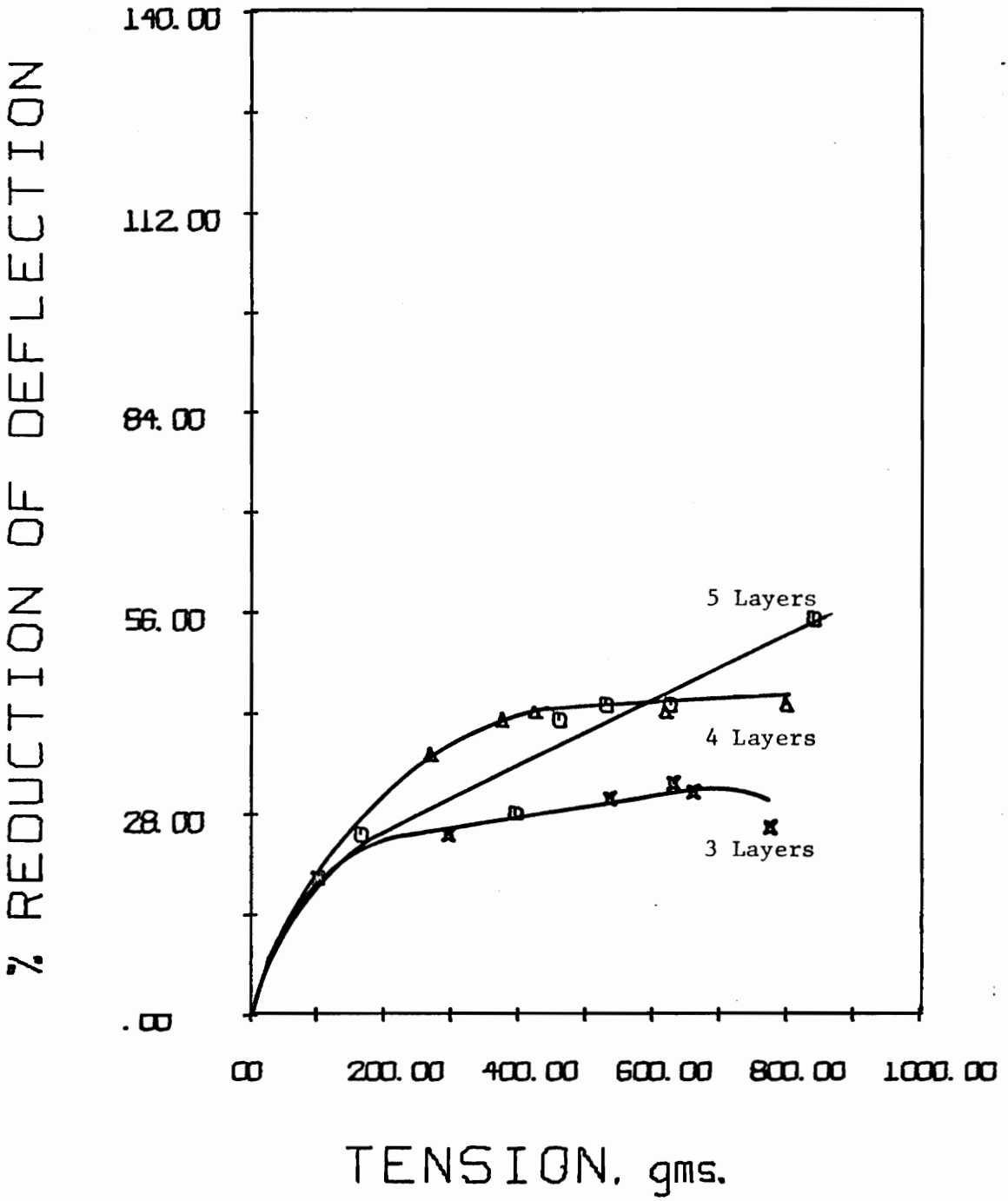

Figure 25. % Reduction of Deflection vs. Truss Tension as a Function of Number of Trussed Roof-layers (dimensions as in Figure 24).

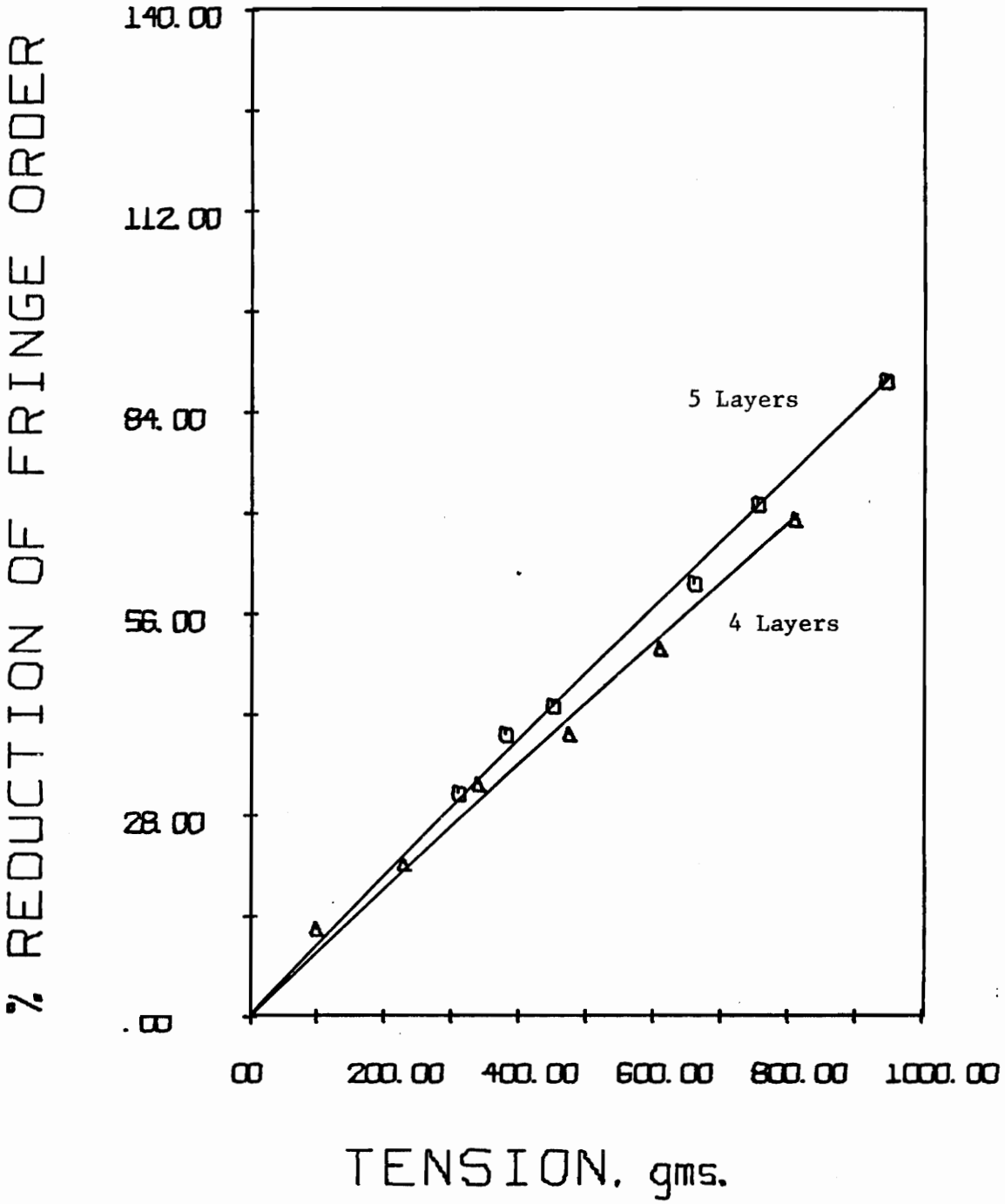

Figure 26. % Reduction of Fringe Order vs. Truss Tension as a Function of Number of Trussed Roof-layers (8" Span, 6" Truss Span, 30^{o} Inclined Holes, .25" Blocking-Point Distances).

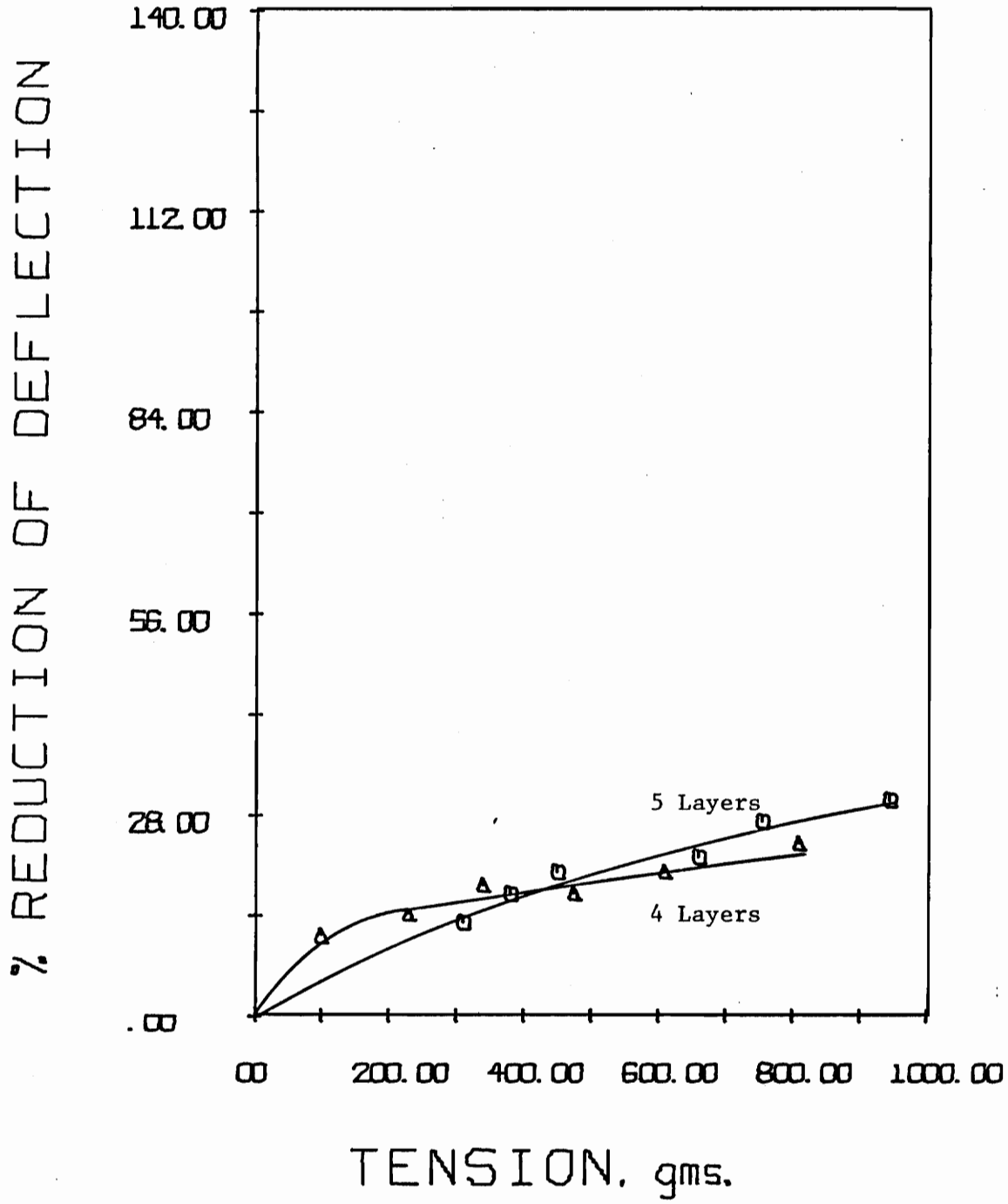

Figure 27. % Reduction of Deflection vs. Truss Tension as a Function of Number of Trussed Roof-layers (dimensions as in Figure 26).

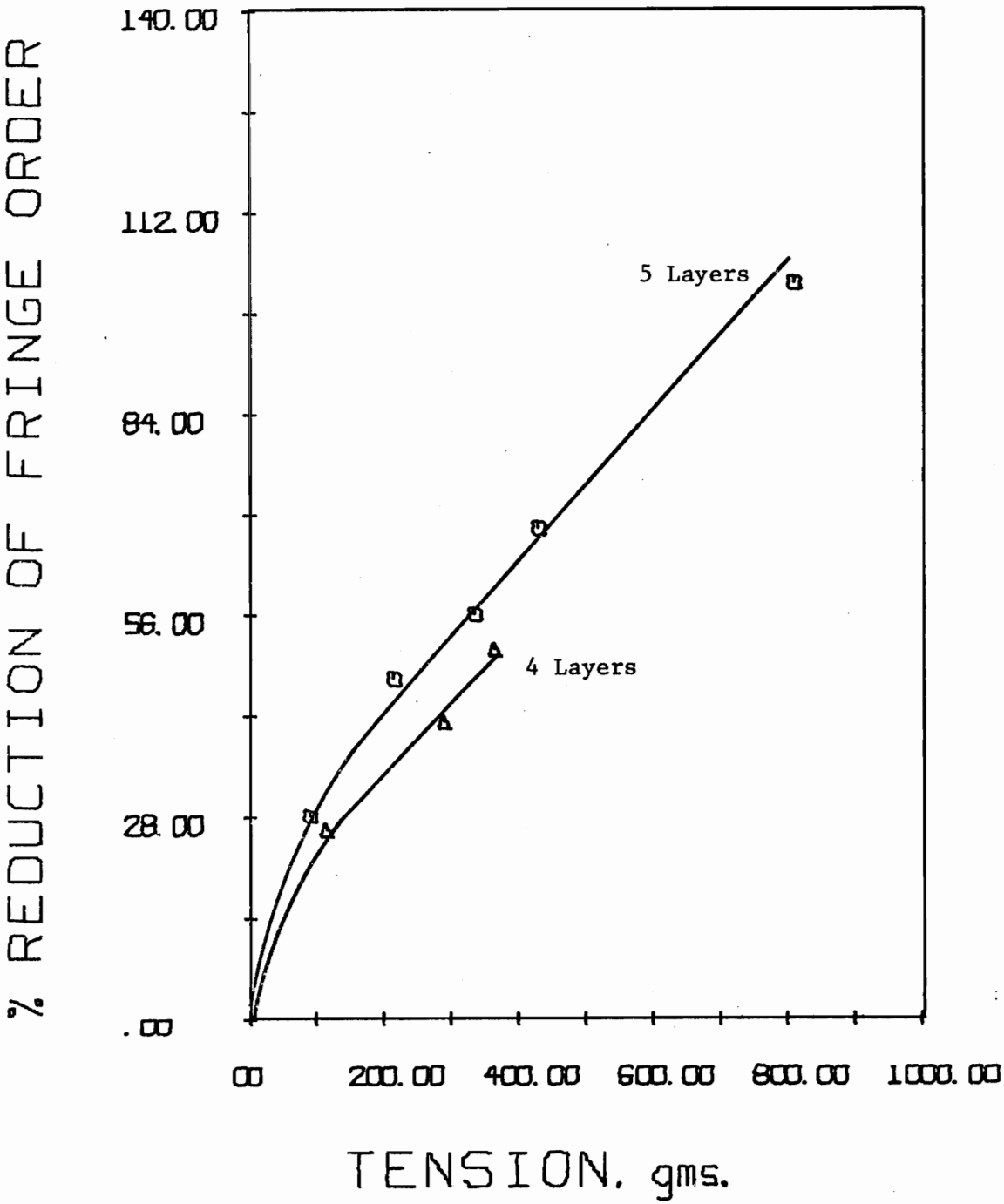

Figure 28. % Reduction of Fringe Order vs. Truss Tension as a Function of Number of Trussed Roof-layers (8" Span, 6" Truss Span, 60° Inclined Holes, .25"Blocking-Point Distances).

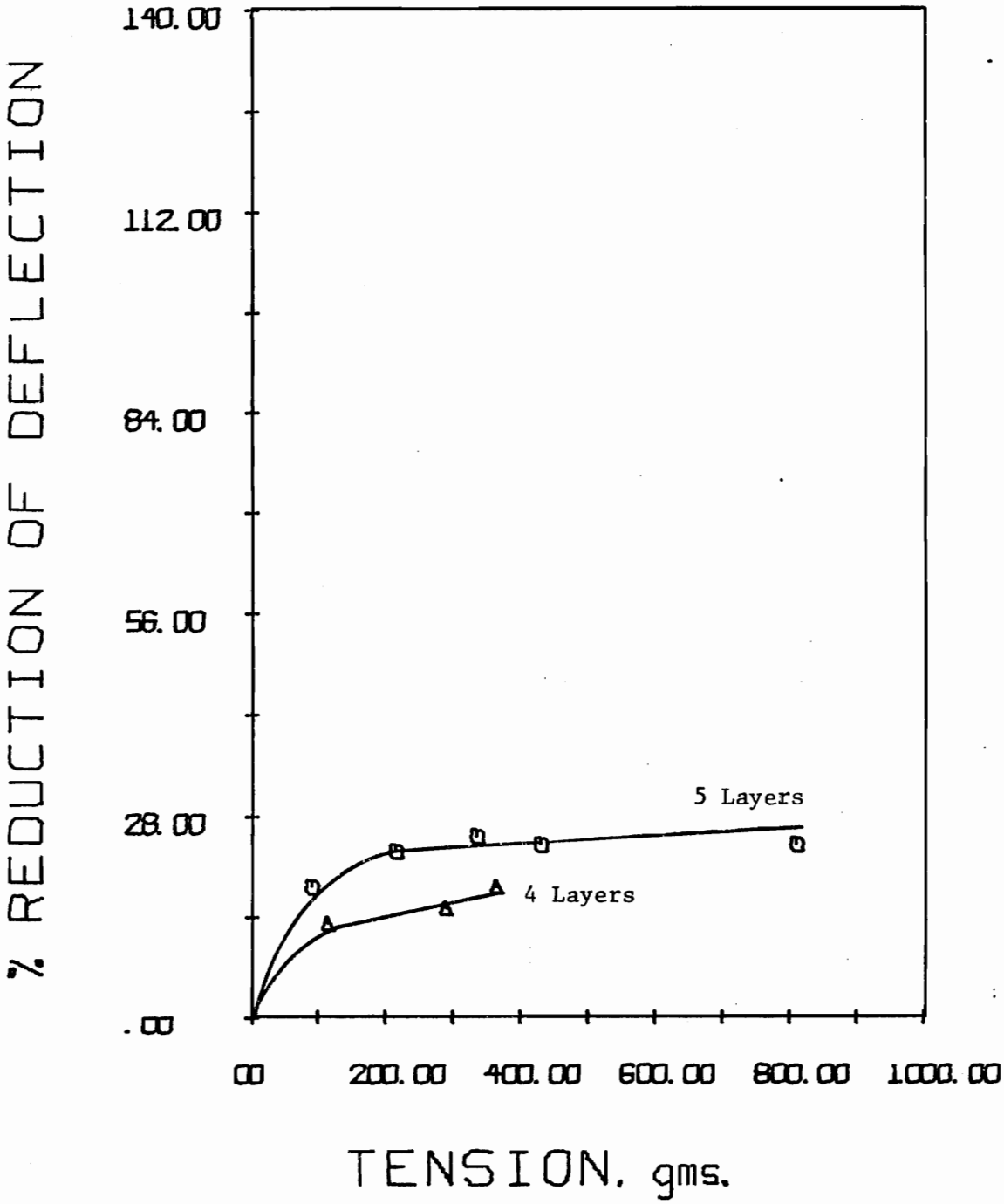

Figure 29. % Reduction of Deflection vs. Truss Tension as a Function of Number of Trussed Roof-layers (dimensions as in Figure 28).

33, 34 and 35, 36 and 37, and 38 and 39 show the results of experimental data when blocking point configurations are changed. From the plots in Figures 30 and 31 it is difficult to choose a preferred configuration because the same general trend is not exhibited in each. A very definite trend is established in the remaining figures, though. In each case the same general trend is exhibited in both the reduction of fringe order and deflection curves, and in each the configuration which is best consists of two blocking points adjacent to the truss holes (.25 in. blocking point distance) and one blocking point at midspan. Additionally, the worst blocking point configuration consists of only two blocking points adjacent to the truss holes. From the above, it would probably be safe to advise the addition of a blocking point at midspan, in addition to the two blocking points which prevent truss-model contact at the holes. This should improve the truss support regardless of the position of the truss in the opening.

Effects of Truss Span Figures 40 and 41 show how the support is related to the location of the truss within the opening. From these graphs several very important factors can be seen. The hole for the 6 in. truss span is collared 1 in. from the rib. The anchor, which is located in the fifth rooflayer (.3 in. thickness/rooflayer), is not over the rib. For the 7 1/2 in. truss span, the anchor is located over the rib. By popular theory the truss anchor should be over the rib and not the opening so that the compressive stress due to the anchor can be 'transferred to the pillar'. By this theory, the

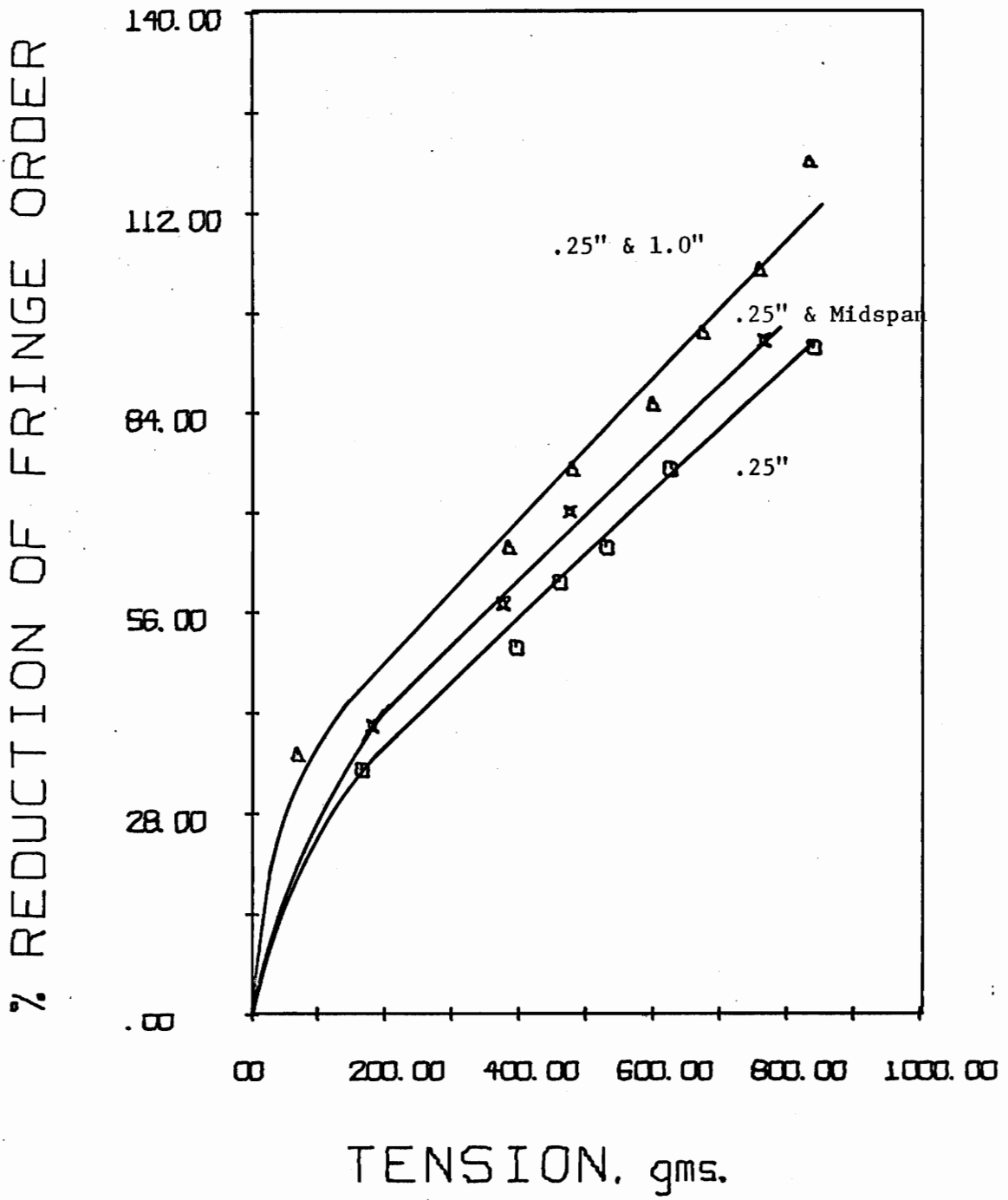

Figure 30. % Reduction of Fringe Order vs. Truss Tension as a Function of Blocking-Point Configuration (8" Span, 6" Truss Span, 45° Inclined Holes, 5 Rooflayers Deep).

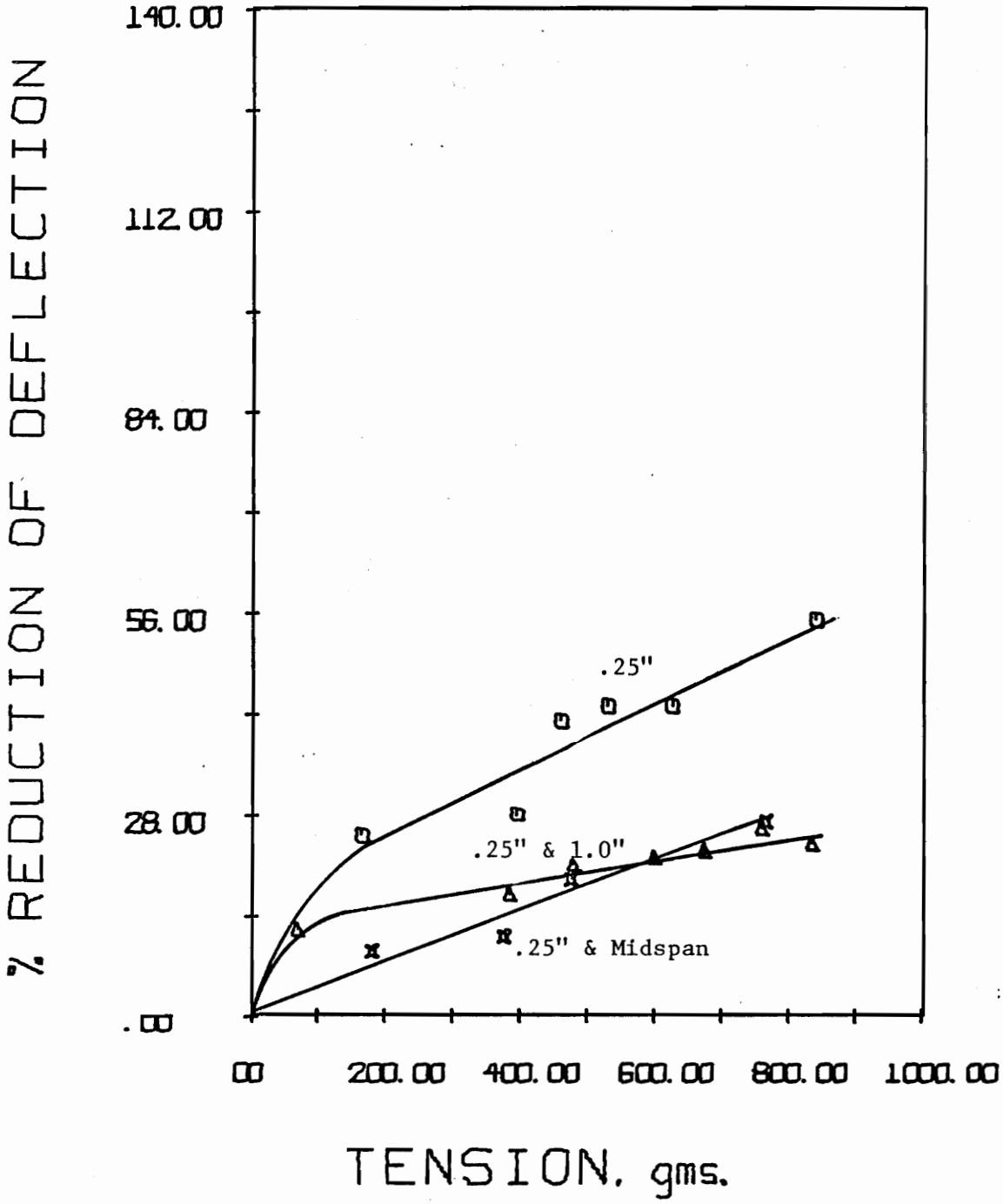

Figure 31. % Reduction of Deflection vs. Truss Tension as a Function of Blocking-Point Configuration (dimensions as in Figure 30).

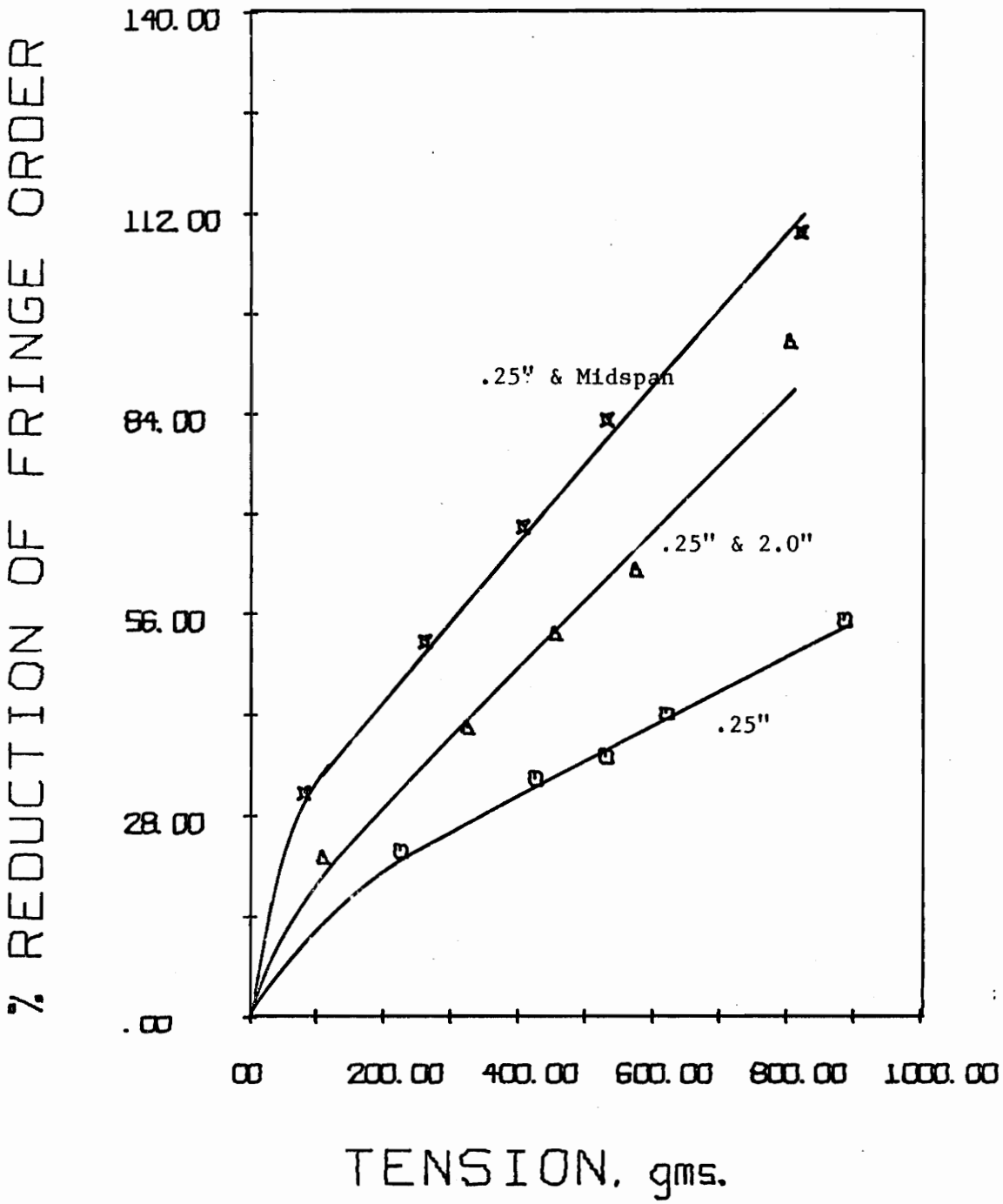

Figure 32. % Reduction of Fringe Order vs. Truss Tension as a Function of Blocking-Point Configuration (8" Span, 7 1/2" Truss Span, 60° Inclined Holes, 5 Rooflayers Deep).

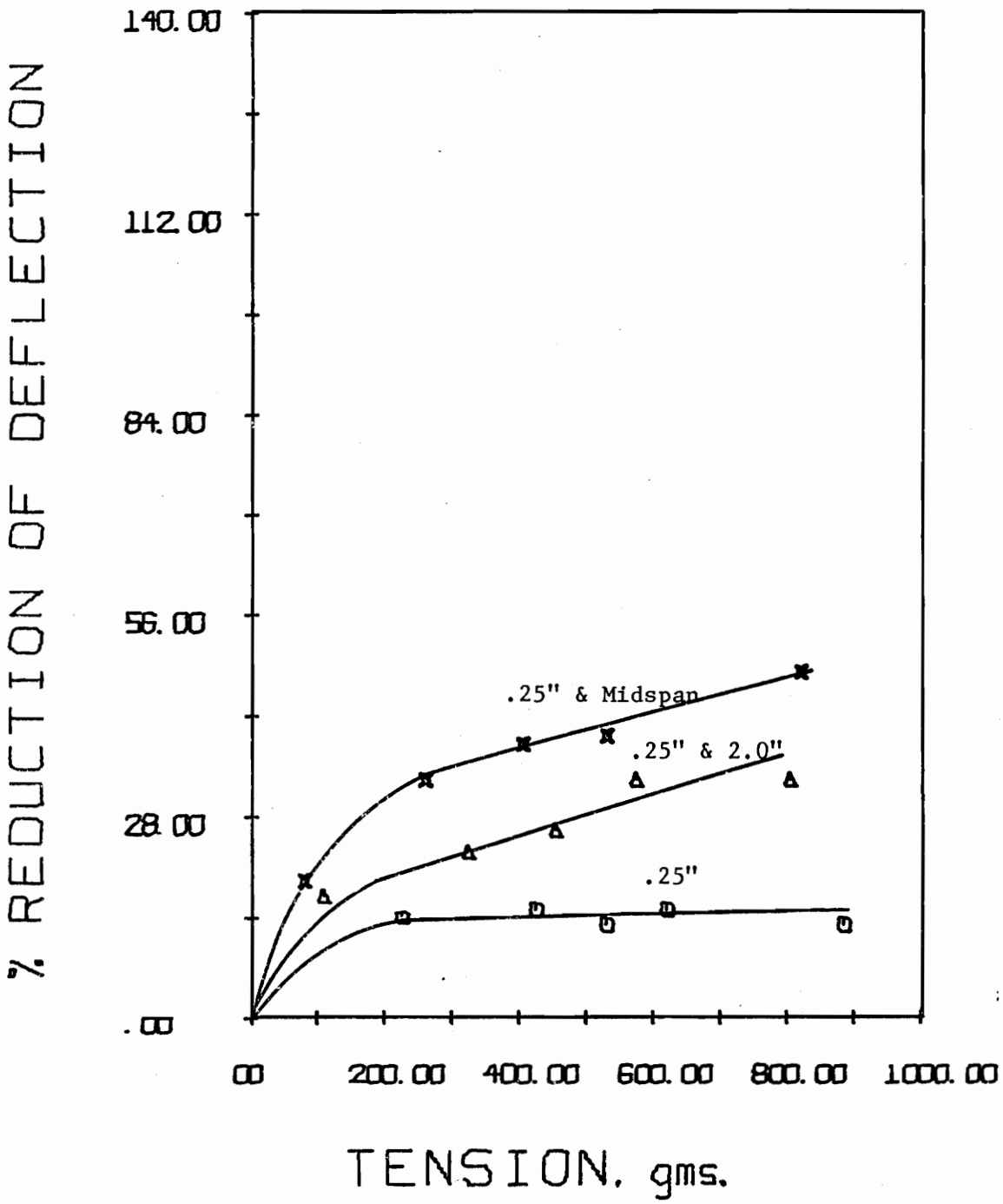

Figure 33. % Reduction of Deflection vs. Truss Tension as a Function of Blocking-Point Configuration (dimensions as in Figure 32).

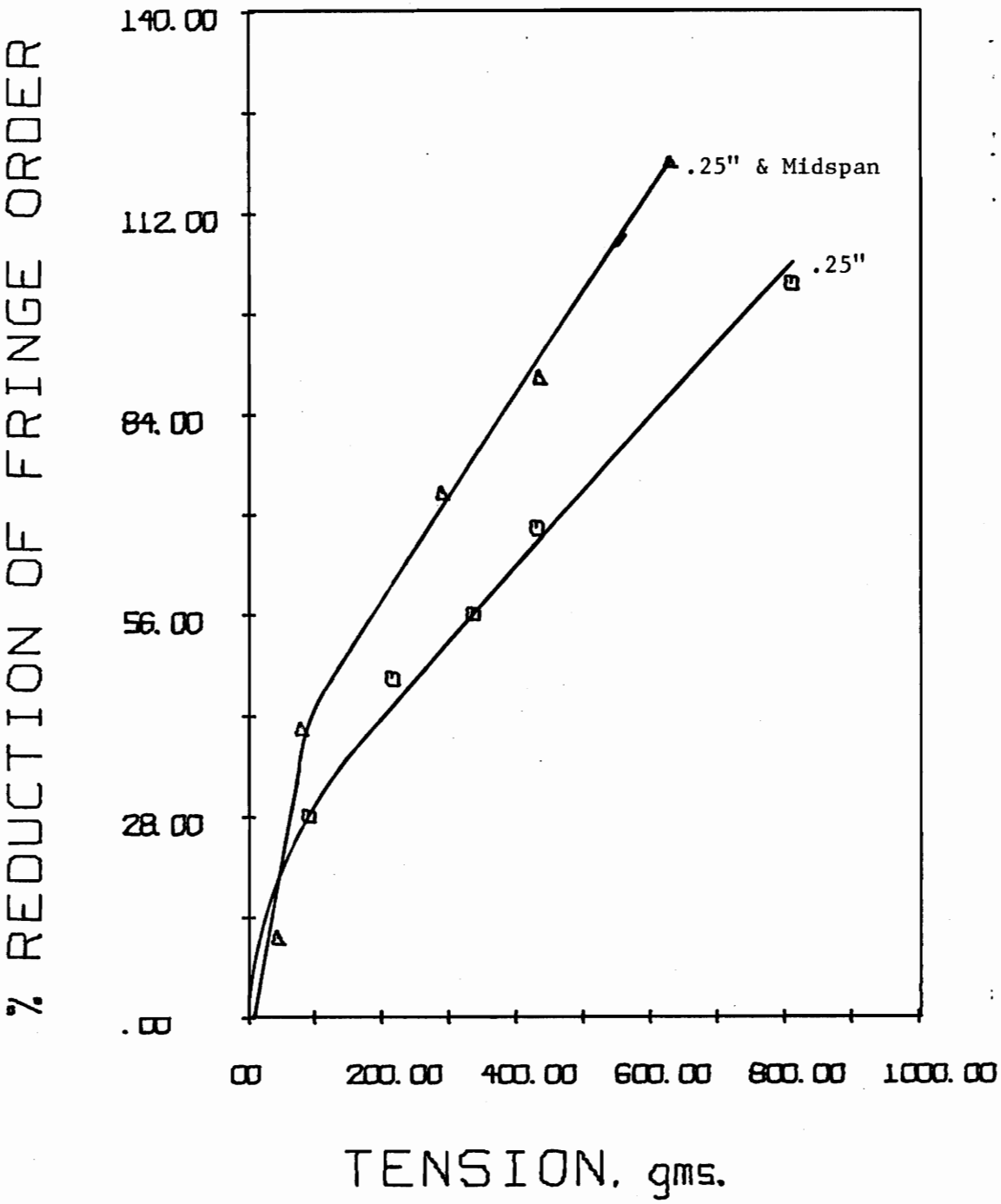

Figure 34. % Reduction of Fringe Order vs. Truss Tension as a Function of Blocking-Point Configuration (8" Span, 6" Truss Span, 60° Inclined Holes, 5 Roof-layers Deep).

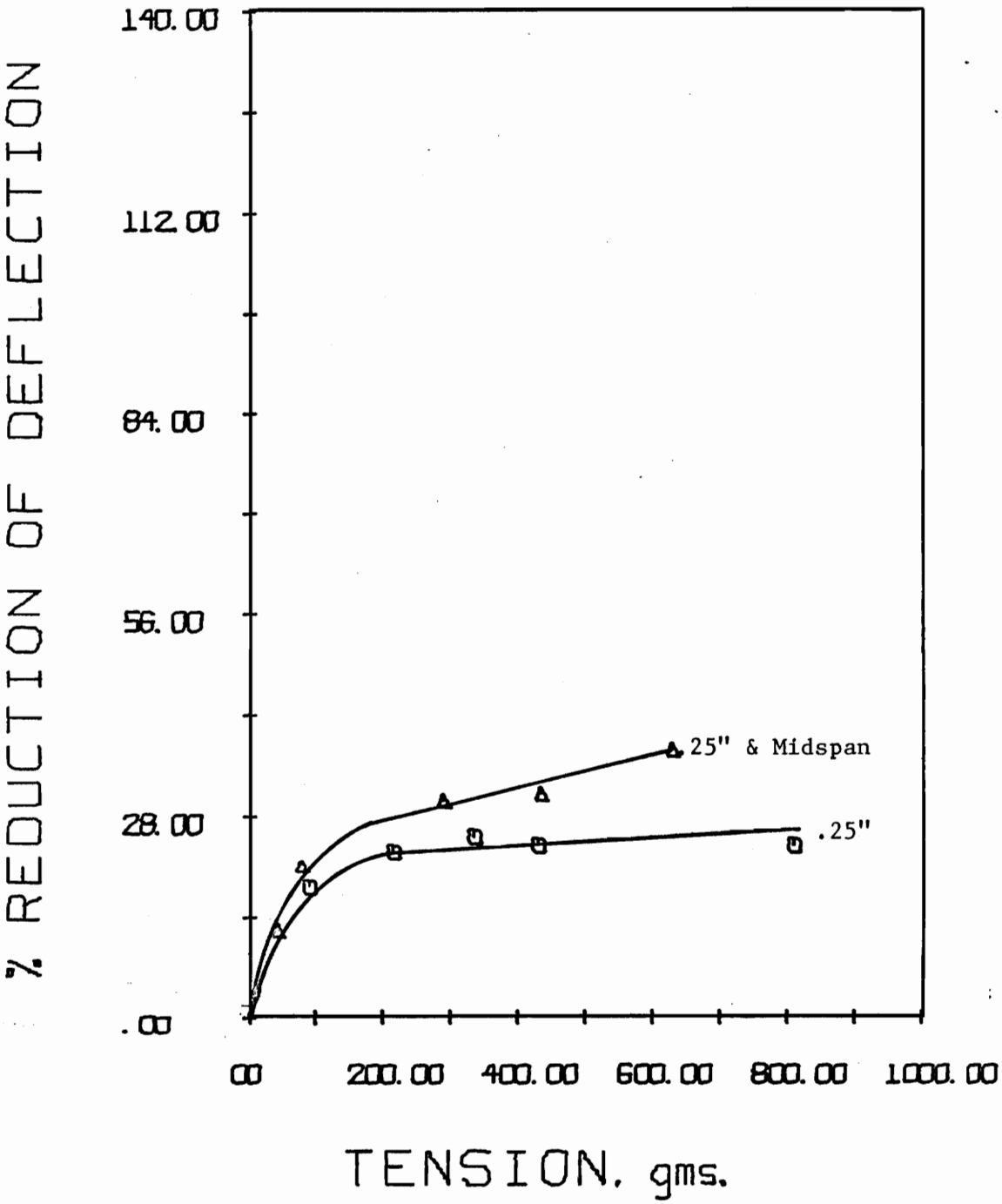

Figure 35. % Reduction of Deflection vs. Truss Tension as a Function of Blocking-Point Configuration (dimensions as in Figure 34).

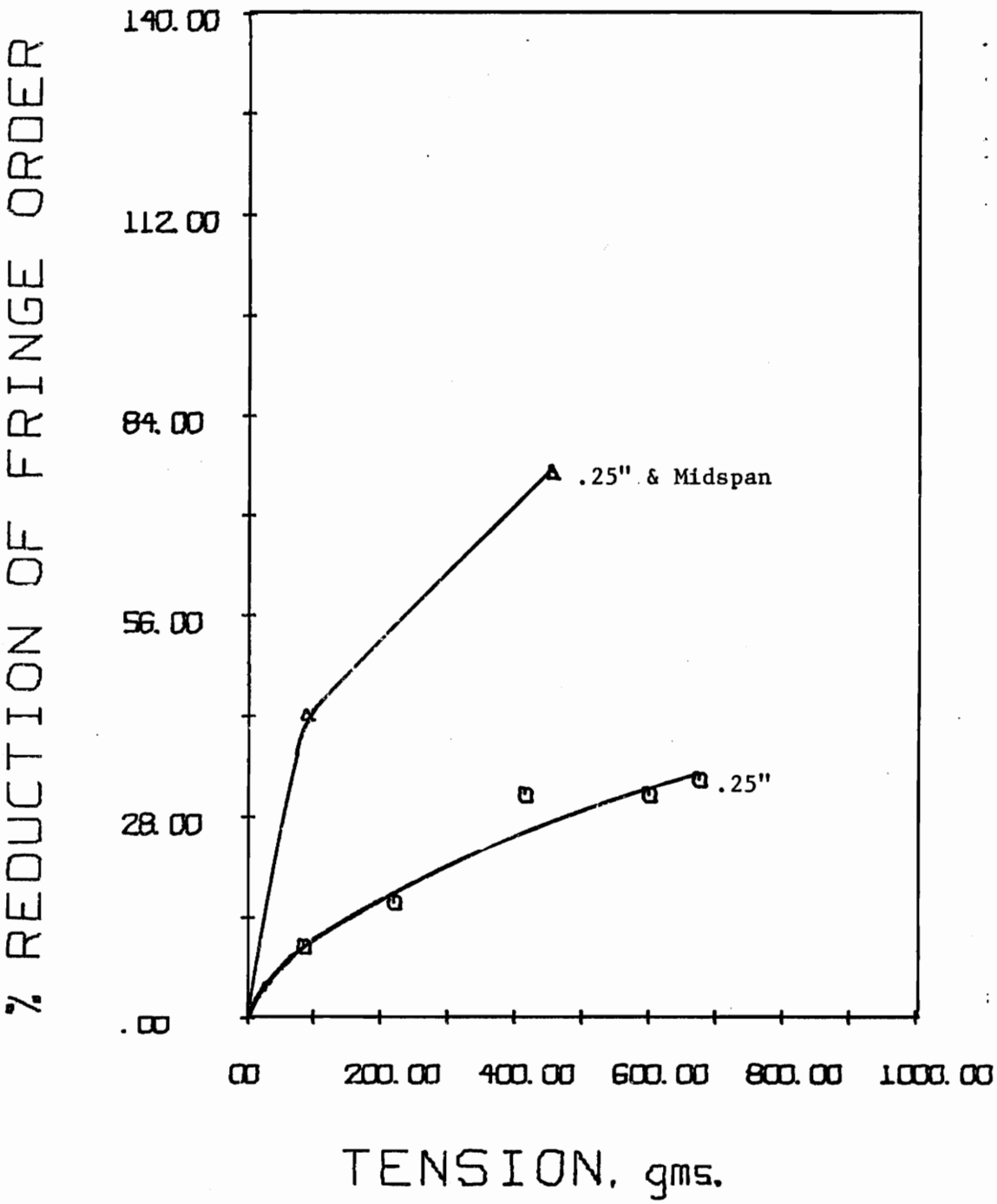

Figure 36. % Reduction of Fringe Order vs. Truss Tension as a Function of Blocking-Point Configuration (9" Span, 7 1/2" Truss Span, 60° Inclined Holes, 5 Rooflayers Deep).

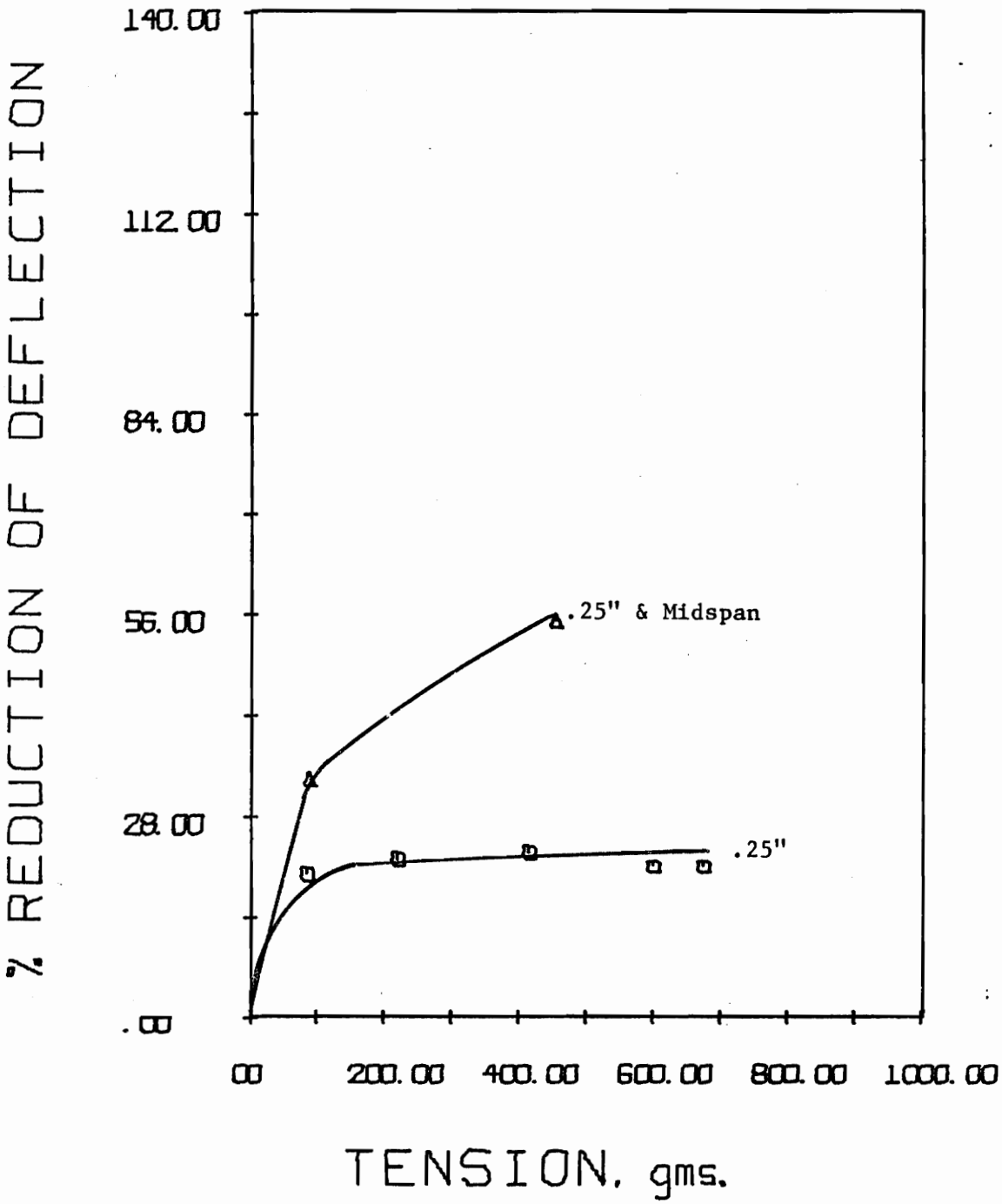

Figure 37. % Reduction of Deflection vs. Truss Tension as a Function of Blocking-Point Configuration (9" Span, 7 1/2" Truss Span, 60° Inclined Holes, 5 Rooflayers Deep).

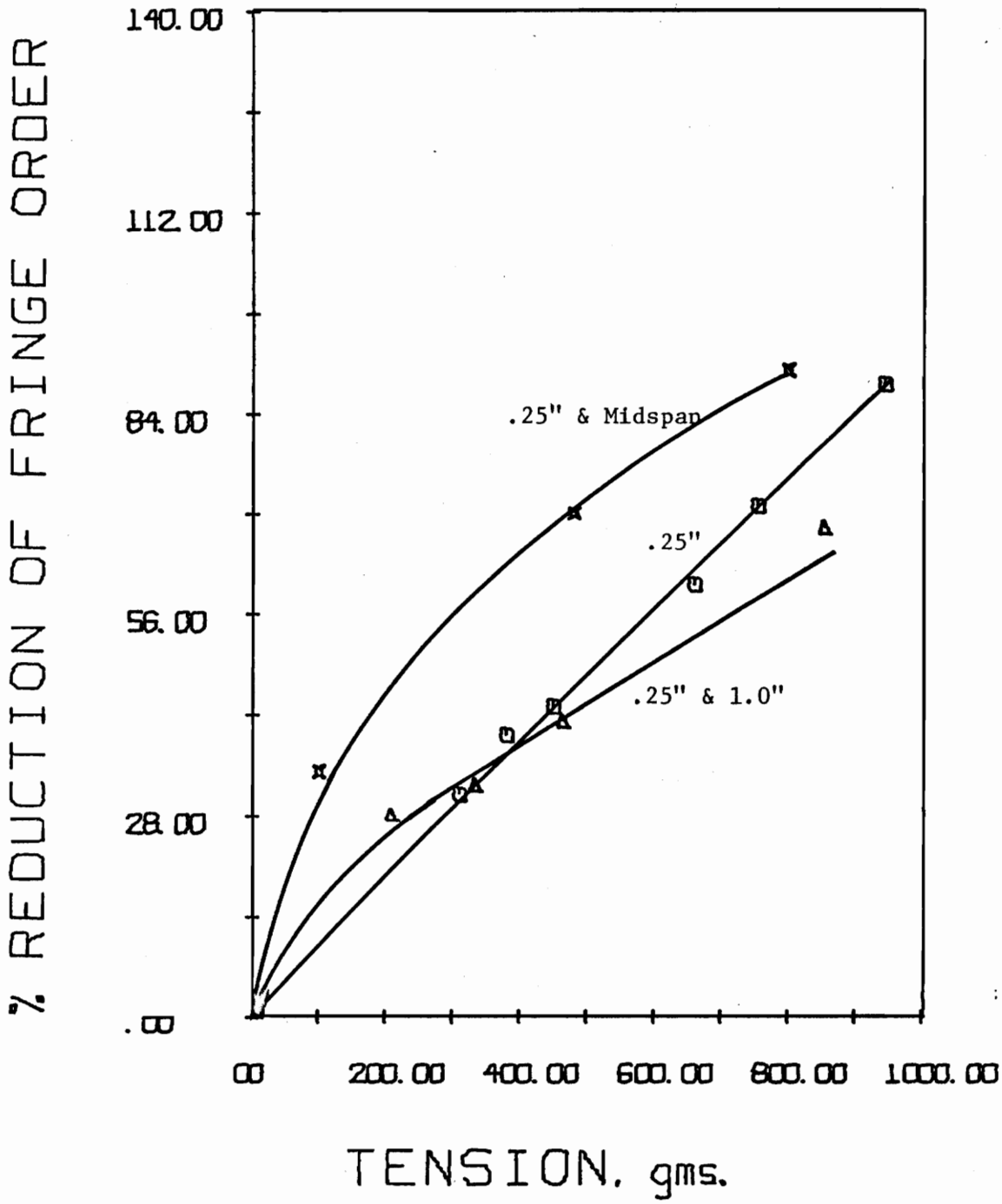

Figure 38. % Reduction of Fringe Order vs. Truss Tension as a Function of Blocking-Point Configuration (8" Span, 6" Truss Span, 30° Inclined Holes, 5 Rooflayers Deep).

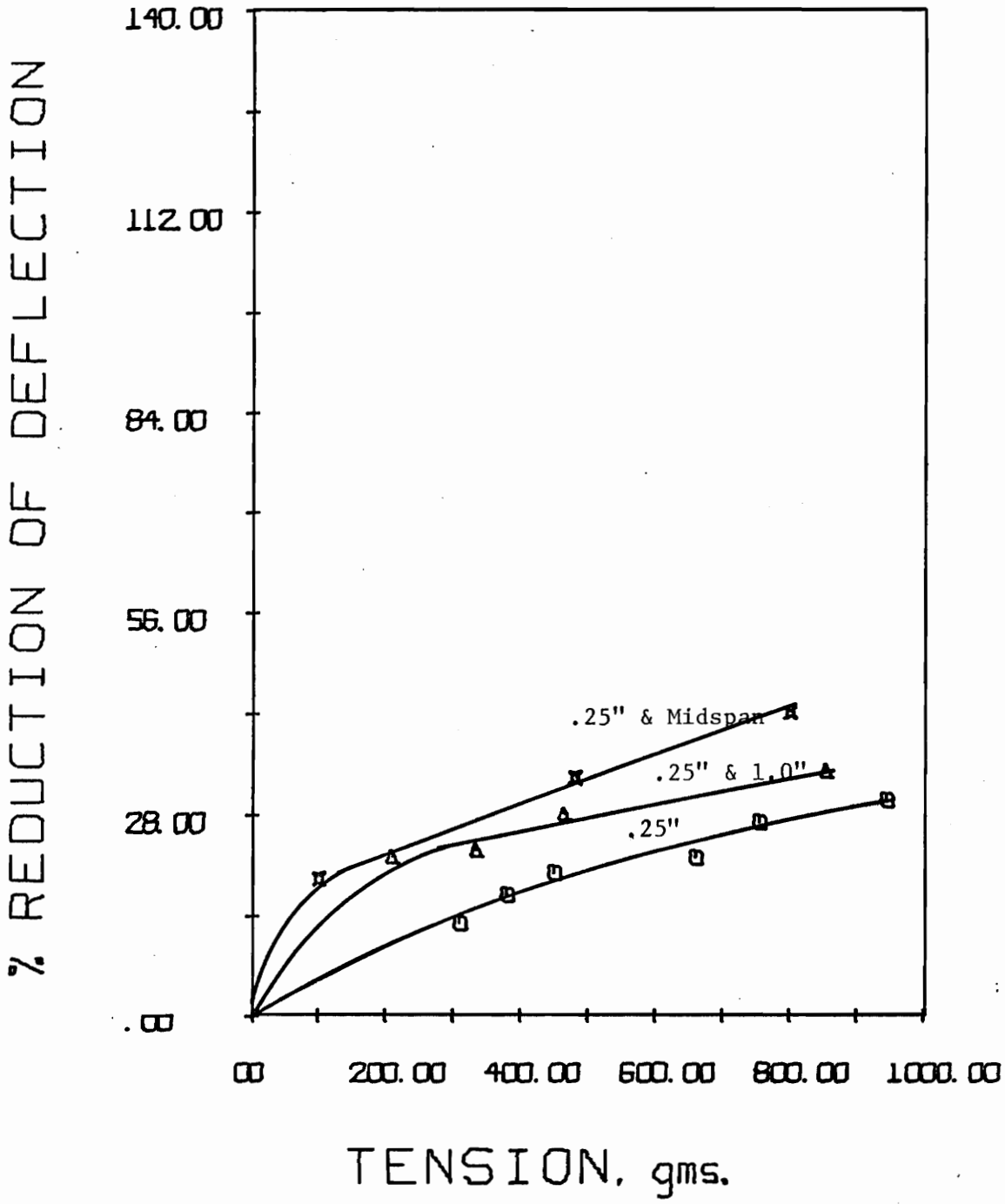

Figure 39. % Reduction of Deflection vs. Truss Tension as a Function of Blocking Point Configuration (8" Span, 6" Truss Span, 30° Inclined Holes, 5 Rooflayers Deep).

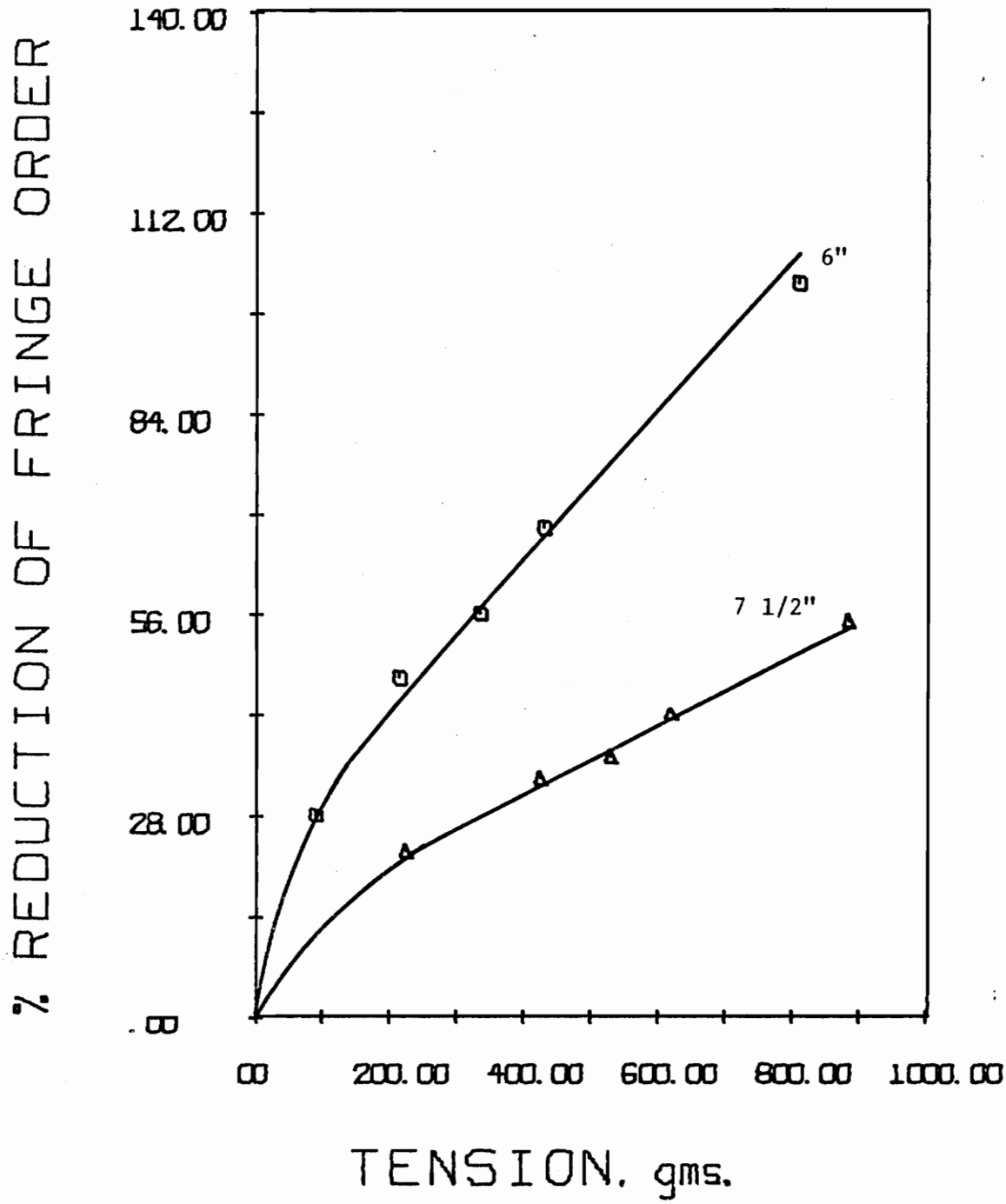

Figure 40. % Reduction of Fringe Order vs. Truss Tension as a Function of Truss Span (8" Span, .25" Blocking-Point Distances, 60° Inclined Holes, 5 Rooflayers Deep).

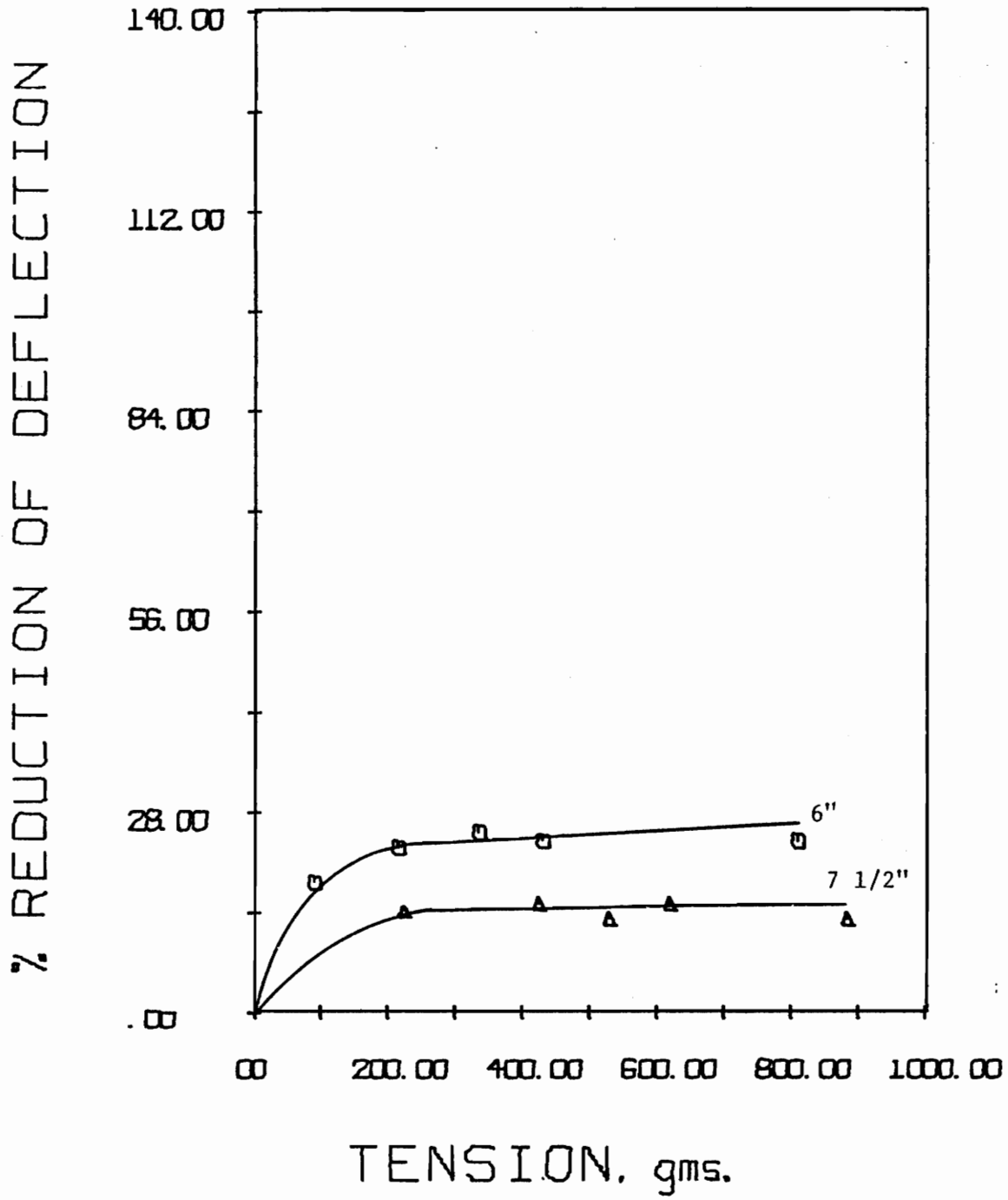

Figure 41. % Reduction of Deflection vs. Truss Tension as a Function of Truss Span (8" Span, .25" Blocking-Point Distances, 60° Inclined Holes, 5 Rooflayers Deep).

7 1/2 in. truss span should be superior to the 6 in. truss span. This is not the case, however. The 6 in. truss span reduces both fringe order and deflection almost twice as much as the 7 1/2 in. truss span.

The belief in the popular theory probably arises from mechanics theory on point and tabular loads in a semi-infinite solid, such as the work done by Boussinesq and Westergaard. The pyramid of stress in soil mechanics is but a simplification of this. By this theory, the further away from the opening the truss is anchored, the lower will be the stress on the opening. The question which is now posed is whether the location of the anchor is more important than the placement of the resultant at each blocking point. Inspecting Figure 2 which breaks down the forces involved in a truss-supported roof, the factors which change are the locations of the anchor and blocking-point resultants. The further over the opening the anchor is located, for a given truss inclination, the greater is the moment which results. This moment is the result of the couple located at the anchor and the blocking point. As this moment resists downward deflection, it is beneficial. At the same time, though, as the moment about the rib increases, so does the shear at the rib due to the increase of stress on the opening from the anchor, and this is detrimental. At some point over the opening, therefore, there should be an optimum location for truss placement. Locating the truss closer to the rib or further away from it would decrease the beneficial support moment faster than it would decrease the shear, or it would increase the moment more slowly than it would increase the shear.

Effects of Opening Width Figures 42 and 43 show the effects of

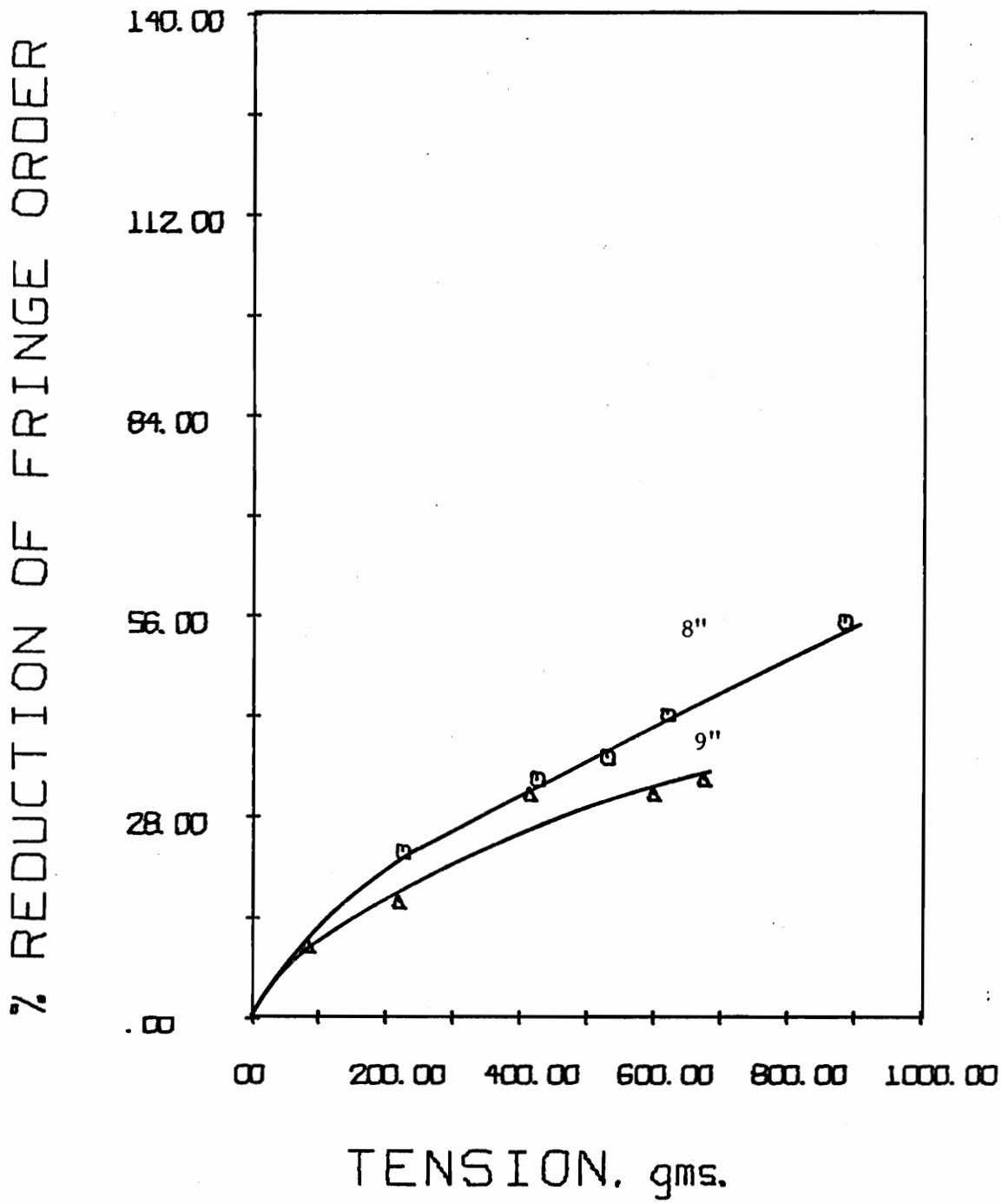

Figure 42. % Reduction of Fringe Order vs. Truss Tension as a Function of Opening Span (7 1/2" Truss Span, .25" Blocking-Point Distances, 60° Inclined Holes, 5 Rooflayers Deep).

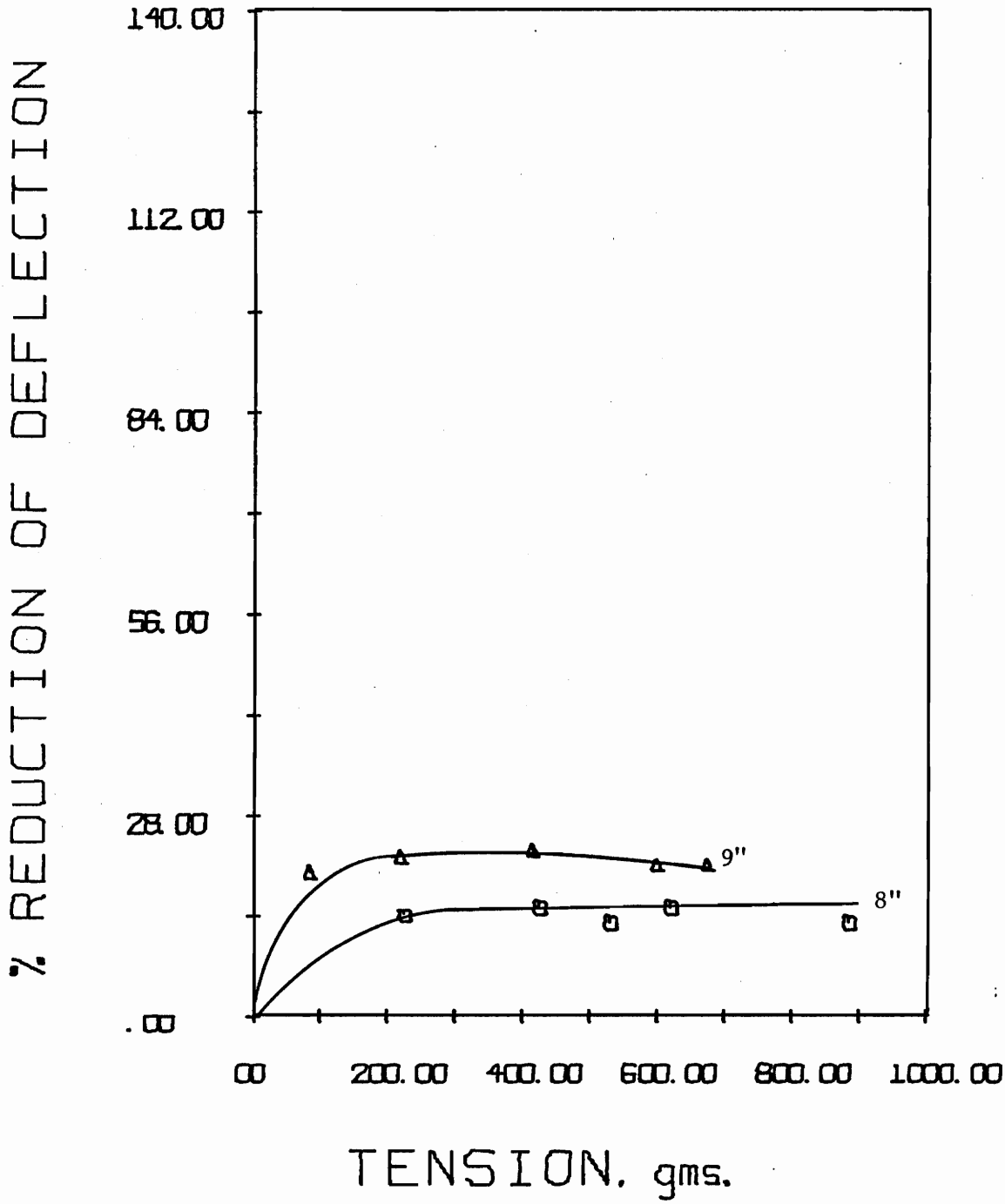

Figure 43. % Reduction of Deflection vs. Truss Tension as a Function of Opening Span (7 1/2" Truss Span, .25" Blocking-Point Distances, 60° Inclined Holes, 5 Rooflayers Deep).

varying the opening width of the mine model with all other variables constant. Because the graphs of reduction of fringe order and reduction of deflection do now follow the same general trend, and because only two tests were performed, it is difficult to reach any conclusions. One would expect the roof truss to be more effective in smaller width openings, however, because of the complex nature of roof truss support and the interdependency of several of the variables upon other variables this may not be the case. An example of the interdependency is the location of the roof truss anchor with respect to the rib. This is a function of not only the truss span and opening width, but also the angle of truss inclination and the depth of the hole. Similarly, for a 9 in. opening and an 8 in. opening, each with a 7 1/2 in. truss span, even though only one of the selected variables was changed, that is the opening width, the distance of the truss hole collar from the rib also changed, and consequently the relative location of the resultant of the blocking points.

Further testing will be required to corroborate or disprove this, however.

Effects of Interlayer Shear Resistance Studying Figures 44 and 45, it is apparent that the roof truss is effective in supporting strata with low interlayer shear resistance, such as might be encountered if layers of clay or softer shale were present between other layers. Again, however, because the same general trends did not appear in both graphs, it is difficult to reach any other conclusions.

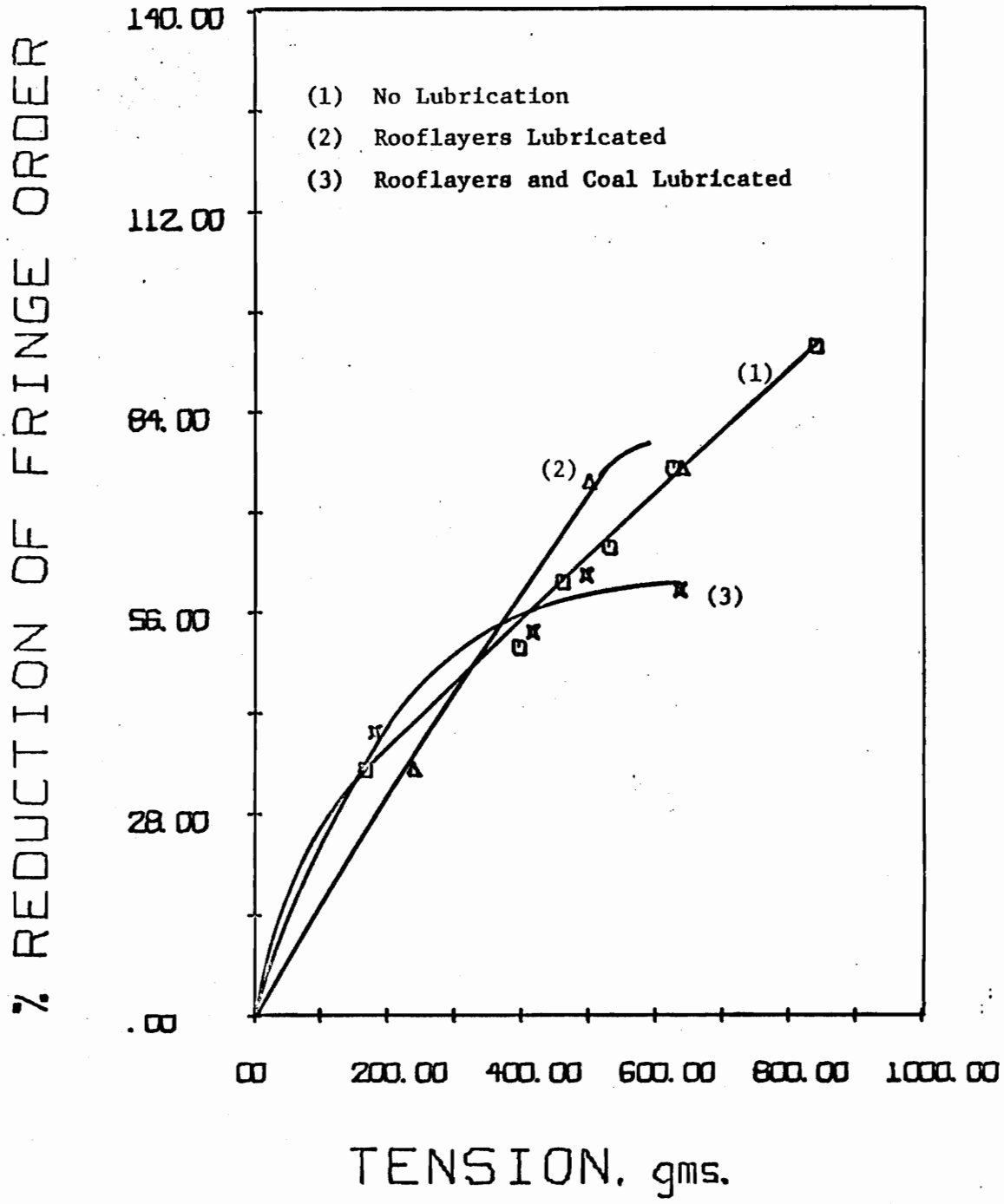

Figure 44. % Reduction of Fringe Order vs. Truss Tension as a Function of Interlayer Shear Resistance (8" Span, 6" Truss Span, .25" Blocking-Point Distances, 45° Inclined Holes, 5 Rooflayers Deep)-

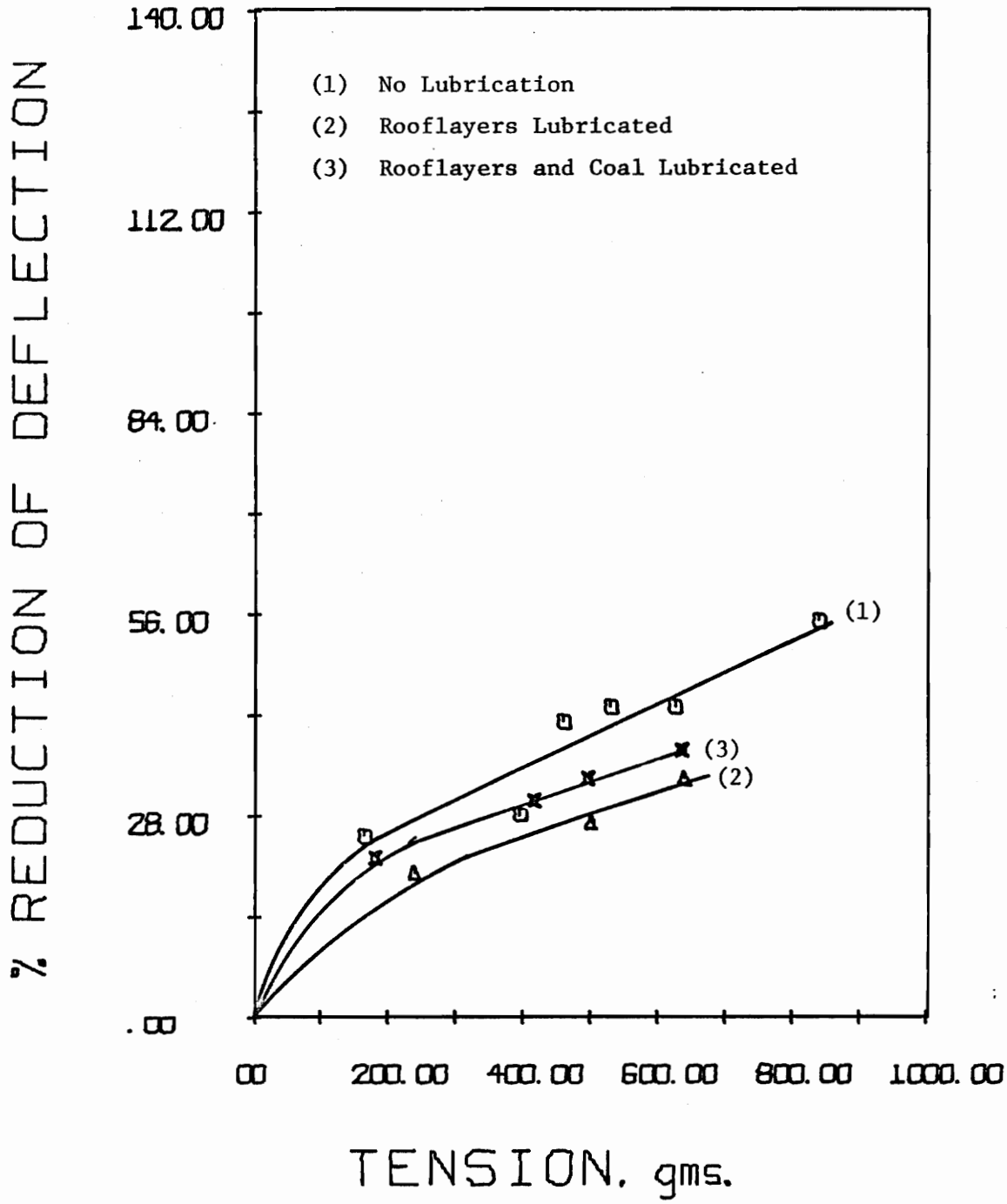

Figure 45. % Reduction of Deflection vs. Truss Tension as a Function of Interlayer Shear Resistance (8" Span, 6" Truss Span, .25" Blocking-Point Distances, 45° Inclined Holes, 5 Rooflayers Deep).

For the unlubricated layers, the static angle of friction was determined to be between 46^{o} and 47^{o}, while for the lubricated layers it dropped to between 24^{o} and 25^{o}, a difference of almost 100 percent.

Superposition of Effects Comparing Figures 32 and 40, and 33 and 41, one can see that the 7 1/2 in. truss span can be improved, and made almost equal in support capacity to the 6 in. truss span, by changing the blocking point configuration. One would assume, then, that similarly the 6 in. truss span could be improved simply by changing the blocking point configuration. Comparing Figures 34 and 40, and 35 and 41, this is immediately confirmed.

Applying the above principle of superposition of effects one would expect the 60^{o} roof truss with the .25 in. and midspan blocking points to be more efficient than the 30^{o} or the 45^{o} case. Again, checking Figures 22 and 23, this is confirmed. Although this superposition principle is not valid for all of the tests performed, it is for the majority. The discrepancies can probably be attributed to experimental error and to the previously mentioned interdependency of variables.

Figures 40 and 42 and 41 and 43 could be related to each other as both deal with the relative location of the roof truss within the opening. This has not been done, however, because of the lack of data. Several other tests with various truss spans and opening spans would be required.

Tables of experimental data may be seen in the appendix.

DISCUSSION

The problems associated with the study of various methods of underground roof support are quite complex, not only because of the anisotropy of the rock being studied, but also because of the uncertainties concerning the stress field which exists.

Classical theory, at this point, cannot adequately describe the phenomena associated with various types of roof support such as the roof truss. The finite-element method seems to give reasonable results, but is not capable, due to limited storage capacity in computers, of modelling a complex multi-layered structure where interlayer bed separation is allowed to take place.

The photoelastic method used in conjunction with low moduli materials has proven to be a useful tool in the study of complex mine models. A certain degree of non-homogeneity could even be built into models by using photoelastic materials with different optical properties and by introducing discontinuities or cracks in the material. This, however, will require extensive testing. The photoelastic method as employed in this series of experiments, though it did not account for varying materials properties, provided useful insight into the area of roof-truss supports.

The problem concerning interpretation of data acquired from an ideal model and the subsequent application of this to actual field operation was recognized in the early stages of this research. As was stated earlier, the application of similitude to scale-model reactions to those of the prototype was not considered because of the complexities

involved. The analysis is further complicated because of the influence that the interlayer shear has on the reaction of the model. Although the coefficient of friction of the model material and its tensile strength (or shear or compressive strength) may be determined and therefore the ratio of the tensile strength (or shear or compressive) to the interlayer shear strength, this value should be the same as the corresponding value for the prototype mine. If these values differ, the difficulty of applying experimental data to field situations is greatly increased. The material properties of the model are fairly accurately known, as are the geometrical properties. This is usually not the case in an operating mine. In the model the roof consists of mechanically descrete layers or beams whereas in some field cases it is difficult to apply this analogy due to the large number of joints and fractures which are present.

The acquisition of field data to substantiate experimental findings was considered, and played an important part in the decision to relate not only stresses to truss tension, but also midspan deflection. The reasons for this are quite apparent to many who have attempted to correlate roof-strain readings with roof stress. Not only is the acquisition of meaninful underground strain-gage data difficult at present, but also its application to theory using experimentally determined mechanical properties is equally difficult. A more practical and acceptable approach, though by no means easy, is the measurement of midspan roof deflection in mines. No material properties are involved, thereby reducing the difficulty of relating model deflections to prototype

deflections.

In the plots of reduction of fringe order and reduction of deflection vs. truss tension, the ratio of the slopes of the curves of the former to the latter averaged about 2 to 3 for the photoelastic experiments. For the finite-element analysis the ratio was about 5. Additionally, almost none of the curves from the photoelastic work were linear, while the plots from the finite-element analysis were. It is suggested that the reason for this non-linearity in the photoelastic work is that separation between layers could, and did, take place. This, in effect, decreased the average layer moment of inertia of the model in the vicinity of the opening, at least as far as reactions to blocking point loads are concerned. Practically speaking, this means that it takes a comparatively smaller force to reduce some initial deflection of the roof, since there is a separation opening above, which will permit the layer to more easily deflect upwards. As this upward deflection is increased, or as downward deflection decreases, and the separation openings are progressively closed up, it also becomes successively more difficult to reduce deflection. This same analogy can be applied to field situations. In addition to interlayer separation, however, interjoint separation can occur. This should tend to further emphasize the above described phenomena.

The support which a roof truss imparts does not appear to increase linearly with truss tension. The slope of the curves representing support increase is greatest when the truss is initially tensioned and tends to decrease with increasing tension. This suggests that at

some point, for a given depth of anchor and other set conditions, increasing truss tension will not provide additional support. Whether this tension is much greater than the capacity of present trusses is still an unanswered question, although from these studies this would appear to be true.

The roof truss is quite sensitive to several variables, and for a given opening width, these variables may be changed so as to optimize truss useage. One of the most sensitive variables appears to be the manner in which the truss is blocked in place. The most efficient method of doing this involves using multiple blocking points, including one at midspan, and one at the collar of each hole to prevent point failure of the rock due to rock-truss contact. An even more efficient way of blocking the roof might involved blocks of varying thickness, so as to achieve uniform blocking stresses across the entire roof, thus making the truss act very similar to a reinforcing bar in concrete, but with the added advantage of a vertical component. Truss placement within the opening also seems to be critical. For a clamped beam, the point at which the tension on the bottom of the beam changes to compression is located approximately 1/5 of the span away from the rib. It would seem reasonable then, to collar the truss hole at this point, so as to provide resistance to tensile failure where it is most needed. The placement of the anchor over the rib, though not indicated necessary by model studies, is suggested due to the presence of discontinuities and other unknown factors. Truss inclination, though important, is not as critical as the preceding factors. An inclination of 60^{o} is sugges-

ted, though not much capacity seems to be lost at 45°. At this point, a compromise could be made regarding the extra depth required of steeper holes, and the decreased capacity of flatter holes. Trusses seem to be capable not only of preventing the downward deflection of roof strata, but also of actually decreasing deflection which has already occurred, a job which standard roof bolting cannot perform. Although some of their effectivenss is lost when interlayer roof friction is decreased, roof trusses are still effective in preventing such problem roof strata from failing. Finally, the depth of the truss anchor should be such that the formation of a failure plane from it to the roof strata is improbable. When anchored over a rib, a vertical depth of 4 ft. is probably sufficient. When not over a rib, additional depth may be required.

The measurement of midspan deflection may not be adequate for relating model reactions to prototype reactions. The radius of curvature of the roof strata should describe the state of stress which exists. If the radius of curvature decreases, the deflection should increase. If the radius of curvature increases the deflection should decrease. It is possible that the radius of curvature could be the same in several different tests, with the deflection readings varying greatly. This would mean that the center of the radius of curvature had deflected downward. In addition, a change in deflection of 1 mm. would mean a large change in the percentage reduction of deflection, whereas it would mean a very small change in the percentage reduction of radius of curvature. This is because the radius of curvature is

so large in comparison to the deflection. In future tests, the radius of curvature will also be determined in an attempt to improve data correlation.

VI. CONCLUSIONS

Based on the performed photoelastic model experiments, the following recommendations are made for conditions as represented by the model:

1. The angle of inclination of the truss should be greater than 45^{o}.
2. Truss installation should involve the use of multiple-blocking points including one at midspan.
3. Truss holes should not be collared too close or too far away from the rib. A distance of 1/5 the opening width is suggested.
4. Trusses can be very effectively used if interlayer friction is low.
5. The number of equal thickness rooflayers which are trussed together does not seem to be as important as the other variables which are invovled.

There are many problems associated with this type of model study and the application of experimental results to field cases. Probably the greatest problem is the presence of interlayer shear and the inability to relate model reactions to those of the prototype. Because of this, extensive field testing will be required to confirm the above results.

It is hoped that this study will help promote more widespread acceptance and use of the roof truss as an economical means of roof support. Two other factors besides the actual support capability of the roof truss are important in this respect, however. The first is the availability of machinery which can readily drill the inclined holes required by the roof truss. The second is the modification of the roof

truss so that it can be tensioned more effectively and efficiently.

Bolting machines are available which will drill inclined holes, and these have been employed to install roof trusses. What is needed, however, is a machine specifically designed so that it can install both roof bolts and roof trusses. It is felt that this could be easily accomplished with existing technology, and that the only reason it has not already been developed has been the absence of requests by the coal mining industry for it.

The roof truss could relatively easily be modified so that it could be tensioned mechanically rather than by hand. This could be realized using one of several methods, but has yet to be tried underground. Higher weight-strength ratio roof trusses might also be employed. These might be constructed from wire rope. Incorporating with this a mechanical truss installer might provide an even more effective answer to the problem of installing roof trusses.

Further laboratory studies are currently being performed to study the variables studied in this paper, but in a much more detailed manner. In addition, several variables not studied in this paper will be evaluated. These include the effects of strata thickness on the support, the effects of coal seam height, and the effects of varying overburden height. The potential for this method of stress analysis of mine models appears to be very promising. In addition to the study of roof trusses, this method will also be employed to study roof bolts, roof pins, and longwall support.

Field correlation of the laboratory studies has just begun with

the selection of several mines for study and the instrumentation of a roof truss with strain gages. This and further studies are recommended, not only to correlate laboratory data with field results, but also to determine when and where roof trusses will be needed to support problem roof strata, and the best combination of roof trusses and roof bolts.

Roof bolts have proven to be an invaluable tool to many coal mine operators. It is hoped that with the further development of design criteria and the appearance of machinery capable of efficiently installing them that they will become an even more valuable method of roof support, perhpas even replacing the roof bolt to a large extent.

REFERENCES

Agarwal, R. K., "Photoelastic Analysis of a Composite Model," Transactions, SME of AIME, December 1968, pp. 495-501.

American Institute of of Steel Construction, Manual of Steel Construction, AISC, 7th edition, 1970.

Bieniawski, Z. T., Van Tonder, C. P. G., "A Photoelastic - Model Study of Stress Distribution and Rock Fracture Around Mining Excavations," Experimental Mechanics, February 1969, pp. 75-81.

Dally, James W., and Riley, William F., Experimental Stress Analysis, McGraw-Hill, 1965.

Dove, Richard C., and Adams, Paul H., Experimental Stress Analysis and Motion Measurement, Merrill Publishing Co., 1964.

Durelli, A. J., and Riley, W. F., "Development of the Grid Method of Experimental Stress Analysis," Proceedings Society for Experimental Stress Analysis, Vol. 14, No. 2, 1956, pp. 91-99.

Everling, G., "Model Tests Concerning the Interaction of Ground and Roof Support in Gate-Roads," Int. J. of R. Mech. & Min. Sci., v. 1, N. 3, May 1964, pp. 319-326.

Frocht, M. M., Photoelasticity, Vols. 1 and 2, New York, John Wiley & Sons, Inc., 1941 and 1948.

Gambrell, S. C., and Haynes, D. C., "In-Situ Roof Trusses vs. Angle Roof Bolts - A Photoelastic Comparison," Transactions SME of AIME, June 1970, pp. 109-110.

Hobbs, D. W., "Scale Model Studies of Strata Movement Around Mine Roadways," Int. J. of R. Mech. & Min. Sci., v. 7, N. 4, March 1970, pp. 183-192.

_____, "Scale Model Studies of Strata Movement Around Mine Roadways," Int. J. of R. Mech. & Min. Sci., v. 6, N. 4, July 1969, pp. 365-414.

_____, "Scale Model Studies of Strata Movement Around Mine Roadways," Int. J. of R. Mech. & Min. Sci., v. 5, N. 3, May 1968, pp. 219-235.

_____, "Scale Model Studies of Strata Movement Around Mine Roadways," Int. J. of R. Mech. & Min. Sci., v. 3, N. 2, May 1966, pp. 101-128.

Hoek, E., "The Design of a Centrifuge for the Simulation of the Gravitational Force Fields in Mine Models," Journal South African Institute of Mining and Metallurgy, April, 1965, pp. 455-487.

Hugon, A., and Costes, A., "Le Boulonnage des Roches en Souterrain," Eyrolles, Paris, 1959.

Jacobi, O., and Everling, G., "Model Tests Illustrating the Effects of Different Roadway Supports," Proceedings of the Third International Strata Control Conference," Paris, 1960.

Kegel, W. G., "Roof Truss Installations," Mining Congress Journal, July, 1969, pp. 22-27.

Ketter, Robert L., and Prawel, Sherwood P., Jr., Modern Methods of Engineering Computation, McGraw-Hill, 1969.

Lang, T. A., "Rock Mechanics Considerations in Design and Construction," Proceedings of the Sixth Symposium on Rock Mechanics, University of Missouri at Rolla, 1964, pp. 561-605.

Mandel, J., "Tests on Reduced Scale Models in Soil & Rock Mechanics, a Study of the Conditions of Similitude," Int. J. of R. Mech. & Min. Sci., v. 1, N. 1, January 1964, pp. 31-42.

Panek, L. A., "Centrifugal Testing Apparatus for Mine Structure Stress Analysis," RI 4883, June 1952, U. S. Bureau of Mines.

Popov, Egor P., Introduction to Mechanics of Solids, Prentice-Hall, 1968.

Proctor, R. V., White, T. L., Rock Tunneling With Steel Supports, Youngstown, Youngstown Printing Co., 1946, Revised 1968.

Rankilor, P. R., "The Construction of a Photoelastic Model Simulating Mining Subsidence Phenomina," International Journal of Rock Mechanics and Mining Sciences, v. 8, N. 5, September 1971, pp. 433-444.

Rankilor, P. R., McNicholas, J. B., "The Preparation and Use of a Stress-Sensitive Material in Multi-Layer Photoelastic Models," Int. J. of R. Mech. & Min. Sci., v. 5, N. 3, 1968, pp. 465-474.

Schvermann, "Richtlinien fuer den ankerausbau," Gluckauf, 3, Umschau, 1960.

Society on Experimental Stress Analysis, Manual on Experimental Stress Analysis, SESA, 2nd edition, 1965.

Sheorey, P. R., Verma, B. P., and Singh, B., "An Analysis of the Roof Truss," Journal of Mines, Metals and Fuels, August 1973, pp. 233-236.

Singh, M. M., and Chugh, Y. P., "Design of Roofbolt Installations in Stratified Deposits," Mining and Minerals Engineering, 4, 1968, pp. 98-104.

Thakur, Devendra Nath, "Some Aspects of Rock Pressure Modelling on Equivalent Materials," Int. J. of R. Mech. & Min. Sci., v. 5, N. 4, July 1968.

Timoshenko, S. and MacCullough, Gleason H., Elements of Strength of Materials, D. Van Nostrand Co., 3rd edition, 1958.

Tincelin, E., and Sinoc, P., "Control of Weak Strata in the Iron Ore Mines of Lorraine," International Journal of Rock Mechanics and Mining Science, 3, 1964, pp. 341-384.

Tsur-Lavie, Y., and Van Ham, F., "The Reinforcement Factor Obtained in Sedimentary Rooflayers by Means of Perpendicular and Oblique Roofbolts," Israel Journal of Technology, Vol. 7, No. 5, 1969.

Van Ham, F., and Tsur-Lavie, Y., "Reinforcement Effect and Action of Perpendicular and Inclined Roofbolts in Layered Rock Formations," Proceedings, Second Congress of the International Society for Rock Mechanics, v. 2, 1970, pp. 457-467.

White, Claude, C., "In-Situ Mine Roof Trusses Combining Rock Compression with Steel Tension Members," Brochure Birmingham Bolt. Co., Birmingham, Alabama.

White, Claude, C., "Roof Bolting Trends in Roof Support," Paper Presented at SME of AIME Spring Meeting, Pittsburgh, Pa., 1970.

Wilson, E. L., "Finite-Element Analysis of Two-Dimensional Structures," Doctor of Engineering Thesis, University of California, Berkeley, 1963.

Appendix 1.

Derivation of Equations for Calculating the Weight of Various Shapes of Potential Failure Zones.

Equation for Parabola

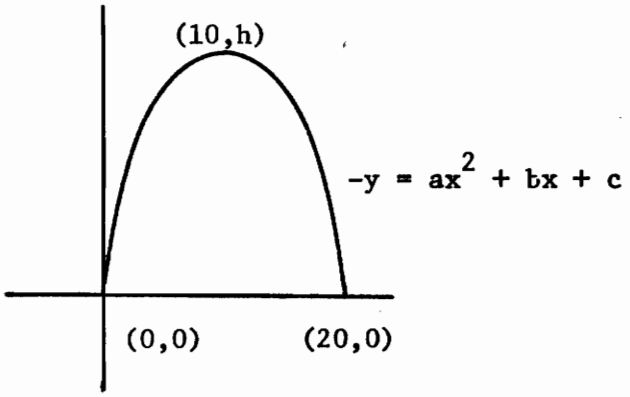

Constraints:

At: $X = 0, Y = 0$

$X = 20, Y = 0$

$X = 10, Y = h$

Solution of constants:

1. $0 = (a)(0)^2 + (b)(0) + (c)$ $\qquad c = 0$

2. $0 = (a)(20)^2 + (b)(20)$

3. $-h = (a)(10)^2 + (b)(10)$

$$0 = 400a + 20b$$

$$-h = 100a + 10b$$

Solving for a:

$$0 = 400a + 20b$$

$$\frac{-2h = 200a + 20b}{2h = 200a} \qquad a = \frac{2h}{200} = \frac{h}{100}$$

Solving for b:

$$0 = 400a + 20b$$

$$\frac{-4h = 400a + 40b}{-4h = +20b} \qquad b = \frac{-4h}{20} = \frac{-h}{5}$$

The general equation for a parabola with the imposed constraints therefore becomes:

$$-y = \frac{h}{100} x^2 - \frac{h}{5} x$$

The area between the x-axis and the above parabola may be found by integration, and is as follows:

$$A = 2 \int_{10}^{0} \left(\frac{h}{100} x^2 - \frac{h}{5} x \right) dx$$

$$= 2 \left(\frac{h}{100} \frac{x^3}{3} - \frac{h}{5} \frac{x^2}{2} \right)_{10}^{0} = (-2) \left(\frac{h}{100} \frac{1000}{3} - \frac{h}{5} \frac{100}{2} \right)$$

$$= (-2) \left(\frac{10h}{3} - 10h \right) = \frac{40h}{3}$$

Assuming the rock weighs 166 pcf, the weight of the potential failure zone for a 20 ft. wide opening can be calculated as follows:

$$(w) = \left(\frac{40h}{3} \text{ ft.}^2 \right) (\text{TS ft.}) (166 \text{ pcf})$$

Where,

w = failed material weight

h = height of failure

TS = truss spacing

Similarly, formulas can be derived for the other geometrical shapes used.

Triangular:

$w = (10h \text{ ft.}^2)(\text{TS ft.})(166 \text{ pcf.})$

Square:

$w = (20h \text{ ft.}^2)(\text{TS ft.})(166 \text{ pcf.})$

Parallelogram

$w = 20h - h^2 \cot\theta$ ft.^{2} (TS ft.)(166 pcf.)

so long as $h \cot \theta \leq \frac{20}{2}$

Where θ is the acute angle of the parallelogram.

Appendix 2

Model Descriptions and Tables of Raw Experimental Data

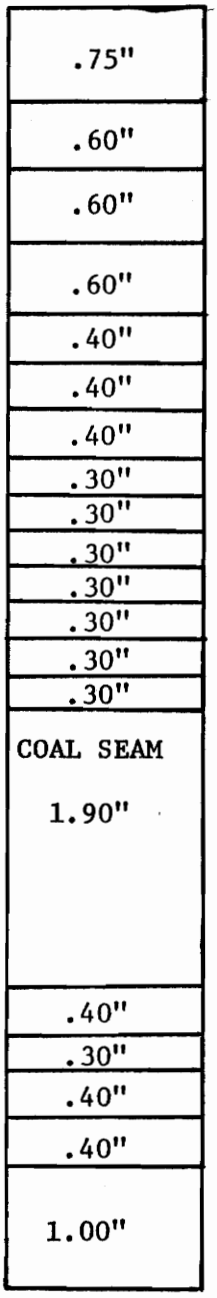

Figure 46. End View of Mine Model Showing Layer Thicknesses.

BEAM TYPE	MIDSPAN DEFLECTION EQUATION
Simple, Uniformly Distributed Load	$\Delta = \frac{(5)(w)(1)^4}{(384)(E)(I)}$
Simple, Uniform Load Partially Distributed at Both Ends	$\Delta = \frac{(w)(a)^2}{(24)(E)(I)} \quad (3(1)^2/2 - a^2)$
Simple, Two Equal Concentrated Loads Symmetrically Placed	$\Delta = \frac{(P)(a)}{(24)(E)(I)} \quad (3(1)^2 - 4(a)^2)$

---

w = uniformly distributed load

1 = beam length between reaction points

E = modulus of elasticity

x = beam length ÷ 2, or (1)/2

a = length of partially distributed load, or distance of concentrated load from reaction point

P = concentrated load

---

polyurethane weight = .037 lb./in.^{3}

I = .00225 in.^{4} for beam 1.0 in. wide by 0.3 in. high

(1) = 8.0 in.

a = 1.5 in. for partially distributed uniform load

a = 1.25 in. for equal concentrated symmetrically placed loads

E = 1000 psi.

Figure 47. Simple Beam Formulas for Midspan Deflections (Fixed End Formulas Yield Answers Approximately 1/3 to 1/5 Simple Beam Deflections).

TABLE 6

Experimental Data for Series 1-A

(8" opening, 6" truss span, .25" blocking point distance, 45° inclined holes 5 rooflayers deep at .3"/rooflayer)

Spring Tension, gms.	Midspan Fringe Order	Fringe Order % Reduction	Midspan Deflection, mm.	Deflection % Reduction
0	1.81	0	2.61	0
165	1.20	34	1.98	25
395	0.88	51	1.88	28
460	0.72	60	1.53	41
530	0.64	65	1.50	43
625	0.43	76	1.49	43
840	0.13	93	1.43	55
0	1.93	0	3.64	0
40	1.76	9	3.40	7
127	1.43	26	3.11	15
182	1.30	33	3.07	16
300	1.06	45	3.01	17

TABLE 7

Experimental Data for Series 2-A

(8" opening, 6" truss span, .25" blocking point distance, 45° inclined holes 4 rooflayers deep at .3"/rooflayer)

Spring Tension, gms.	Midspan Fringe Order	Fringe Order % Reduction	Midspan Deflection	Deflection % Reduction
0	1.82	0	2.82	0
270	0.75	59	1.80	36
375	0.55	70	1.66	41
425	0.42	77	1.64	42
620	0.12	93	1.63	42
800	-0.19	110	1.60	43

TABLE 8

Experimental Data for Series 3-A

(8" opening, 6" truss span, .25" blocking point distance(s), 45^{o} inclined holes 3 rooflayers deep at .3"/rooflayer)

Spring Tension, gms.	Midspan Fringe Order	Fringe Order % Reduction	Midspan Deflection, mm.	Deflection % Reduction
0	2.08	0	3.75	0
100	1.47	29	3.03	19
295	1.21	42	2.81	25
535	0.65	69	2.63	30
630	0.49	76	2.56	32
660	0.43	79	2.60	31
775	0.39	81	2.78	26

TABLE 9

Experimental Data for Series 4-A

(8" opening, 6" truss span, .25" and 1.0" blocking point distance(s), 45° inclined holes 5 rooflayers deep at .3"/rooflayer)

Spring Tension, gms.	Midspan Fringe Order	Fringe Order % Reduction	Midspan Deflection, mm.	Deflection % Reduction
0	1.73	0	3.52	0
70	1.10	36	3.09	12
385	0.60	65	2.91	17
480	0.42	76	2.77	21
600	0.26	85	2.75	22
675	0.08	95	2.70	23
760	-0.06	104	2.61	26
835	-0.33	119	2.68	24

TABLE 10

Experimental Data for Series 5-A

(8" opening, 6" truss span, .25" and 3" blocking point distance(s), 45° inclined holes 5 rooflayers deep at .3"/rooflayer)

Spring Tension, gms.	Midspan Fringe Order	Fringe Order % Reduction	Midspan Deflection, mm.	Deflection % Reduction
0	2.09	0	3.92	0
180	1.25	40	3.58	9
375	0.89	57	3.48	11
475	0.63	70	3.17	19
765	0.12	94	2.88	27

TABLE 11

Experimental Data for Series 6-A

(8" opening, 6" truss span, .25" blocking point distance(s), 45° inclined holes 5 rooflayers deep at .3"/rooflayer, rooflayers, but not coal seam, lubricated)

Spring Tension, gms.	Midspan Fringe Order	Fringe Order % Reduction	Midspan Deflection, mm.	Deflection % Reduction
0	1.60	0	3.70	0
240	1.05	34	2.97	20
500	0.41	74	2.69	27
640	0.39	76	2.48	33

TABLE 12

Experimental Data for Series 7-A

(8" opening, 6" truss span, 3.0" blocking point distance(s), 45° inclined holes 5 rooflayers deep at .3"/rooflayer, rooflayers lubricated and top of coal seam lubricated)

Spring Tension, gms.	Midspan Fringe Order	Fringe Order % Reduction	Midspan Deflection, mm.	Deflection % Reduction
0	2.01	0	4.11	0
180	1.23	39	3.20	22
415	0.94	53	2.89	30
495	0.79	61	2.76	33
635	0.82	59	2.58	37

TABLE 13

Experimental Data for Series 1-C

(8" opening, 6" truss span, .25" blocking point distance(s),
30° inclined holes 5 rooflayers deep at .3"/rooflayer)

Spring Tension, gms.	Midspan Fringe Order	Fringe Order % Reduction	Midspan Deflection, mm.	Deflection % Reduction
0	1.87	0	3.75	0
310	1.30	31	3.26	13
380	1.15	39	3.11	17
450	1.06	43	3.02	20
660	0.75	60	2.93	22
755	0.55	71	2.75	27
945	0.23	88	2.63	30

TABLE 14

Experimental Data for Series 2-C

(8" opening, 6" truss span, .25" blocking point distance(s),
30^{o} inclined holes 4 rooflayers deep at .3"/rooflayer)

Spring Tension, gms.	Midspan Fringe Order	Fringe Order % Reduction	Midspan Deflection, mm.	Deflection % Reduction
0	2.14	0	4.34	0
100	1.88	12	3.85	11
230	1.69	21	3.73	14
340	1.46	32	3.56	18
475	1.30	39	3.62	17
610	1.06	51	3.48	20
810	0.67	69	3.31	24

TABLE 15

Experimental Data for Series 3-C

(8" opening, 6" truss span, .25" and 1.0" blocking point distance(s), 30^{o} inclined holes 5 rooflayers deep at .3"/rooflayer)

Spring Tension, gms.	Midspan Fringe Order	Fringe Order % Reduction	Midspan Deflection, mm.	Deflection % Reduction
0	2.10	0	3.83	0
210	1.51	28	2.98	22
335	1.43	32	2.95	23
465	1.25	41	2.78	28
855	0.67	68	2.54	34

TABLE 16

Experimental Data for Series 4-C

(8" opening, 6" truss span, .25" and 3" blocking point distance(s), 30° inclined holes 5 rooflayers deep at .3"/rooflayer)

Spring Tension, gms.	Midspan Fringe Order	Fringe Order % Reduction	Midspan Deflection, mm.	Deflection % Reduction
0	2.11	0	3.91	0
100	1.40	34	3.15	19
480	0.63	70	2.62	33
800	0.21	90	2.28	42

TABLE 17

Experimental Data for Series 1-D

(8" opening, 6" truss span, .25" blocking point distance(s),
60^{o} inclined holes 5 rooflayers deep at .3"/rooflayer)

Spring Tension, gms.	Midspan Fringe Order	Fringe Order % Reduction	Midspan Deflection, mm.	Deflection % Reduction
0	2.00	0	3.66	0
90	1.45	28	3.02	18
215	1.07	47	2.88	23
335	0.89	56	2.76	25
430	0.64	68	2.78	24
810	-0.04	102	2.77	24

TABLE 18

Experimental Data for Series 2-D

(8" opening, 6" truss span, .25" blocking point distance(s), 60^{o} inclined holes 4 rooflayers deep at .3"/rooflayer)

Spring Tension, gms.	Midspan Fringe Order	Fringe Order % Reduction	Midspan Deflection, mm.	Deflection % Reduction
0	2.12	0	3.11	0
115	1.58	26	2.72	13
290	1.25	41	2.65	15
365	1.05	51	2.56	18

TABLE 19

Experimental Data for Series 3-D

(8" opening, 6" truss span, .25" and 3" blocking distance(s), 60^{o} inclined holes 5 rooflayers deep at .3"/rooflayer)

Spring Tension, gms.	Midspan Fringe Order	Fringe Order % Reduction	Midspan Deflection, mm.	Deflection % Reduction
0	2.14	0	3.53	0
45	1.90	11	3.10	12
80	1.29	40	2.79	21
290	0.57	73	2.48	30
435	0.23	89	2.45	31
630	-0.40	119	2.22	37

TABLE 20

Experimental Data for Series 4-D

(8" opening, 7 1/2" truss span, .25" blocking point distance(s), 60^{o} inclined holes 5 rooflayers deep at .3"/rooflayer)

Spring Tension, gms.	Midspan Fringe Order	Fringe Order % Reduction	Midspan Deflection, mm.	Deflection % Reduction
0	1.90	0	4.07	0
225	1.47	23	3.49	14
425	1.27	33	3.46	15
530	1.22	36	3.53	13
620	1.10	42	3.45	15
885	0.85	55	3.53	13

TABLE 21

Experimental Data for Series 5-D

(8" opening, 7 1/2" truss span, .25" and 2.0" blocking point distance(s), 60^{o} inclined holes 5 rooflayers deep at .3"/rooflayer)

Spring Tension, gms.	Midspan Fringe Order	Fringe Order % Reduction	Midspan Deflection, mm.	Deflection % Reduction
0	2.11	0	4.03	0
110	1.64	22	3.33	17
325	1.26	40	3.12	23
455	1.00	53	3.00	26
575	0.81	62	2.71	33
805	0.13	94	2.70	33

TABLE 22

Experimental Data for Series 6-D

(8" opening, 7 1/2" truss span, .25" and 3.75" blocking point distance(s), 60^{o} inclined holes 5 rooflayers deep at .3"/rooflayer)

Spring Tension, gms.	Midspan Fringe Order	Fringe Order % Reduction	Midspan Deflection, mm.	Deflection % Reduction
0	2.08	0	3.83	0
80	1.43	31	3.11	19
260	1.00	52	2.57	33
405	0.67	68	2.36	38
530	0.36	83	2.34	39
820	-0.19	109	2.01	48

TABLE 23

Experimental Data for Series 7-D

(9" opening, 7 1/2" truss span, .25" blocking point distance(s), 60^{o} inclined holes 5 rooflayers deep at .3"/rooflayer)

Spring Tension, gms.	Midspan Fringe Order	Fringe Order % Reduction	Midspan Deflection, mm.	Deflection % Reduction
0	2.45	0	3.29	0
85	2.20	10	2.64	20
220	2.06	16	2.55	22
415	1.69	31	2.53	23
600	1.70	31	2.60	21
675	1.65	33	2.59	21

TABLE 24

Experimental Data for Series 8-D

(9" opening, 7 1/2" truss span, .25" and 3.75" blocking point distance(s), 60^{o} inclined holes 5 rooflayers deep at .3"/rooflayer)

Spring Tension, gms.	Midspan Fringe Order	Fringe Order % Reduction	Midspan Deflection, mm.	Deflection % Reduction
0	2.33	0	3.30	0
90	1.36	42	2.21	33
455	0.56	76	1.48	55

VITA

George M. Neall III was born on March 7, 1949, in Salisbury, Md. He attended elementary and high school in Annandale, Va., and graduated from Annandale High School in June 1967. In June, 1971, he obtained his B.S. Degree in Mining Engineering from Virginia Polytechnic Institute and State University. He worked as a Mining Engineer with Cities Service Co. and Mine Contractors from June, 1971, to August, 1973, and returned to VPI & SU to do graduate study in the field of Rock Mechanics.

George M. Neall III

A PHOTOELASTIC STUDY OF ROOF-TRUSS ROOF INTERACTIONS IN A MULTILAYERED MINE MODEL

by

George M. Neall III

(ABSTRACT)

The available literature on roof trusses and model studies is reviewed and several variables associated with roof truss support are selected for further theoretical and experimental study.

Four theoretical approaches are initially taken in an attempt to construct a simple mathematical model. The theoretical methods employed were elastic beams solutions, rock load solution, transformation of sections, and the finite element method. The insight gained from the theoretical study of the model is used to help explain some of the conclusions which are reached from the photoelastic study.

A multilayered body-loaded photoelastic mine model made from polyurethane plastic is described. The equipment and procedures used to construct the model and to obtain the experimental data, as well as the method of analyzing the data, are included in the discussion. Results from the experiments are presented and an optimum roof truss configuration for the model is selected from the experimental data. Correlation of experimental data with field data is discussed in addition to the potential for further model studies and suggestions for improving the experimental procedure.